Co-expression of lung alveolar epithelial type I and II cell-selective proteins in response to injury

Gareth Roger Clegg

Presented for the degree of Doctor of Philosophy

The University of Edinburgh

2005

Declaration of Authorship

All of the work contained in this thesis, including figures and manuscript preparation, is my own except where explicitly stated. This work has not been submitted for any other degree or professional qualification.

Gareth Roger Clegg,

Edinburgh, November 2005

Abstract

The internal surface of the lung is covered by alveolar epithelial type I (ATI) and II (ATII) cells. In response to injury ATII cells proliferate and transdifferentiate to ATI cells. Currently, there are no simple methods to identify transdifferentiation in vivo. This study used a novel combination of ATI and ATII cell-selective antibodies to investigate the phenotype of the alveolar epithelium following *Staphylococcus aureus*-induced 'direct' lung injury. Imaging using confocal laser scanning microscopy with 2D and 3D image analysis allowed qualitative and quantitative investigation of the epithelial response to injury. Following distal airway instillation of *S. aureus*, the alveolar epithelium was covered with ATII cells (MMC4/$RTII_{70}$-positive cells) and ATI cells (RTI_{40}-positive cells) as seen in control lungs. However, the surface area covered by ATII cells was significantly increased, while the surface area covered by ATI cells was significantly decreased, in comparison with controls. Ultrastructural studies confirmed the decrease in ATI cell numbers following *S. aureus*-inoculation. The alveolar wall of *S. aureus*-injured lungs also contained cells that co-stained with a unique combination of ATI and ATII cell proteins, RTI_{40} and MMC4. To determine whether RTI_{40}/MMC4-positive cells were likely to be intermediates in the transition of ATII to ATI cells I examined ATII cells as they transformed to ATI-like cells in culture (day 0 to 5). Only cells on day 1 of culture were RTI_{40}/MMC4 positive. I also examined the developing lung for RTI_{40}/MMC4 positive cells. Co-staining cells were not found in the developing alveolar epithelium, but they were present in small airways. I also developed a rat model of haemorrhagic shock induced 'indirect' alveolar epithelial injury as a platform for future work. Here I have developed a robust technique for imaging ATII cell transdifferentiation in vivo and in vitro. This work has identified a novel alveolar epithelial phenotype, RTI_{40}/MMC4, in repairing lungs and in ATII cells as they transdifferentiate to ATI-like cells in vitro. These data suggest that RTI_{40}/MMC4-positive cells can be used to both visualize alveolar epithelial intermediates in vivo and to investigate the regulation of ATII cell transdifferentiation following injury.

Table of Contents

Declaration of Authorship ii

Abstract iii

Table of Contents iv

List of Tables vii

Abbreviations viii

Acknowledgements x

Introduction 12

Defining the problem - Acute Lung Injury and Acute Respiratory Distress Syndrome 12
The extent of the problem - incidence of ALI/ARDS 13
The severity of the problem - outcomes after ALI/ARDS 15
Alveolar epithelial cell injury is a crucial component of ALI 16
Constituents of the normal adult lung alveolar epithelium 16
Consequences of alveolar epithelial disruption 17
Alveolar epithelial recovery is key to surviving ALI/ARDS 18
The ATII cell has a pivotal role in the response to alveolar epithelial injury 19
The replacement of damaged alveolar epithelium 19
The role of the ATII cell in epithelial repair - the empirical evidence 19
ATII cells as progenitors 21
Extra-alveolar stem cells 22
ATII cells and lung fibrosis 22
Does alveolar epithelial regeneration recapitulate ontogeny? 24
Immunotargeting as a means of studying cell types 27
The panel of antibodies used 27
Laser Scanning Confocal Microscopy 29
Combining Immunotargeting and LSCM in lung cell research 30
Experimental model of alveolar epithelial injury 31

Aims of this thesis 33

Hypotheses: 34

Materials and Methods 35

Alveolar epithelial type II cell isolation and culture system 35
Modified Papanicolau staining for assessment of purity. 37
Rat pneumonia models: *Staphylococcus aureus* and *Streptococcus pneumoniae.* 37

Harvesting, fixation and frozen sectioning of control and instilled adult rat lungs for immunohistochemistry and electron microscopy 39
Harvesting and fixation of developing rat lung tissue for immunohistochemistry 40
Immunohistochemistry for fluorescence microscopy 41
Confocal microscopy using the *Zeiss LSM 510* 42
Multi track versus single track scanning with the *Zeiss LSM 510* 42
Capturing tiled images using the *Zeiss LSM 510* 43
Image Density Slicing using *Openlab* 44
Cell counting with *Openlab* 45
Quantification of epithelial surface area staining using *Openlab.* 45
Z-plane scanning and 3D reconstruction with *Volocity* 46
Deconvolution of image stacks using Huygens 2 (SVI) software 46
Rat haemorrhagic Shock Model 47
BAL protein content assay 48
Results 1: Control lung alveolar epithelium **49**
Introduction 49
The phenotype of the alveolar epithelium in control lungs defined using anti-RTI_{40}, MMC4, anti-$RTII_{70}$, anti-Pro-SP-C, and anti-SP-D antibodies 49
Three dimensional imaging of control lung tissue 50
Immunophenotyping – staining controls **52**
Auto-fluorescence 52
Secondary only negative controls 52
Isotype-specific negative controls 53
Results 2: Repairing lung alveolar epithelium **54**
Introduction 54
The phenotype of the alveolar epithelium following *S. aureus*-induced lung injury 54
The phenotype of the alveolar epithelium following *S. pneumoniae*-induced lung injury ... 56
Ultrastructure of the alveolar epithelium in inflamed lungs 57
Results 3: Alveolar epithelial cells in vitro and in development **58**
Introduction 58
Analysis of freshly isolated type II cells - modified Papanicolau staining 58
Phenotype of Cultured Alveolar Epithelial Type II cells 58
The alveolar epithelium in development 59
Results 4: Haemorrhagic Shock - a model of indirect acute lung injury **61**

Introduction 61

Alveolar epithelial injury after profound hypotension followed by fluid resuscitation and positive pressure ventilation 61

Discussion **63**

Overview 63

Imaging the lung alveolar epithelium. 63

Demonstration of staining pattern in control lungs 65

Quantification of epithelial staining 66

Demonstration of lung inflammation and injury caused by *S. aureus* and *S. pneumoniae* ... 66

Lung tissue biochemistry 67

Biochemistry - ATI cell markers: 68

Biochemistry - ATII cell markers 68

Primary ATII cell culture - in vitro corroboration of the *in vivo* findings 69

Development 71

A current scheme for epithelial repair 72

Alveolar epithelial repair in the context of other tissues 73

Healing in the lung – avenues for further work 74

Summary 76

Figures **78**

Appendix A: List of solutions **i**

Stock solutions for ATII cell isolation i

'With' Ca/Mg buffer i

'Without' Ca/Mg buffer ii

Coating IgG plates ii

Standard cell culture medium. ii

Solutions for immunohistochemistry: ii

Appendix B: Published work arising from thesis **i**

Coexpression of RTI_{40} with alveolar epithelial type II cell proteins in lungs following injury: identification of alveolar intermediate cell types i

Bibliography **i**

List of Tables

Table 1. Clinical disorders associated with development of ARDS, as identified by the American-European Consensus Conference Committee on ARDS 1994 (Bernard, Artigas et al. 1994)..... 13

Table 2. Recommended criteria for ALI and ARDS, American-European Consensus Conference Committee on ARDS 1994 (Bernard, Artigas et al. 1994)..... 13

Table 3. Attributable mortality for acute lung injury and comparison diseases (adapted from (Rubenfeld 2003)) 14

Table 4. ATI and ATII cell-specific or selective proteins 29

Table 5: Histological and biochemical alterations in pulmonary and extrapulmonary acute respiratory distress syndrome. (Pelosi, D'Onofrio et al. 2003)..... 32

Table 6. Secondary antibodies used in immunohistochemistry 41

Table 7. Isotype specific primary antibody negative controls 53

Abbreviations

10^5 person-years	100,000 person-years
^{3}HT	Tritiated Thymidine
ALI	Acute Lung Injury
ARDS	Acute Respiratory Distress Syndrome
ARDSnet	Acute Respiratory Distress Syndrome Network
ATI-cell	Type I Alveolar Epithelial Cell
ATII-cell	Type II Alveolar Epithelial Cell
BAB	Blood Agar Base
BAL	Broncho-alveolar lavage
BB	Blocking Buffer
BBT	Blocking Buffer with Triton
BM	Branching Morphogenesis
CVP	Central Venous Pressure
DDW	Double Distilled Water
DIC	Differential Interference Contrast
DMEM	Dulbecco's Modified Eagle's Medium
ECM	Extracellular Matrix
EGF	Epidermal Growth Factor
FiO_2	Oxygen Fraction
FCS	Foetal Calf Serum
FGF	Fibroblast Growth Factor
HGF	Hepatocyte Growth Factor
ICU	Intensive Care Unit
IgG	Immunoglobulin G

IPF	Idiopathic Pulmonary Fibrosis
KGF	Keratinocyte Growth Factor
LLD	Lung Liquid Drainage
LSCM	Laser Scanning Confocal Microscope
Mab	Monoclonal antibody
MAP	Mean Arterial Pressure
MMP	Matrix Metalloproteinase
MOF	Multi- or Multiple Organ Failure
MPA	Macula Pomifera Lectin
NO_2	Nitrogen Dioxide
OCT	Optimal Cutting Temperature Compound
Pap	Papanicolau
PBS	Phosphate Buffered Saline
PDGF	Platelet Derived Growth Factor
PEEP	Positive End Expiratory Pressure
Pro-SP-C	Pro-Surfactant Protein C
RDU	Relative Density Units
SP-C	Surfactant Protein C
SP-D	Surfactant Protein D
TGF-beta	Transforming Growth Factor-beta
TH Broth	Todd Hewitt Broth
TLC	Total Lung Capacity
TO	Tracheal Occlusion
UK	United Kingdom of Great Britain and Northern Ireland
USA	United States of America

Acknowledgements

I would like to gratefully acknowledge the help of the following people in the preparation of this thesis:

Firstly my supervisors: Professor Chris Haslett who was instrumental in getting the project off the ground, Professor David Harrison for consistent good advice and practical support, and Dr Mary McElroy without whose patience and personal investment in the project the whole thing would not have been possible.

Thanks to Stuart McKechnie for moral support, excellent conversation – occasionally about work – and collaboration with animal and cell culture work. Bob Morris and Susan McIntyre for technical and logistical assistance, Kirsty Tyrrell for essential help with animal work. Thanks to Linda Wilson for holding my hand through the first faltering steps into the world of confocal microscopy.

Spike Clay gave help in setting up our haemorrhage model. Chris Baig helped enormously with preparation of foetal lung sections, Stuart McKenzie patiently taught me how to use the electron microscope and Shirley O'Dea was there right at the beginning to provide a solid introduction to the ways of the lab. Sharon Hannah kindly helped with final manuscript assembly.

Thanks to the following investigators for their generous provision of reagents and materials:

Professor Leland G Dobbs, Cardiovascular Research Institute, University of California, San Francisco: anti-RTI_{40} and anti-$RTII_{70}$ antibodies. Professor Michael Beers, University of Pennsylvania Medical Center, Philadelphia: anti-pro-SP-C and anti-SP-D antibodies. Dr Tim Foster, Department of Microbiology, Moyne Institute of Preventive Medicine, Trinity College, Dublin: *S. aureus* strain 8325-4. Dr Tim Mitchell, Division of Infection and Immunity, University of Glasgow: *S. pneumoniae* strain D39, NCTC 7466.

Finally, a heartfelt thank-you to my family. My wife Alice for somehow managing to produce three children and cope with moving house along with my preoccupations during the course of the PhD. My fantastic children David, Emily, Matthew and Charlotte for helping me retain some perspective on the important things in life.

This work was supported by a Training Fellowship from the Wellcome Trust.

Introduction

Defining the problem - Acute Lung Injury and Acute Respiratory Distress Syndrome

Ashbaugh and colleagues published the first description of 'Respiratory Distress Syndrome' in the Lancet in 1967 (Ashbaugh, Bigelow et al. 1967). They describe 12 patients with a pattern of acute dyspnoea, cyanosis refractory to oxygen therapy and loss of lung compliance. These clinical features were accompanied by 'diffuse alveolar infiltration' on chest X-ray and a mortality of nearly 60% (7/12). In speculating on the possible pathogenesis of the syndrome the authors postulate 'a common mechanism of injury' to explain the stereotyped end-point after a variety of stimuli. Reflecting on the possible cause of loss of lung compliance, refractory cyanosis and microscopic atelectasis they implicate the alveolus as 'a likely source of trouble.'(Ashbaugh, Bigelow et al. 1967).

Since these initial comments by Ashbaugh and colleagues much has been discovered about the 'Acute Respiratory Distress Syndrome' (ARDS). A key instrument in facilitating the collection of epidemiological data, and allowing comparison of clinical trial data, has been the widespread adoption of a standard definition of ARDS. In 1994 the American-European Consensus Conference Committee on ARDS agreed that the term 'acute lung injury' (ALI) could be applied to a 'wide spectrum' of the clinical presentations of this condition, but that the term 'acute respiratory distress syndrome' be reserved for the most severe end of this spectrum (Bernard, Artigas et al. 1994). Therefore, 'all patients with ARDS have ALI, but not all patients with ALI have a ARDS' (Bernard, Artigas et al. 1994). The 1994 Consensus committee defined ALI as a syndrome of inflammation with injury to the air-blood barrier. The group offered a list of common precipitants, citing sepsis syndrome, aspiration, primary pneumonia and multiple trauma as the commonest **(table 1)**. The committee further recommended operational criteria for the identification of patients with ALI and ARDS **(table 2)**. Although the simplicity of this definition has its detractors, as it does not include assessment of the many factors influencing outcome from ALI and ARDS (e.g. underlying cause, dysfunction of other organ systems), it has improved the

standardisation of clinical research and trials (Ware and Matthay 2000).

Table 1. Clinical disorders associated with development of ARDS, as identified by the American-European Consensus Conference Committee on ARDS 1994 (Bernard, Artigas et al. 1994).

I. Direct Injury	II. Indirect Injury
Aspiration	Sepsis syndrome, with or without hypotension
Diffuse pulmonary infection	Severe non-thoracic trauma
Near drowning	Hypertransfusion for emergency resuscitation
Toxic inhalation	Cardiopulmonary bypass (rare)
Lung contusion	

Table 2. Recommended criteria for ALI and ARDS, American-European Consensus Conference Committee on ARDS 1994 (Bernard, Artigas et al. 1994).

	Timing	Oxygenation	Chest Radiograph	Pulmonary Artery Wedge Pressure
ALI criteria	Acute onset	PaO2:FiO2 ≤ 300mmHg (regardless of PEEP level)	Bilateral infiltrates seen on frontal chest radiograph	≤18mm Hg when measured or no clinical evidence of left atrial hypertension
ARDS criteria	Acute onset	PaO2:FiO2 ≤ 200mmHg (regardless of PEEP level)	Bilateral infiltrates seen on frontal chest radiograph	≤18mm Hg when measured or no clinical evidence of left atrial hypertension

The extent of the problem - incidence of ALI/ARDS

Accurate assessment of disease incidence is fundamental to estimating the societal burden of a disease, tracking trends, and informing decisions regarding allocation of research money and resources. Estimates of the incidence of ALI and ARDS have varied significantly, from 75 per 100,000 person-years (10^5 person-years) in an early study from the USA (National Institutes of Health 1977), to between 1.5 and 8.3 per 10^5 person-years in more recent studies from the UK and USA (Webster, Cohen et al. 1988; Villar and Slutsky 1989; Thomsen and Morris 1995). Figures vary according to definitions employed, methodological assumptions made and the populations studied.

The first published study employing the 1994 consensus definitions reported Scandinavian figures of 17.9 per 10^5 person-years for ALI and 13.5 per 10^5 person-years for ARDS. As definitions and methodology have become increasingly standardised, a recent study utilising the screening logs of the multi-centre Acute Respiratory Distress Syndrome Network (ARDSnet) randomized trial and data from the American Hospital Association has estimated the annual incidence of ALI/ARDS in the USA as 64.2 per 10^5 person-years (Goss, Brower et al. 2003). Corroborative estimates of the likely incidence of ARDS can be derived by examining the incidence of the commonest aetiological factors (i.e. sepsis, pneumonia and severe trauma) and combining these figures with epidemiological data indicating what proportion of these patients will go on to develop ARDS. Rubenfeld and Neff have performed this exercise and estimate an incidence of ARDS associated with sepsis of 45-64 cases per 10^5 person-years and with severe trauma (injury severity score > 15) of 11-18 per 10^5 person-years (Rubenfeld 2003). They also point to further sources corroborating these higher incidence rates (Rubenfeld 2003). Armed with this estimate of incidence for the disease, and assuming a mortality rate of approximately 40% (consistent with the recent literature - see below) the authors then go on to calculate the Attributable Mortality for ALI by multiplying these two values, giving a figure for the USA of around 17,000 - 43,000 deaths per year (Rubenfeld 2003). This figure is put into context with other diseases having important public health impact in **table 3**.

Table 3. Attributable mortality for acute lung injury and comparison diseases (adapted from (Rubenfeld 2003))

Disease	Attributable Mortality
ALI	17,000-43,000
Acute respiratory failure	60,000-120,000
Acute myocardial infarction	199,454
Breast cancer	41,528
HIV disease	14,802
Asthma	4,657

The severity of the problem - outcomes after ALI/ARDS

Until recently, perhaps the most disappointing aspect of the study of ALI/ARDS was the fact that in over three decades since it was first described, there had been little change in the reported mortality rate. Most studies report a mortality rate of 40 - 60 percent (Bell, Coalson et al. 1983; Fowler, Hamman et al. 1983; Montgomery, Stager et al. 1985; Suchyta, Clemmer et al. 1992; Doyle, Szaflarski et al. 1995; Heffner, Brown et al. 1995; Milberg, Davis et al. 1995; Zilberberg and Epstein 1998). Recently studies have begun to report a decline in mortality. Milberg et al reported a steady improvement in outcome beginning in 1989 with mortality reaching a low of 36% in 1993 (Milberg, Davis et al. 1995). Similarly, in the UK Abel et al. found a decrease in mortality from 66% in 1990-93 to 34% in 1993-97 (Abel, Finney et al. 1998). These gradual changes in mortality do not appear to reflect the success of a particular therapy, but rather a non-specific improvement in the delivery of ICU care (Abel, Finney et al. 1998). Indeed, a recent systematic review of therapies for ALI and ARDS found that the evidence does not support the use of any specific pharmacological intervention (Adhikari, Burns et al. 2004). Most encouragingly, the ARDSnet trial, comparing ventilatory strategies used in the support of patients with ARDS reported a mortality rate of 31% in patients treated with low tidal volume ventilation (i.e. 6ml per kg body weight compared to a traditional 12ml per kg body weight) (2000).

In the majority of cases of ARDS death is attributed to sepsis or multi organ failure - rather than primary respiratory failure. It is likely, however, that lung dysfunction contributes significantly to these processes. Pulmonary dysfunction in ALI/ARDS usually necessitates mechanical ventilation, which is not only a potential cause of further lung injury (Dreyfuss and Saumon 1998), but also predisposes to pulmonary infection (Kollef 1999; Bonten, Kollef et al. 2004), and results in a systemic inflammatory response which could worsen extra-pulmonary organ dysfunction

(Slutsky and Tremblay 1998; Ranieri, Giunta et al. 2000). The 2000 ARDSnet trial also lends empirical support to the concept of 'injurious' ventilation. This landmark study showed not only a reduction in absolute mortality of around 10% with low tidal volume ventilation, but also an increase in days free from multi-organ failure (MOF) - suggesting that mechanical ventilation has played a significant part in the pathogenesis

of ARDS as well its treatment.

Alveolar epithelial cell injury is a crucial component of ALI

The pathological process affecting the lung after a range of injurious events can be described as occurring in a series of stages (Albertine 1998). Acutely, extensive endothelial and epithelial damage cause airspace flooding during the first few days (<7days) after the onset of injury. This has also been termed the 'exudative' phase (Tomashefski 2003). The alveoli are filled with protein rich exudate, inflammatory cells and fibrin. Histologically, injury is most evident at the alveolar epithelial component of the air-blood barrier - in particular to the alveolar type I (ATI) cells which appear to be more sensitive to many forms of injury than their counterparts the type II (ATII) cells (Adamson and Bowden 1974). The second histopathological stage in the natural history of acute lung injury is much more variable. The 'proliferative' phase is defined by the onset of epithelial cell regeneration. ATII cells proliferate along alveolar septa from around day 3 after injury and begin to line the alveolar surface (Tomashefski 2003). Fibroblasts and myofibroblasts proliferate also, and migrate through breaks in the alveolar basement membrane into the fibrinous intra-alveolar exudates. During this period, a proportion of patients will achieve rapid reabsorption of oedema fluid, repair of the injured air-blood barrier and restoration of lung function. A significant number, however, will have a very different outcome, with persistence of oedema fluid organisation of the alveolar debris and intra-alveolar fibrosis. During this third 'fibrotic' phase, lung architecture is distorted and lung dysfunction worsens.

Constituents of the normal adult lung alveolar epithelium

The epithelium of the 300 million or so alveoli in each adult lung has a total surface area of approximately 40-80m^2 (Weibel and Gomez 1962). This enormous area is covered exclusively by ATI cells and ATII cells:

Alveolar type I (ATI) cells: cover ~95% of the surface area of the lung with its large attenuated cytoplasmic processes. The cells are large, (surface area of ~5000μm^2), and very thin (thickness ~0.2μm) (Weibel 1984; Pinkerton, Gehr et al. 1992) providing the surface for gas exchange in the lung. ATI and capillary endothelial cells, resting on the same basement membrane, form the air-blood barrier. Because of its paucity of

organelles or other obvious internal structure, the ATI cell had been thought of as having little or no function other than facilitating gas exchange. More recently it has become clear that these cells are important in regulating alveolar fluid balance (Johnson, Widdicombe et al. 2002), and transduction of mechanical deformation for control of surfactant secretion (reviewed in (Williams 2003)).

Alveolar type II (ATII) cells: have a very different role. Described as early as 1977 as the 'Defender of the alveolus' (Mason and Williams 1977), a concept endorsed and expanded by Fehrenbach in the light of 24 years of research (Fehrenbach 2001) the ATII cell covers a fraction of the epithelial surface (<10%) but occurs in roughly equal numbers to the ATII cell. ATII cells are cuboidal in shape, with an apical surface covered by microvilli. Flanked by ATI cells they typically occur singly, occupying the 'corners' of alveolar airspaces. Also known as the 'great pneumocyte' or 'granular cell' ('granules' being the phospholipid rich lamellar bodies which are the *sine qua non* of the ATII cell) these cells have a plethora of functions (reviewed in (Fehrenbach 2001)) including:

1. Surfactant production and recycling
2. Ion transport
3. Regeneration of damaged epithelium
4. Production of a variety of signalling molecules for integration of inflammatory and repair processes.

Consequences of alveolar epithelial disruption

Disruption of the alveolar epithelial barrier has several important consequences:

1. **Alveolar Flooding:** Under normal circumstances, the epithelium is much less permeable to fluid than the endothelium (Wiener-Kronish, Albertine et al. 1991). Loss of epithelial integrity removes a significant physical barrier to alveolar flooding.
2. **Impaired Alveolar Fluid Clearance:** Loss of epithelial integrity and damage to ATII and ATI compromises the epithelial fluid transport machinery and impairs fluid removal from the air-spaces. (reviewed in (Matthay, Folkesson et al.

2002)).

3. **Surfactant Abnormalities:** ATII cell injury interrupts the cycle of surfactant production, secretion and recycling (reviewed in (Baudouin 2004)). This in turn reduces surfactant production and alters its composition leading to loss of surface tension reducing phospholipids, alveolar instability and some compromise of innate immune function. (Haitsma, Papadakos et al. 2004).
4. **Invasion of Pathogenic Micro-Organisms:** Loss of the physical epithelial barrier can provide a portal to the circulation for pathogenic micro-organisms.
5. **Fibrosis.** Disruption of normal epithelial-mesenchymal cross-talk after severe epithelial injury may facilitate lung fibrosis (Rhodes, Lykke et al. 1989; Adamson, Hedgecock et al. 1990; Fang 2000; Selman, King et al. 2001).

Alveolar epithelial recovery is key to surviving ALI/ARDS

It is not surprising then that alveolar epithelial recovery is recognised as being crucial to survival after significant lung injury (Berthiaume, Lesur et al. 1999; Ware and Matthay 2000). Clinical studies have found a correlation between recovery of alveolar epithelial fluid transport and patient outcomes (Matthay and Wiener-Kronish 1990; Ware and Matthay 2001). The method used by investigators to assess alveolar epithelial fluid transport relies on the fact that protein is removed from the alveoli more slowly than fluid. An estimate of the rate of fluid clearance by the alveolar epithelium can be obtained by measuring the change in alveolar protein concentration over time: the magnitude of protein concentration change equates to the rate of liquid clearance (Berthiaume, Sapijaszko et al. 1991). In human studies, these measurements can be achieved by aspirating sequential samples of undiluted pulmonary oedema fluid from the distal airways of intubated patients by passing a suction catheter via the endotracheal tube (Matthay and Wiener-Kronish 1990).

Most patients with ARDS have impaired alveolar epithelial transport, which is associated with more prolonged respiratory failure and higher mortality. Ware and Matthay, divided patients with ARDS into those with maximal fluid clearance (defined as >14% per hour) and those with impaired clearance <14% per hour). Hospital mortality was significantly lower in the group whose epithelial fluid clearance was

maintained (Ware and Matthay 2001).

The ATII cell has a pivotal role in the response to alveolar epithelial injury

Two important aspects of the role of the ATII cell after epithelial injury have been studied in detail by investigators:

a) Replacement of damaged ATII and ATI cells.

b) Modulation of the fibrotic process in the alveolus.

The replacement of damaged alveolar epithelium

An important function of the ATII cell compartment is in re-epithelialisaton of the alveolus after injury. One of the first groups to ascribe this role to the ATII was Adamson et al in 1974. They found that after a hyperoxic insult, ATII cells were relatively unharmed compared to the ATI population (Adamson and Bowden 1974). Using thymidine incorporation as a measure of DNA synthesis they found that maximal epithelial cell proliferation occurred between 3 and 4 days after injury. Induction of mitotic arrest using colchicine revealed that epithelial cell division was occurring solely within the ATII cell population, with no dividing ATI cells seen. Sequential study of epithelial cells labelled with tritiated thymidine after injury showed a reduction of ATII labelling over time, with a corresponding increase in ATI labelling. No labelled ATII cells were found in broncho-alveolar lavage (BAL) fluid. This finding provides compelling circumstantial evidence that the ATII cell population provides a 'reservoir of dividing cells for the replacement for the injury-susceptible [ATI cell] epithelium' (Adamson and Bowden 1974).

The role of the ATII cell in epithelial repair - the empirical evidence

The current paradigm for the role of ATII cells in epithelial repair after injury began to emerge in the early 1970s largely out of the work of two groups - Adamson and in Winnipeg and Evans in California (Evans, Stephens et al. 1972; Adamson and Bowden 1974; Adamson and Bowden 1975; Evans, Cabral et al. 1975). Adamson's 'Cytodynamic Study in Mice After Exposure to Oxygen' illustrates the methodological approach (Adamson and Bowden 1974). Using electron microscopy to phenotype epithelial cells according to specific ultrastructural characteristics Adamson and co-

workers examined the response of the rat lung to an injury induced by a six-day exposure to 90% oxygen followed by recovery in room air. By injecting animals with intravenous tritiated thymidine (^{3}HT) and colchicine 4 hours before death, it was possible to examine lung alveolar epithelial cell kinetics during recovery. Tritiated thymidine is a weak beta emitter, and after being incorporated into DNA during the S phase of cell division the isotope is then detectable by autoradiography, demonstrating which cells have begun DNA synthesis since labeling. Colchicine inhibits microtubule polymerization and so prevents formation of the mitotic spindle - arresting cell division in metaphase and providing a 'snapshot' allowing the identification of cells undergoing mitosis. The pattern of hyperoxic lung injury was typical with interstitial oedema, epithelial necrosis and hyaline membrane formation. Alveolar epithelial cell damage appeared to be limited to the ATI cells, with ATII cells relatively spared. Cell proliferation after injury was maximal after 2.5 days and by 7 days post oxygen exposure the lung structure was normal. ^{3}HT labeling was initially confined mostly to the ATII cell population. The absence of any ATI cells caught in metaphase by colchicine confirmed the impression that proliferation during recovery was confined to the ATII cell population. In an extension to this study cells were labeled using a single pulse of ^{3}HT at 2.5 days post exposure - the point of maximum epithelial proliferation. The number of silver grains over the nuclei of alveolar epithelial cells was then counted at daily intervals. Importantly the mean grain count over the nuclei of ATII cells fell to approximately half, with this decrease beginning 2 days post labelling. Meanwhile the ATI cells population, which was initially unlabeled, began to acquire nuclear grains in similar quantities. Analysis of BAL fluid showed that labeled ATII cells were not disappearing by simply sloughing off into the airspaces. The conclusion drawn by Adamson from these observations was that the initial process of alveolar epithelial repair involves multi-focal proliferation of ATII cells. Some of these cells are then transformed into ATI cells. The finding of a morphologically 'intermediate' population of epithelial cells, having a 'more flattened than cuboidal' shape, microvilli but no lamellar bodies provides support for this hypothesis. In a similar fashion Evans and colleagues used a lung injury model based on nitrogen dioxide (NO_2) exposure to show that ATI cell damage was followed by ATII cell proliferation. ^{3}HT labeling, Autoradiography and electron microscopy showed ATII cell proliferation and transfer

of ^{3}HT from the ATII to the ATII cell populations apparently via a morphologically intermediate cell stage (Evans, Cabral et al. 1975). Uhal summarizes the prevailing view of cell lineage in alveolar epithelial repair at this time as 'the model circa 1980' (Uhal 1997) **(figure 1A).** Since then there has been significant supplementation of this view, though the basic structure remains intact (Uhal 1997).

ATII cells as progenitors

The traditional view of stem cell biology is that self-renewing tissues retain a cohort of tissue-specific 'adult somatic stem cells' which maintain the cell population (reviewed in (Neuringer and Randell 2004)). In the adult lung, the epithelial cell proliferation rate is normally very low, but increases dramatically in response to injury (reviewed in (Uhal 1997)). This conditional nature of lung cell proliferation (i.e. proliferation in response to stimulus) sets it apart from better understood systems with continuous turnover e.g. skin, gut and haematopoietic system (Marshman, Booth et al. 2002; Alonso and Fuchs 2003; Kondo, Wagers et al. 2003). Current thinking derived from examination of these other tissues is that stem cells inhabit specific microenvironments (niches) that provide cues that modulate cell fate (Watt and Hogan 2000). Broadly, unicellular organisms and invertebrates tend to use 'invariant' mechanisms to generate stem cell progeny. Here, each stem cell division is asymmetric and predictable, giving rise to one stem cell daughter, and a further daughter which goes on to differentiate (Morrison, Shah et al. 1997). In contrast to this it is thought that the dividing strategy used by stem cells in most mammalian self-renewing tissues is one of 'populational asymmetry' (reviewed in (Watt and Hogan 2000)). Here a stem cell gives rise to two daughter cells, which can be either stem cells or committed 'progenitors', destined for differentiation. This mechanism allows a degree of flexibility in the progeny produced, allowing response to environmental factors at a population level. It is likely that to conserve stem cells they cycle infrequently and the majority of cell replacement is accomplished through the division of committed progenitors: the so-called 'transiently amplifying compartment' (Neuringer and Randell 2004). The prevailing view is that the ATII cell is the alveolar epithelial progenitor cell.

Extra-alveolar stem cells

It is possible that after severe injury to the alveolar epithelium, repair mechanisms may involve progenitor cells originating from outside the alveolus. Examination of the distal airway epithelium of the mouse 28 days after bleomycin injury revealed a subpopulation of epithelial cells containing Clara cell-specific protein (CC10) mRNA, present in alveolar-like structures (Daly, Baecher-Allan et al. 1998). The inference drawn by Daly et al. from this finding was that alveolar epithelial progenitors could arise from the bronchiolar epithelium.

More controversially, recent work challenges the dogma that tissues are maintained solely by organ-specific stem cells. There is evidence that adult stem cells from the bone marrow are able to regenerate a variety of cell types, including the alveolar epithelium (Kotton, Ma et al. 2001; Grove, Lutzko et al. 2002; Theise, Henegariu et al. 2002; Kleeberger, Versmold et al. 2003). In experimental models, injury appears to increase incidence of engraftment of donor bone marrow cells into the lung e.g. (Ortiz, Gambelli et al. 2003; Hashimoto, Jin et al. 2004). It is still unclear how these cells take on alveolar epithelial phenotypes, and whether or not they must transit through an 'intermediate' stage. Some of the appearances of cells containing both non-lung and lung cell markers after injury can be explained by cell fusion (Spees, Olson et al. 2003). Alternatively, marrow cells may actually change tissue type. Despite the above findings, the actual significance of circulating cells in the process of lung epithelial repair after injury remains controversial and unanswered.

ATII cells and lung fibrosis

The original hypothesis of the pathogenesis of pulmonary fibrosis postulated an initial injury to the lung led to chronic inflammation, this in turn inducing fibrogenesis and later scar formation. More recent observations, however, provide evidence that this scheme is not central to the pathogenesis of interstitial lung disease and puts alveolar epithelial repair firmly at the centre of the interplay of factors leading to conditions such as idiopathic pulmonary fibrosis (IPF), or end-stage ARDS (reviewed in (Geiser 2003)).

Recognition of the fact that fibrotic foci are much more prominent than evidence of inflammation in lung tissue during fibrosis (Kuhn, Boldt et al. 1989), and the lack of

efficacy of anti-inflammatory interventions in the treatment of IPF or ARDS (2000), (Adhikari, Burns et al. 2004) has led to a focus on the fibrotic pathway itself (Selman, King et al. 2001). Increasing evidence suggests that fibrosis results from alveolar epithelial injury, with subsequent abnormal wound repair characterised by alterations in mesenchymal-epithelial interactions at the level of the alveolus (Selman, King et al. 2001; Gauldie, Kolb et al. 2002; Selman and Pardo 2002). After injury, efficient alveolar epithelial repair can inhibit the development of pulmonary fibrosis (Adamson, Hedgecock et al. 1990). The ability of an intact alveolar epithelium to suppress fibrosis has been demonstrated in animal models (Adamson, Young et al. 1988), with delayed alveolar re-epithelialisation seeming to facilitate fibrosis. Attempting to facilitate restoration of epithelial integrity by blocking ATII-cell apoptosis results in reduced fibrosis after bleomycin injury in rats (Wang, Ibarra-Sunga et al. 2000) and mice (Kuwano 2001). Actively promoting ATII proliferation with Keratinocyte Growth Factor (KGF), also known as Fibroblast Growth Factor-7 (FGF-7), can protect the lung if given prior to a variety of injurious agents including bleomycin or oxygen (Guo, Yi et al. 1998), radiation (Takeoka, Ward et al. 1997), alpha-naphthylthiourea (Mason, Guery et al. 1996) and *Pseudomonas* pneumonia (Viget, Guery et al. 2000). Similarly another ATII cell mitogen Hepatocyte Growth Factor (HGF) can reduce injury caused by intratracheal hydrochloric acid if given post exposure (Ohmichi, Matsumoto et al. 1996).

Epithelial and mesenchymal cells signal each other 'bidirectionally and dynamically' (Fang 2000). On a molecular level, the interactions between epithelium and mesenchyme have yet to be worked out, but appear to occur in two main ways. Firstly there is release of soluble mediators in a paracrine fashion. Epithelial cells release TGF-beta and platelet derived growth factor (PDGF), which modulate fibroblast proliferation and matrix deposition. Conversely, fibroblasts influence epithelial cell function by releasing epidermal growth factor (EGF), KGF and HGF among other things. A second means of communication occurs via direct intercellular contact in an anatomical region conceptually termed 'the attenuated fibroblast sheath' (Evans, Van Winkle et al. 1999). The epithelium and mesenchyme communicating in this way form a notional 'epithelial-mesenchymal trophic unit' within which it is thought that ATII cells exert a restraining influence on fibroblast proliferation, this may be lost when epithelial injury interferes

with this relationship (Fang 2000). Anatomical evidence in support of the notion of close epithelial-mesenchymal contact in human lungs comes from examination of uninjured lung tissue by scanning electron microscopy. It appears that fibroblasts maintain physical communication between ATI/ATII cells and the mesenchyme by spanning apertures visible in the basal lamina of the epithelium (Sirianni, Chu et al. 2003).

It seems clear that successful repair of the alveolus after injury requires timely re-epithelialisation and restoration of the epithelial component of this integrated system allowing normalisation of epithelium-mesenchymal communications. Failure of alveolar repair and unchecked signalling between compartments leads to excessive matrix deposition, intra-alveolar fibrosis and progressive lung disease (Adamson, Hedgecock et al. 1990; Fang 2000; Selman, King et al. 2001; Sheppard 2001)

Does alveolar epithelial regeneration recapitulate ontogeny?

Parallels in the genetic control of development and repair: Lung development and repair are controlled by complex stimulatory and inhibitory signalling mechanisms (Warburton, Schwarz et al. 2000). Analysis of the genetic machinery central to governing early lung morphogenesis reveals a high degree of stereotypy suggesting a degree of genetic 'hard wiring' (Warburton and Bellusci 2004). Pattern formation in the airways is not well understood, but it is likely that the raw material for the process of branching morphogenesis (BM) arises out of the physical properties of a 2D epithelial cell sheet 'fingering' as it penetrates the mesenchyme (Fleury and Watanabe 2004). A layer of order and control is superimposed by tempero-spatial patterns of gene expression (Warburton and Bellusci 2004). Significant parallels have been drawn between the genetic mechanisms governing BM in flies, mice and humans (Metzger and Krasnow 1999; Beitel and Krasnow 2000). FGF receptor tyrosine kinase signalling is required for the initiation and maintenance of tracheal branching in the fly, and also crucial to all stages of lung morphogenesis in the mouse. Fgf10 null mutants have no bronchial modelling distal to the carina (Min, Danilenko et al. 1998; Sekine, Ohuchi et al. 1999), whereas double null mutation of Fgfr3 and Fgfr4 abrogates postnatal alveolar morphogenesis (Weinstein, Xu et al. 1998). Similar studies on the *sprouty* family, are cited as further evidence of functional conservation of key regulatory elements across

phyla during development (Warburton and Bellusci 2004).

In adult ATII cells survival, migration and proliferation during remodelling after hyperoxic injury is stimulated by culture on fibronectin, and exposure to Epidermal Growth Factor (EGF) (Buckley, Driscoll et al. 2001). The highly conserved nature of the mechanisms controlling lung development, and the involvement of some of these signals in the repair of adult lungs have been cited as evidence that the same processes are involved in development and repair (Warburton and Bellusci 2004).

'Intermediate' cells are identified in alveolar development and repair: Cells which have a morphology combining ATII and ATI cell features have been reported after a variety of injuries to the alveolar epithelium (Adamson and Bowden 1974; Evans, Cabral et al. 1975; Takahashi, Aida et al. 1994), and are visible after KGF induced hyperplasia (Fehrenbach, Kasper et al. 1999). The proposition that the appearance of these cells represents the activation of a developmental process during repair is supported by descriptions of similar cells observed during alveolar development.

Flecknoe et al. have performed a series of studies examining the development of the alveolar epithelium (Flecknoe, Harding et al. 2000; Flecknoe, Wallace et al. 2002; Flecknoe, Wallace et al. 2003; Flecknoe, Boland et al. 2004). Their experimental paradigm involves the alteration of basal lung expansion in the foetal sheep - increasing expansion by tracheal occlusion (TO) or decreasing expansion by lung liquid drainage (LLD) - for a period of several days. Composition of the alveolar epithelium was then surveyed by electron microscopic examination of epithelial cell morphology in random tissue sections, with corroborating information on numbers of functional ATII-cells from the quantification of surfactant protein mRNA. The group have assigned four distinct cell morphologies: 1. 'Alveolar epithelial stem cells', having cuboidal shape and containing abundant cytoplasmic glycogen deposits. 2. 'Type I alveolar epithelial cells' with long flattened cytoplasmic extensions, flattened elongated nuclei and little perinuclear cytoplasm. 3. 'Type II alveolar epithelial cells' were rounded with apical microvilli and lamellar bodies. 4. 'Intermediate cells' displayed both ATI and ATII features, but were a heterogeneous group. To qualify, cells were required to have a flattened nucleus and elongated cytoplasm, but also lamellar bodies and usually apical microvilli (Flecknoe, Harding et al. 2000).

The group found that control foetal lungs (113-120/147 days gestation) contained around 29% ATII, 65% ATI and 6% morphologically intermediate cells (Flecknoe, Harding et al. 2000). These proportions could be manipulated by altering basal lung expansion and/or glucocorticoid infusion. Tracheal occlusion produced a decrease in ATII cell numbers to 9% after 2 days with a corresponding increase in 'intermediate' cells to 24%. There was no change in ATI cell number at this early time point, but after 10 days of TO ATI cells made up 90% of the alveolar epithelial population with intermediate cell number back down to control levels (Flecknoe, Harding et al. 2000). The group inferred that an increase in basal lung expansion by tracheal occlusion had caused ATII cells to differentiate into ATI cells via an 'intermediate' stage. Further work using this model yielded empirical evidence to suggest that this change in the proportion of ATII and ATI cells following TO is reversible if the foetus is then subjected to lung liquid drainage to chronically reduce basal lung expansion (Flecknoe, Wallace et al. 2002). A comparison of the contributions of reduced lung expansion, and cortisol infusion to the increase in ATII-cell numbers showed that each had an additive effect, but probably exercised through different mechanisms (Flecknoe, Boland et al. 2004).

While this approach to identifying cell type using ultrastructural markers has been widely used, and still remains the gold standard for individual cell phenotyping, it has significant limitations. It is usually only practicable to survey a very small area of lung by electron microscopy. Even with careful attention to sampling technique in order to try and obtain representative images, it is difficult to place the very high magnification phenotyping-information-rich images from the electron microscope into the context of the tissue or organ under examination without losing access to morphological markers of cell-type.

Williams and Dobbs (Williams and Dobbs 1990) used an immunotargeting approach to lung epithelial cell phenotyping, avoiding some of the limitations inherent in a solely morphology based approach. Using immunofluorescence and immunoblotting to detect ATI and ATII cells specific markers during development they found that RTI_{40}, a ATI cell specific marker, first appeared on the apical surfaces of lung cells at day 15 (by immunofluorescence, but was not present in concentrations detectable by immunoblot until day 17). Macula pomifera agglutinin (MPA), a ATII-cell marker, was first

observed on day 16. By day 20, staining with both markers was widespread throughout the alveolar epithelium, and a population of cells was detected which appeared to express both markers simultaneously. The authors were unable to stain the same lung section with both markers at the same time and instead stained 'serial frozen sections' to detect colocalisation of markers. Because the thickness of sections (4-6μm) was less than the diameter of the epithelial cells under examination it was suggested that staining visible in two consecutive sections arising from the same place on the slide was likely to originate from the same cell.

Immunotargeting as a means of studying cell types

Adamson and Bowden in their seminal paper allude to the difficulty involved in studying the behaviour of the alveolar epithelium because of "...the problems of combining adequate numerical analysis with precise cellular identification." (Adamson and Bowden 1974). 'Immunotargeting' is a term used by Funkhouser to describe the use of antibodies to antigens specific to a particular cell lineage or stage of differentiation to isolate cell subpopulations of interest (Funkhouser and Peterson 1989). Used in this way, immunofluorescence is a powerful tool for characterising cell populations and analysing their interactions. I used a panel of ATI and ATII cell specific antibodies to investigate the alveolar epithelium in control lungs, after lung injury, during lung development and in primary cell culture.

The panel of antibodies used

Classification of proteins: McElroy and Kasper have differentiated between marker proteins expressed by ATI cells, by grouping them according to cell specificity (McElroy 2004). Cell-specific proteins are expressed by the target epithelial cell (in this case ATI-cells) in the lung and nowhere else. Cell-selective proteins are expressed by the target cells, and other lung cells but not other cells in the same tissue compartment (in this case the alveolar epithelium). Cell associated proteins are expressed more abundantly by target cells than other cells in the same tissue compartment. In this study I have used antibodies against the following panel of cell-specific and cell-selective proteins:

Aminopeptidase N, p146, MMC4 antigen: Aminopeptidase N was first located on the

apical membranes of ATII cells in the rat lung during a search for rat lung epithelial cell specific proteins using monoclonal antibodies (Funkhouser, Cheshire et al. 1987). The membrane glycoprotein was initially labelled p146, though subsequent isolation and partial sequencing revealed that it was identical to aminopeptidase N (Funkhouser, Tangada et al. 1991). Similarly Boylan et al. raised a monoclonal antibody, MMC4, specific to rat ATII cells and Clara cells in the distal airways (Boylan, Pryde et al. 2001). Later identification of the MMC4 antigen by immunoprecipitation and mass spectrometry has shown it to recognise aminopeptidase-N (Franklin 2004). Speculating on the probable functions of aminopeptidase-N in the lung by analogy with its role in other contexts, Funkhouser et al suggest that these may include regulation of autocrine and paracrine signals, post translational modification of proteins (e.g. surfactant associated proteins) and possibly activation of antibacterial peptides (Funkhouser, Tangada et al. 1991).

Rat type II cell 70-kDa protein ($RTII_{70}$): Anti-$RTII_{70}$ is a monoclonal antibody, specific to the apical surface of rat ATII cells. The function of the $RTII_{70}$ protein antigen is not known (Dobbs, Pian et al. 1997).

Pro-Surfactant Protein C (Pro-SP-C): Surfactant protein C (SP-C) is produced from proteolytic cleavage of a larger precursor; pro-SP-C. Beers et al. have produced an anti-pro-SP-C polyclonal antibody, and demonstrated that pro-SP-C is unique to the intracellular compartment of ATII cells in the lung (Beers, Wali et al. 1992; Beers, Kim et al. 1994).

Surfactant protein D (SP-D): Surfactant protein D (SP-D) is a product of ATII cells involved in the opsonisation of inhaled pathogens and allergens. Lung inflammation significantly increases the quantity of SP-D in BAL fluid (Haczku, Atochina et al. 2001). Cao et al. have produced a rabbit polyclonal antibody using peptides from the N- and C-terminal regions of human SP-D. This antibody recognises rat, murine and human SP-D (Cao, Tao et al. 2004).

Rat type I cell 40-kDa protein (RTI_{40}), Type I cell alpha protein (TI-α): This is an apical membrane protein that is specific to ATI cells in the lung. The protein was discovered by Dobbs et al. as part of an effort to produce antibodies with which to characterise ATI cells (Dobbs, Williams et al. 1988). RTI_{40} protein is also detected

outside the rat lung in the choroid plexus and ciliary epithelium (Williams, Cao et al. 1996). A monoclonal antibody against RTI_{40} has enabled identification of the rat gene, and revealing homology with proteins expressed by a number of other cell types including an osteoblast cell line, rat kidney podocytes, mouse thymus, a mouse osteoblast cell line and mouse keratinocytes (reviewed in (McElroy 2004)). The role of RTI_{40} in the lung is unknown, but mice with targeted mutations at the RTI40 locus die at birth with respiratory failure (Ramirez, Millien et al. 2003; Schacht, Ramirez et al. 2003). It is speculated that the protein may be important in initiating and maintaining the extended and flattened ATI phenotype (Williams 2003; McElroy 2004).

Table 4. ATI and ATII cell-specific or selective proteins

Name (reference)	Cell specificity in the rat lung	Antibody isotype
MMC4 (Boylan, Pryde et al. 2001)	ATII & Clara	IgG2a
Anti-$RTII_{70}$ (Dobbs, Pian et al. 1997)	ATII	IgG3
Anti-Pro-SP-C (Beers, Wali et al. 1992)	ATII	Rabbit polyclonal
Anti-RTI_{40} (Dobbs, Williams et al. 1988)	ATI	IgG1
Anti-SP-D (Cao, Tao et al. 2004)	ATII & Clara	Rabbit polyclonal

Laser Scanning Confocal Microscopy

The concept of the confocal microscope was first invented by Marvin Minsky (patented in 1957) to visualise neurons. The key feature of the confocal microscope is the 'spatial confinement' of detected light (signal) that reduces image blurring caused by light scatter. This is done by imaging one 'point' at a time.

A confocal imaging system achieves rejection of out-of-focus signal by two strategies:

a) Illumination of a single point of the specimen at any one time with a focused beam, so that illumination intensity drops off rapidly above and below the plane

of focus.

b) Use of a pinhole aperture so that light emitted away from the point in the specimen being illuminated is blocked from reaching the detector.

Figure **(figure 2A)** shows a simplified diagram of the optics of a confocal microscopy system, and illustrates how emitted light from above or below the optical plane of interest is screened from the detection device by a detector pinhole. **(figure 2B)** Shows a schematic of the implementation of this type of system, as used in the present study.

In general, a confocal microscope that is set up correctly will always give a better image than can be obtained with a standard epifluorescence system because of its rejection of out-of-focus interference. The improvement can vary between marginal, in the case of very flat specimens, to spectacular in the case of large, whole-mount specimens. In fact, it can be almost impossible to gain useful information from a large, microscopically thick specimen with conventional microscopy, yet obtain clear optical sections with the confocal microscope **(figure 3)**. Use of a confocal system will also increase the effective image resolution achievable, and improve signal to noise ratio. By allowing the imaging of multiple single thin optical sections at different focal planes through a thick specimen ('z-stack'), confocal microscopy also provides the ability to image in three dimensions.

Combining Immunotargeting and LSCM in lung cell research

Use of LSCM technology has become an increasingly popular tool in imaging biological systems since the 1980's. LSCM has often been used simply to obtain a clearer version of the image that would have been obtainable using epifluoresence, ignoring the other possibilities opened up by this technology. The lung in particular, with its complex three dimensional structure and intricate distal airspaces lends itself to LSCM imaging. In this project I have combined modern LSCM technology and image analysis tools with immunotargeting using novel antibody combinations to achieve the following:

a) **Cell phenotyping:** Electron microscopy has been the tool of choice for phenotyping lung cells using morphological markers (Evans, Stephens et al. 1972; Adamson and Bowden 1974; Adamson and Bowden 1975; Evans, Cabral

et al. 1975) and remains so for many investigators (Flecknoe, Wallace et al. 2003; Flecknoe, Boland et al. 2004). This approach requires the identification of cell type based solely on morphology, which does not distinguish between morphologically similar cells that are destined for different pathways of differentiation during development or repair.

b) **Immunotargeting with colocalisation:** Phenotyping by immunofluorescence often demands accurate assessment of colocalisation of antibody staining on a single cell. An important requirement for this is the ability to image at a high enough resolution to avoid the confounding influence of 'pseudo-colocalisation' i.e. where two discrete and differently labelled objects are adjacent, but too small to be individually resolved by the imaging system used and appear as a single dual stained entity. LSCM, with deconvolution of images (see below) is a much more powerful technique than standard epifluorescence to accomplish this.

c) **Examination of 3D structure of airspaces:** Volume rendering of image stacks after immunotargeting allows examination of antigen distribution, cell phenotypes, and cell-cell relationships in three dimensions.

d) **Quantification:** A survey of the cells in a tissue section or cell culture is difficult using morphology based electron microscopic criteria for phenotyping. The demands of tissue preparation for electron microscopy are such that only a very small amount of tissue can be visualised at a time. Immunotargeting combined with LSCM provides a powerful phenotyping tool while allowing large areas of tissue (even sections of entire organs) or cell culture to be surveyed contiguously.

Experimental model of alveolar epithelial injury

To carry out our investigation I sought to use a clinically relevant model of lung injury. As indicated earlier the commonest clinical disorders associated with ALI/ARDS can be broadly grouped according to their mechanism of injury to the lung. This distinction has been postulated for some time and was recognised by the American-European Consensus Conference Committee on ARDS in 1994 **(table 1)**. Disorders resulting in a

'direct' injury to the alveolar air-blood barrier (most commonly gastric aspiration and pulmonary infection) appeared to inflict damage to the alveolar-capillary membrane via an intense inflammatory infiltrate producing oxidants and proteases. Conversely 'indirect' injury to the lung (caused most often by sepsis syndrome, severe non-thoracic trauma or massive blood transfusion) was thought to be predominantly the result of circulating chemokines, cytokines and other mediators generated initially by extra-pulmonary sources of inflammation. This largely speculative distinction was given weight by the clinical observations of Gattinoni et al. who reported differences in respiratory mechanics and response to positive end-expiratory pressure in what they described as 'pulmonary ARDS' (ARDSp) compared to patients with 'extra-pulmonary ARDS' (ARDSexp) (Gattinoni, Pelosi et al. 1998). Further observations confirm the likely existence of two distinct pathogenic pathways for ARDS having different morphological aspects, respiratory mechanics and response to ventilatory strategies (Pelosi, D'Onofrio et al. 2003), though it is not clear how these differences affect clinical outcomes. The main difference in histology and biochemistry in ARDSp compared to ARDSexp are summarised in **table 5.**

Table 5: Histological and biochemical alterations in pulmonary and extrapulmonary acute respiratory distress syndrome. (Pelosi, D'Onofrio et al. 2003)

	ARDSp	**ARDSexp**
Alveoli		
Alveolar epithelium	↑↑ Damage	Damage
Altered ATI and ATII cell	↑↑ Damage	Normal
Alveolar Neutrophils	Prevalent	Rare
Apoptotic Neutrophils	Prevalent	Rare
Fibrinous exudates	Present	Rare
Alveolar collapse	↑↑ Increased	Increased
Local interleukin	Prevalent	Rare
Interstitial space		
Interstitial oedema	Absent	High
Collagen fibres	↑↑ Increased	Increased
Elastic fibres	Normal	Normal
Capillary endothelium	Normal	↑↑ Damaged
Blood		

Interleukin	Increased	↑↑ Increased
TNF-α	Increased	↑↑ Increased

I chose initially to use a rat model of unilateral pneumonia. This was primarily designed to cause a sub-lethal 'direct' lung injury, primarily affecting the alveolar epithelium, allowing examination of subsequent epithelial repair. Inoculation of the animals with *Staphylococcus aureus* strain 8325-4, or *Streptococcus pneumoniae* strain D39 was performed via the oral route to avoid animal injury and facilitate uncomplicated recovery **(figure 4A-D).** The efficacy of this method of unilateral inoculation has been confirmed by Bakker-Woudenberg, who instilled X-ray contrast medium using the same technique, then followed with X-ray examination **(figure 4F)** (Bakker-Woudenberg 2003). Advantages of this approach include a reproducible infectious disease model, with low variation between individuals (Bakker-Woudenberg 2003). *S. aureus* 8325-4 has been shown previously to cause an acute injury to the air-blood barrier in the lung at the inoculating dose we used. McElroy et al. found histological evidence of inflammation, and increased leukocytes and protein in the BAL fluid at 4 hours post instillation (McElroy, Harty et al. 1999).

We also investigated the use of an 'indirect' model of injury secondary to haemorrhage. The haemorrhage model offered the possibility of a more finely controlled and homogeneous lung injury, which could be combined with positive pressure ventilation of the anaesthetised animal in order to provide an approximation to the clinical scenario in the intensive care unit. We used a system similar to that used by Modelska et al. which has been shown to cause endothelial injury and alterations in alveolar epithelial barrier function (Modelska, Matthay et al. 1997). Our initial work involved detection of any injury to the alveolar epithelium sustained during a brief period of haemorrhage, resuscitation and mechanical ventilation. These initial observations were intended to provide a platform for further work.

Aims of this thesis

(a) Development of a robust and informative method of 'immunotargeting' the lung alveolar epithelium using a combination of antibodies to cytotypic (cell-specific) antigens, including qualitative and quantitative analysis of the lung alveolar

epithelium using laser scanning confocal microscopy and subsequent image analysis.

(b) Set up of a system for the isolation and culture of rat lung epithelial type II cells.

(c) To define the phenotype of lung alveolar epithelial cells using a novel combination of cell-specific antibodies.

(d) To examine the phenotype of the alveolar epithelium during repair in a model of *S. aureus* pneumonia, and in *S. pneumoniae* pneumonia using the same panel of antibodies.

(e) To examine the rat lung epithelium during development and ATII cells in culture to look for immunotypic features common to:

- alveolar epithelial cells during repair in the *in vivo* pneumonia model
- during alveolar expansion in lung development
- cell phenotype changes over time in the *in vitro* cell culture system.

(f) To examine the extent of injury to the alveolar epithelium of the rat after haemorrhage and resuscitation, with a view to developing a model of 'indirect' lung injury.

Hypotheses:

(a) After *Staphylococcus aureus* injury, the repairing alveolar epithelium contains 'intermediate' cells with a unique 'differentiation' phenotype.

(b) The process of epithelial regeneration after *Staphylococcus aureus* injury is generic, and evidence of the same process should be detectable in other *in vivo* models of lung injury, in cell culture, and in lung alveolar epithelial development.

Materials and Methods

All reagents were obtained from Sigma-Aldridge Ltd (Poole, Dorset, UK) unless otherwise indicated. Anaesthetics and other veterinary pharmaceuticals were supplied by Genusxpress Ltd, Aberdeen UK. A list of the composition of stock solutions is given in **Appendix A**. Animal work was carried out in accordance with the Animals Scientific Procedures Act 1986.

Alveolar epithelial type II cell isolation and culture system

The cell isolation procedure used was modified from that of Dobbs et al. (Dobbs, Geppert et al. 1980).

1. Dulbecco's Modified Eagle's Medium (DMEM), and Phosphate Buffered Saline (PBS) solutions were warmed to 37°C.
2. Adult male Sprague-Dawley rats (specific-pathogen-free. Harlan, UK) weighing 150-200g were terminally anaesthetized using a mixture of heparin sulphate 500 units and pentobarbital 0.5mls.
3. The descending aorta was cut and the animal exsanguinated. A small cannula was inserted into the trachea. The lungs were perfused with approximately 20mls of warmed 'with'-Ca/Mg buffer solution **(see Appendix A)** via the right ventricle/pulmonary artery using a 26G needle and 20mls syringe. A nick was made in the left atrium using a pair of fine scissors to allow escape of perfusate. The lungs were ventilated with air during the perfusion using a 10ml syringe attached to the tracheal cannula. Perfusion and ventilation were continued until the lungs were white in colour.
4. The lungs were placed in warmed isotonic saline until ready, then lavaged 8 times using 'without'-Ca/Mg buffer.
5. Elastase solution 12.5% (wt/vol) was freshly prepared by dissolving 5mg of elastase (porcine pancreas, specific activity of powder 105 units/mg at 25°C, Roche Ltd, UK) in 40mls of 'with'-Ca/Mg buffer per rat.
6. Lungs were lavaged a further 2 times using 'with' Ca/Mg buffer. Lungs were lavaged once with elastase solution. Elastase solution was then used to inflate

the lungs to total lung capacity (TLC). The lungs were then suspended in beaker of water, in a water bath at 39°C. A plastic 2.5 mls syringe was used as a funnel, and attached to the tracheal catheter to allow periodic addition of elastase solution to maintain inflation. Total elastase inflation time was 25 minutes

7. DNAase solution was freshly prepared using 2mg DNAase (DNase I Bovine Pancreas, Grade II. Roche Diagnostics, Mannheim Germany) per rat diluted in 2mls of 'with' Ca/Mg buffer. Lobes of the digested lungs were dissected free of other remaining non-lung tissue and added to DNAase solution before chopping finely (~5mm cubes). 4mls of Foetal Calf Serum (FCS) was added to the lung tissue, topped up to 40mls using 'with' Ca/Mg buffer and hand shaken for 3 minutes.

8. The crude tissue suspension was passed through progressively finer filters: 2 layer gauze, 4 layer gauze. 150μm, 15μm and 7μm mesh. The cell suspension was then centrifuged at 1100rpm for 6 minutes then resuspended in 20mls of warmed DMEM.

9. IgG coated plates were washed 5 times with PBS before use. 10mls of cell suspension was then plated onto each IgG coated plate and incubated at 37°C for 20-30mins. Plates were then removed from the incubator and the supernatant containing non-adherent ATII cells retrieved. The IgG plates were washed with a further 5mls DMEM which was added to the ATII cell supernatant.

10. The cell suspension was spun down at 1100rpm for 6 minutes and cells resuspended in culture medium (see Appendix A). Cells were counted then spun down and resuspended as appropriate to obtain the desired concentration for plating.

Cell Plating: Correct plating density was achieved by counting the final cell suspension using a haemocytometer and diluting to the required concentration. Cells were plated on circular coverslips, pre-coated with fibronectin (1:50 solution of fibronectin allowed to stand on the coverslips overnight at 4°C, and excess liquid removed before plating) and placed at the bottom of the wells in a 24-well plate.

Modified Papanicolau staining for assessment of purity.

This standard technique for assessing the purity of freshly isolated ATII cells is based on the method described by Dobbs (Dobbs 1990).

1. Cell in a suspension of $2x10^5$ cells per ml were cytospun onto slides at 300rpm for 3 minutes and left to air-dry overnight.
2. Slides were first dipped in hematoxylin (Harris' Formulation) for 3 minutes, then rinsed in distilled water.
3. Dipped for 2 min in lithium carbonate solution. (i.e. 2mls of saturated lithium carbonate solution in 158mls of water. Saturated solution made by dissolving of 256mg lithium carbonate in 20mls of DDW) then rinsed by dipping slides in double-distilled water for 5 sec.
4. Dipped in 50% ethanol for 90 sec, 80% ethanol for 15 sec, 95% ethanol for 15 sec, 100% ethanol for 30 sec.
5. Dipped in xylene:ethanol 1:1 for 30 sec
6. Dipped in xylene for 1 min
7. Mounted using a cover-slip.

Rat pneumonia models: *Staphylococcus aureus* and *Streptococcus pneumoniae*.

The rat pneumonia model by direct instillation of bacteria into the lower airways was based on the technique previously described by Bakker-Woudenberg et al. (Bakker-Woudenberg, de Jong-Hoenderop et al. 1979). Instillate preparation, animal inoculation and tissue harvesting were performed by Christine Tyrrell. The *Staphylococcus aureus* strain used in this study was 8325-4, and was provided by Dr Tim Foster, Department of Microbiology, Moyne Institute of Preventive Medicine, Trinity College, Dublin, Ireland. The *Streptococcus pneumoniae* used was serotype 2 strain D39, NCTC 7466 and was obtained from Dr Tim Mitchell, Division of Infection and Immunity, University of Glasgow, UK.

1. Bacteria were plated out from glycerol stocks onto Blood Agar Base (BAB) plates (Tryptic soy agar plates + 5% sheep's blood, BD Biosciences, Oxford, UK). Bacterial stocks were kept on dry ice to minimise freeze/thawing. A

scraping of glycerol stock was spread onto the BAB plate using an inoculation loop in a sterile Class II cabinet. Plates were incubated at 37°C overnight.

2. Overnight cultures were started in Todd Hewitt (TH) Broth (BD Biosciences, Oxford, UK), from a single colony. 3mls of TH Broth was inoculated with a single bacterial colony using inoculation loop. The broth was then incubated overnight at 37°C (approx 18 hrs). (*S. aureus* containing broth was shaken at approximately 220rpm. while incubating, *S. pneumoniae* broth was not shaken as this had an adverse effect on subsequent bacterial growth).

3. **Making up bacterial instillate:** Bacterial broths were kept on ice and agitated periodically to ensure bacteria remained in suspension. The optical density (O.D.) of overnight cultures was measure using spectrophotometer (600nm wavelength) to estimate bacterial concentration. The required quantity of bacterial suspension was aliquotted into a sterile container. Cells were washed twice with sterile endotoxin free PBS (with Mg/Ca), centrifuging for 3 minutes at approx 13,000 rpm and resuspending between spins. The bacterial pellet was finally resuspended in 1.5mls sterile PBS and kept on ice.

4. **Anaesthetising rats:** Rats (specific-pathogen-free Sprague-Dawley males, 300-350g, Harlan, UK) were anaesthetised with an intraperitoneal injection of Fentanyl citrate 0.315 mg/ml (1 mg/kg/i.p.) and Fluanisone 10mg/ml (33 mg/kg/i.p.) mixed with Midazolam hydrochloride 5mg/ml (17 mg/kg/i.p.).

5. **Instillation:** Rats were maintained in a vertical position by suspension on a horizontal wire by the front upper incisors **(figure 4A)**. An intubation wedge (in the form of a modified 2ml Eppendorf tube, Fisher Scientific, Leicester, UK) was placed in the mouth and a tracheal catheter (0.96 external diameter, Portex Fine Bore Polythene Tubing, Portex Ltd, Kent UK) inserted. 0.5ml bacterial suspension (or PBS control) was instilled into the lungs via the tracheal catheter using a 1ml syringe. **(figure 4B-E)**. A further blast of air was blown into the lungs to aid instillation. A successful tracheal instillation resulted in a transiently increased respiratory rate.

6. **Recovery:** Rats were given an intraperitoneal injection of 3 mls warmed sterile saline and recovered in cage with heating pad, inside a Class II cabinet (animals

were removed from the cabinet after 24 hours).

7. **Determination of concentration of organisms:** Bacterial suspension was plated onto BAB plates to determine concentration or organisms expressed as the number of colony forming units (cfu). 50μl of bacterial suspension at 10^{-3} dilution was plated onto half of a BAB plate, and an erythromycin antibiotic disc placed on the inoculated half of the plate, to confirm sensitivity. 50μl of a 10^{-6} dilution of bacteria was plated onto the other half of the plate, spreading with inoculation loop. The plate was incubated overnight at 37°C.

Harvesting, fixation and frozen sectioning of control and instilled adult rat lungs for immunohistochemistry and electron microscopy

1. At the appropriate time point post inoculation, rat lung perfusion was performed in a similar way to the ATII cell isolation technique. After the lungs had been perfused with saline and were blanched, they were inflated with 4% paraformaldehyde in PBS (wt/vol) solution through the tracheal cannula. Care was taken to avoid causing a leak by over inflating. The tracheal cannula was clamped using haemostat to maintain inflation and the lungs submerged in a beaker containing 4% paraformaldehyde.
2. After ~30 minutes, tissue was cut into slices using razor blade and re-submerged in 4% paraformaldehyde for further 1-2 hours.
3. **Tissue Selection:** The left upper lobe was used consistently for in control animals. When harvesting lungs from the pneumonia model the inflamed/consolidated area of lung was identified macroscopically as paler than the rest of the tissue. This was removed and cut into 5mm cubes for sectioning. A non-inflamed area of the same lung was also removed and treated in the same way. Tissue cubes were processed either for frozen sectioning and immunohistochemistry of preparation for electron microscopy:

Preparation of lung tissue for immunohistochemistry:

1. Tissue was left in 30% sucrose solution at 4°C overnight for cryoprotection. The following day blocks of tissue were submerged in Optimal Cutting Temperature Compound (OCT) and frozen in Freon 22 initially then plunged into liquid

nitrogen. ~3μm sections were cut using a Bright cryostat (Huntington, UK).

2. Tissue sections were stored at -70°C until used.

Preparation of lung tissue for electron microscopy:

1. Lung tissue was first cut into 1mm cubes, then fixed in 3% glutaraldehyde in sodium cacodylate buffer for 4 hours (minimum) to overnight (maximum) at 4°C.

2. After washing in 0.1M sodium cacodylate buffer tissue was fixed in 1% osmium tetroxide in sodium cacodylate buffer for 2 hours at 4°C.

3. Tissue was dehydrated through a series of grades of ethanol (15 minute changes at lower grades, 3x30 minute changes at 100% ethanol), washed in propylene oxide (2 changes at 20 mins each change) and impregnated with Araldite epoxy resin for 2-3 hours.

4. After embedding in fresh Araldite epoxy resin 50 nanometer sections were cut on a LKB Nove ultramicrotome and placed onto 300 mesh copper grids. Grids were stained with uranyl acetate and lead citrate.

5. Grids were viewed on a Jeol 100CXII electron microscope.

Harvesting and fixation of developing rat lung tissue for immunohistochemistry

1. Timed pregnant Sprague-Dawley rats (Harlan, UK) were euthanased at the appropriate time points using carbon dioxide.

2. **Embryonic day 16:** The foetuses were harvested and placed in 4% paraformaldehyde solution at 4°C for 2 hours then switched to 30% sucrose solution and left overnight at 4°C.

3. **Embryonic day 17 - day 21:** Lungs were removed separately and placed in a 4% paraformaldehyde fixative solution containing 10% OCT (vol/vol). After 2 hours at 4°C, tissue was switched to sucrose and left at 4°C overnight.

Immunohistochemistry for fluorescence microscopy

Protocol for staining frozen sections: See **table 4** for a list of primary antibodies. Alexa secondary antibodies **(table 6)** were obtained from Molecular Probes, Invitrogen Ltd, UK.

1. Frozen sections were treated with Blocking Buffer with Triton (BBT) for 10 minutes then washed three times with Phosphate Buffered Saline (PBS)
2. 100μl of primary antibody solution was added to each slide for 20 minutes (primary antibodies were diluted at 1:100 except for anti-$RT1_{40}$=1:50, and anti-pro-SP-C=1:10).
3. Tissue was washed three times with PBS before adding 100μl secondary antibody (dilution 1:100 in BBT for Alexa secondaries) for 15 minutes.
4. Washing was carried out as before and 100μl of TO-PRO-3 (Molecular Probes, Invitrogen Ltd, UK) added for 10 minutes (dilution 1:1000 in PBS).
5. After further washing, a coverslip was mounted using fluorescence mounting medium (DakoCytomation, UK).

Table 6. Secondary antibodies used in immunohistochemistry

Primary antibody	Antibody Isotype	Alexa secondary antibodies used
MMC4	Mouse IgG2a	Alexa Fluor 546 goat anti-mouse IgG2a (A-21133)
Anti-$RTII_{70}$	Mouse IgG3	Alexa Fluor 647 goat anti-mouse IgG3 (A-21243)
Anti-Pro-SPC	Rabbit polyclonal	Alexa Fluor 488 goat anti-rabbit IgG (A-11070)
Anti-RTI_{40}	Mouse IgG1	Alexa Fluor 488 goat anti-mouse IgG1 (A-21121) Alexa Fluor 647 goat anti-mouse IgG1 (A-21240)
Anti-SPD	Rabbit polyclonal	Alexa Fluor 488 goat anti-rabbit IgG (A-11070)

Protocol for staining cells fixed on coverslips used in cell culture:

The protocol for staining coverslips with adherent ATII is similar to that for frozen sections with the following modifications:

1. Cells were fixed at the appropriate experimental juncture using 4% paraformaldehyde solution. Before staining, fixative solution was washed off the cells using PBS.
2. Blocking buffer, and antibody application were carried out as above.
3. The staining solutions were applied to the cells by retrieving the coverslip from the bottom of its 24-well plate and placing it cell-side down onto a piece of laboratory film (Parafilm, Pechiney Plastic Packaging, Chicago USA). A small drop of the required solution (antibody, blocking buffer etc.) was pre-positioned on the film and formed a capillary across the cells.
4. Washing was done by gentle irrigation of the coverslip while holding carefully in fine forceps.

Confocal microscopy using the *Zeiss LSM 510*

Basic laser/filter set up: Images were captured using confocal laser scanning microscopy with the Zeiss LSM 510 scanning head fitted to an Axiovert 100M research microscope. Both are fully motorized and can be controlled via the LSM software. Three lasers were used: Argon/Krypton (488nm), Helium/Neon (543nm), Helium/Neon (633nm). The Alexa secondary antibodies used for staining have emission spectra which peak at wavelengths 546nm (Alexa 546 appears red), 488nm (Alexa 488 appears green) and 647nm (Alexa 647 appears blue). Alexa 647 emissions were filtered through a Low Pass 650nm filter, Alexa 488 emissions through a Band Pass 500-530nm filter, and Alexa 546 emissions through a Band Pass 565-615 filter (**figure 5**). Images were captured as three channel (red, green, and blue) 8-bit grey scale TIFFs, at a resolution of 1024 x1024 pixels. A further 'transmitted', or visible light image of the specimen was also captured to record morphology at the light level.

Multi track versus single track scanning with the *Zeiss LSM 510*

Scanning of each channel was performed sequentially *(multi-track imaging)* - that is the lasers were used one at a time, exciting the specimen with each wavelength of laser light and detecting emission before moving on to the next. This was a crucial part of the image acquisition strategy, as the alternative technique - simultaneous *(single track)* excitation and detection at all wavelengths used can lead to serious artefactual 'spectral

spill', or cross-talk of signal between channels. In our system, cross-talk occurred particularly between the red and green channels during single track scanning, but was effectively eliminated by multi-tracking. This problem is illustrated below. **Figure 5A** shows the excitation spectra for the fluorophores used. The band pass filter system used in detection limits the signal seen by each detector to excitation of the fluorophore of interest. The success of this configuration allows independent detection of multiple fluorophores simultaneously during a single scan, reducing scan times and photobleaching of the specimen. A problem occurs using this single track technique when the excitation spectra for the fluorophores used significantly overlap - in this case the Alexa 488 and Alexa 546 fluorophores (**figure 5B**). Alexa 488 emission excited by the Argon/Krypton 488 laser is detected mainly in the 'green' channel, whose sensitivity is windowed around the peak signal wavelength (500-530nm). Single track scanning using Alexa 488 and Alexa 546 would mean simultaneous detection of the signal generated by excitation of the 546 fluorophore windowed around its peak (565-615nm). It can be seen from the figure that the 'red' signal is potentially contaminated by the 'tail' of the 'green' fluorophore emission. In practical terms, this means that imaging a specimen with a strong Alexa 488 (green) signal by single tracking can result in the appearance of a co-localised positive signal in the 'red' channel, in the absence of any actual staining with a 'red' (565-615nm emitting) fluorophore. By exciting and detecting each channel separately, multi-track scanning eliminates this type of cross-talk.

Capturing tiled images using the *Zeiss LSM 510*

In order to capture images of large contiguous areas of sections at high magnification image tiling was used. Large images composed of a number of smaller tiles allow detailed examination of a significant area of tissue, scanned at the same time, with the same microscope settings. Tiling facilitates quantification by measuring or counting without the bias introduced by simply choosing a number if interesting looking fields of view. The procedure adopted was as follows:

1. A 'scout' image was captured using the x5 objective. A tile was created using 25 contiguous fields of view (i.e. 5x5 fields). 2.
2. This tile was inspected and areas of interest determined and marked - the LSM

510 is able to record stage positions and return to a given point providing the slide is not moved.

3. Higher powered views (20x or 63x objectives) were then obtained, and further high magnification tiles captured which could be further processed e.g. cell counting, quantification of antibody colocalisation etc. The maximum size of tile obtainable using the Zeiss LSM 510 system is 4096x4096 pixels. This equates to 4x4 fields of view using the x63 objective (a specimen area of 585μm^2), or 4x4 fields of view using the x20 objective (specimen area 1843μm^2) using the capture settings detailed above.

Image Density Slicing using *Openlab*

Crucial to counting the numbers of a particular cell type or determining the area of epithelial surface colocalising particular proteins was the facility to isolate the areas of an image which are positively stained with a given fluorochrome. This was achieved using the *Density Slice ...* and *Boolean Operations ...* functions in *Openlab 3.5.2*. Tiled images were first opened in Openlab after reducing the size to a maximum of 4080x4080 pixels (This was done using GraphicConverter *Picture>Size>Add/Remove Margins ...* Openlab is unable to deal with larger images). The RGB TIFF tiles were then split into their constituent red green and blue channels *(Layers>Split RGB)*. Each layer could then be analysed to select areas above a given intensity threshold using the *Image Density* slice function. The threshold for 'positivity' was arrived at by polling the pixel value of a positive area using the *HSI (Hue, Saturation, Intensity) Colorspy* palette or by selecting a positive area (Region of Interest - *ROI*) in the image (e.g. a positively stained cell) and using the *Grab from ROI* function in the *Density Slice dialog*. Positively stained areas in the red, green and blue channels could be selected using the Density Slice function, and a further layer produced containing a simple single colour outline of the positive parts of a given image - a so called *binary layer*. This Binary layer could then be overlaid on the original image and the positive areas counted or measured using Openlab's *Measurement* tools. *Boolean Operations ...* allow binary layers to be combined in useful ways - to highlight colocalisation for example. Openlab is able to look at the binary layer for all positive 'green' (e.g. Alexa 488 labelled antibody) staining areas AND all 'red' (e.g. Alexa 546 labelled antibody) staining areas.

The resulting combined binary layer shows only those pixels in the image containing green and red intensities above the positive threshold value that is, the areas corresponding to positive staining with both antibodies.

Importantly, images used for quantification were not digitally enhanced in any way. Pixel intensity values were left unaltered after image capture to avoid the introduction of artefact.

Cell counting with *Openlab*

Cultured cells were fixed and stained as detailed above. A 'tiled' image of an area of cells was then obtained using the confocal microscope. Areas of positive fluorescent staining or colocalisation could then be determined using density slicing in *Openlab*. Overlaying the binary map showing the cells of interest on the DIC image of all of the cells enabled counting using the *Measurements* facility in Openlab. Because of cell clumping, the DIC image alone was not always sufficient to provide an accurate denominator for cell counts. The addition of a channel showing staining of all nuclei (with TO-PRO-3) increased reliability of counts.

Quantification of epithelial surface area staining using *Openlab.*

Analysis of the proportion of the alveolar epithelium covered by cells of a particular phenotype cannot be done by global biochemical analysis of lung proteins. In order to make a quantitative assessment of alveolar epithelial composition, the epithelial cells must be typed, and then some form of measurement made. I chose to use length of alveolar epithelial surface visible in a section of lung as a representative measure of the alveolar epithelial area present. In particular, as a measure with which to compare control lungs and inflamed lungs. The total length of exposed alveolar epithelial surface was imaged using the tiled image capture technique detailed above. This surface was then traced using Openlab and a Wacom graphics tablet and pen (**figure 6A, C**). Density slicing to create binary layers demarcating the positively staining areas of epithelium allowed these also to be measured in the same way (**figure 6B, D**). The contribution to the alveolar epithelial cell surface made by cells of various immuno-phenotypes could be quantified as a percentage of the total exposed surface. This process was repeated for control lung sections, and sections from inflamed lungs.

Localisation of different proteins in the cytoplasm of epithelial cells and on the epithelial cell membrane surface was investigated using this technique.

Z-plane scanning and 3D reconstruction with *Volocity*

A particular advantage of the confocal laser scanning microscope (LSCM) is its ability to produce optical sections - each having a very small depth of field, with no contribution to the section from out of focus regions of the specimen above or below the plane of interest. This feature, coupled with the ability to scan below the surface of tissue specimens allows capture of a series of sections which may be arranged to form an image 'stack' viewable as a three dimensional image. I employed this range of techniques to investigate the 3D distribution of cell-selective proteins on the cells of the alveolar epithelium in control and inflamed lungs. Cells or tissue sections were fixed and stained in the usual way. Multi-track scanning was performed as before, but with the additional step of determining the positions of the top and bottom of the specimen by scanning at different focal planes (i.e. different z-positions). The specimen was then scanned at a series of different levels to create an image stack. The number of images in the stack, and vertical distance between sequential images (z-step) were adjusted to achieve an image of sufficient z-resolution to be useful, while avoiding destructive photobleaching of the specimen. As the laser scans the specimen, it is selectively bleached in the xy plane and non-selectively bleached in the z plane. As the specimen is scanned one plane at a time, not only is that plane bleached, but all other cross-sectional planes above and below are also bleached. There is of necessity a compromise between better z-plane resolution and 'total slice capacity' (or the fixed number of images that can be sampled from a specimen before the data becomes artefactual).

Deconvolution of image stacks using Huygens 2 (SVI) software

For three-dimensional viewing of alveolar wall membranes where resolution of the final image was critical, image stacks were acquired using Nyquist settings (the Nyquist criterion determines the minimal sample density needed to capture *all* information from the microscope into the image. When the sampling distance is larger than the Nyquist distance information about the image is lost). The raw data were deconvoluted using Huygens 2 (SVI) software and reconstructed and analyzed for co-localization using

Imaris 4.0 Software (Bitplane AG, Zurich)(Duncan, Greaves et al. 2003). Deconvolution involves the recovery of information about an object from an image that is degraded by blurring and noise. In LSCM the blurring is largely due to diffraction limited imaging by the instrument; the noise is usually photon noise. Deconvolution involves the application of An MLE (Maximum Likelihood Estimation) algorithm to the image stack dataset, which calculates the object distribution with the highest likelihood of having produced the output image, taking into account the nature of the noise and the imaging properties of the microscope.

Rat haemorrhagic Shock Model

The rat haemorrhagic shock model was developed jointly with Stuart McKechnie. Experiments were performed jointly, but subsequent biochemical analysis of broncho-alveolar lavage fluid was performed by Stuart McKechnie.

Animal preparation: Specific pathogen-free male Sprague-Dawley rats (250-300g, Harlan UK) were anaesthetised using intraperitoneal injection of midazolam (5mg/kg) and ketamine (75-100mg/kg) and placed supine on a temperature-regulated heating pad. After shaving, a transverse incision of the neck was made and the trachea, right common carotid artery and left jugular veins exposed by blunt dissection. The common carotid was clamped proximally and cannulated using PE50 tubing (Becton Dickinson) facilitating continuous measurement of arterial blood pressure using a modified *Propaq Encore* monitor (WelchAllyn, Bucks, UK), and arterial blood sampling. The left internal jugular vein was cannulated in a similar manner, but without proximal clamping, to allow central venous pressure monitoring (using the *Propaq* as above) and administration of drugs and fluids. Anaesthesia was maintained by an intravenous infusion of Propofol (0.5mg/kg/min) and muscle relaxation with pancuronium bromide (2mg/kg/h). Normal saline was administered intravenously such that intravenous fluids, including medications, totalled 1.5ml/h. A tracheostomy was performed and the trachea cannulated using an 18G monoject blunt needle (Harvard Apparatus), and rats ventilated using a volume-controlled ventilator (Small Animal Ventilator Model 683, Harvard Apparatus). A tidal volume of 6ml/kg, positive end expiratory pressure (PEEP) of 5cmH_20, inspired oxygen fraction (FiO_2) of 1.0 and a respiratory rate of 55-60 breaths/min were delivered and adjusted to maintain a pH of between 7.3 and 7.45.

Experimental Protocol (figure 8): After a 30 min stabilisation period, blood was removed from the carotid artery in 500μl aliquots, lowering the mean arterial pressure (MAP) to 30-40mmHg. This level of haemorrhagic shock was maintained for 30 min, followed by resuscitation over 15-30 minutes using warmed intravenous normal saline to restore the MAP to ≥80mmHg whilst maintaining a CVP of ≤10mmHg. The variation in MAP over the course of a typical experiment is shown in **figure 8 (B).** Animals were subsequently ventilated for an additional 4 hours and then exsanguinated. Blood was collected from the abdominal aorta and the lungs lavaged with 2x10mls of sterile endotoxin and Ca/Mg free PBS to obtain BAL fluid for analysis. Control animals underwent surgery without subsequent haemorrhage. Lavage fluid was analysed to determine total protein content, differential cell count, and MMC4 and RTI_{40} protein content. MMC4 and RTI_{40} proteins were quantified using an ELISA-based dot blot assay as previously described (McElroy, Pittet et al. 1995; Boylan, Pryde et al. 2001).

BAL protein content assay

Protein concentrations in aqueous solution were determined using the Bio-Rad, also known as Bradford (Bradford 1976), protein assay. This is a dye-binding assay based on the concentration-dependent shift of the absorbance maximum of an acidic solution of Coomassie Brilliant Blue G-250 from 465 nm to 595 nm upon binding protein. Protein concentrations were obtained from the linear range of a standard curve constructed by plotting absorbance against concentration (0-1.4 mg/ml) of bovine serum albumin. Absorbance of samples was read at 630 nm using a plate reader.

Results 1: Control lung alveolar epithelium

Introduction

Control lung sections were stained with a panel of antibodies in order to establish their specificity when used in combination to identify ATI and ATII cells **(table 4)**. The distribution of staining was examined in 2D and 3D using laser scanning microscopy, and the imaging technique developed to avoid confounding sampling artefact. Antibodies fell into two main groups: those which stained membrane associated proteins, and those having an affinity for cytoplasmic/secreted proteins:

The phenotype of the alveolar epithelium in control lungs defined using anti-RTI_{40}, MMC4, anti-$RTII_{70}$, anti-Pro-SP-C, and anti-SP-D antibodies

Membrane associated proteins: RTI_{40} is a membrane associated protein expressed on the apical surface of ATI cells (Dobbs, Williams et al. 1988). Examination of control rat lungs stained with **anti-RTI_{40}** showed that the majority of the epithelial surface area was comprised of RTI_{40} positive cells **(figure 8)**. **MMC4** is a monoclonal antibody (mab) which has been shown in the lung to stain only the apical membranes of ATII and Clara cells (Boylan, Pryde et al. 2001). **Anti-$RTII_{70}$** is also a ATII cell membrane specific mab (Dobbs, Pian et al. 1997). Control rat lungs displayed MMC4/$RTII_{70}$ positive cells at the corners of the alveolar air spaces, flanked by RTI_{40} positive cells **(figure 8C)**. Small airways that appeared in control lung sections featured epithelial cells with typical Clara morphology (cuboidal non-ciliated cells) that were also MMC4 positive at their apical surfaces but did not stain with $RTII_{70}$ **(figure 8D)**.

Secreted intracellular proteins: Surfactant protein C (SP-C) is a hydrophobic peptide that is specific to the lung (Beers, Wali et al. 1992). Production of SP-C occurs *exclusively* in ATII cells involving the proteolytic cleavage of a larger molecule pro-SP-C (p-SP-C) (Beers, Wali et al. 1992). Anti-pro-SP-C antibody is therefore a very useful ATII cell specific marker. I found that p-SPC was localised to the cytoplasm of cuboidal cells in a typical ATII position at the corners of the alveoli. **(figure 9)**. Cells staining with p-SP-C in the cytoplasm also stained positively for MMC4 at their apical membranes, and did not stain with RTI_{40}, confirming their ATII phenotype **(figure 9)**.

Similarly **surfactant protein D (SP-D)** is secreted by ATII cells, but in contrast to p-SP-C, is also produced by Clara (non-ciliated bronchiolar epithelial) cells (Wong, Akiyama et al. 1996). SP-D is not localised to lamellar bodies but is found in the endoplasmic reticulum of ATII cells, and in the secretory granules of Clara cells. Though it is highly expressed in conducting airways of rats SP-D is found sparsely in the conducting airways in humans (Mason, Greene et al. 1998). In the control sections examined SP-D was present in the cytoplasm of typical ATII cells **(figure 10)**, alveolar macrophages also appeared to have a low level of staining **(figure 10A white arrows)**. This is consistent with the finding that SP-D has a significant role to play in innate immunity in the lung, and has receptors on the surface of a variety of cell types including alveolar macrophages (Miyamura, Leigh et al. 1994; Holmskov, Lawson et al. 1997).

Three dimensional imaging of control lung tissue

Examination of control lung tissue using laser scanning confocal microscopy allowed optical slicing of tissue, and reconstruction of images in three dimensions using imaging software (Volocity 3.0, Improvision UK). This technique was useful in showing the non-uniform distribution of proteins in the cytoplasm and on cell membranes.

The problem of depth: Frozen tissue sections were variable in thickness, and range from around 3μm to 10μm. This size approaches the order of magnitude of the diameter of a ATII cell apical surface (around 7μm). It is possible for positively stained cells to be invisible to the LSCM if scanning is performed in only one z ('vertical') plane. This is illustrated in **(figure 11)**, where the alveolar epithelial surface has been sectioned *en face*. Here a ATII is visible staining characteristically with MMC4 and $RTII_{70}$ giving a pink circular appearance to the apical membrane, surrounded by green RTI_{40} staining ATI cells **(figure 11A)**. If the same section is scanned a few microns lower in the z-plane the ATII cell almost disappears, as the optical section is now cutting through the tissue below the level of the apical membrane staining

Image stacks as a solution to the problem of depth: (figure 11D) shows a 3D reconstruction of the field of view that has been rotated to give perspective. This 3D volume rendered image is derived from a stack of 60 optical sections, each aligned in the xy plane. Volume rendering is a technique whereby the object or phenomenon of

interest is sampled or subdivided into many cubic volume elements or voxels. A voxel is the 3-D counterpart of the 2-D pixel and is a measure of unit volume. Each voxel is assigned an intensity value and is represented by a unit cube. The 3-D voxel sets are assembled from multiple 2-D images (i.e. the LSCM image stack), and are displayed by projecting these images into 2-D pixel space - displayed on the 2-D computer screen. Volumes rendered in this manner have been likened to a translucent suspension of particles in 3-D space. The 3-D reconstruction can be interrogated to show the appearance of an object from different perspectives, or 'cut' in any plane to show the internal structure of an object. This is illustrated in **(figure 12)** where the 3-D image is shown as if seen from different points of view, providing useful information about the spatial relationship of the cells in the tissue section.

More accurate quantification of sections: The LSCM scans a thin optical section in a plane perpendicular to the optical axis of the microscope. The stage is carefully balanced with a spirit level prior to each session so that the microscope slide is parallel to the plane of optical sectioning. Because the tissue sections to be examined are seldom absolutely flat, however, the specimen on the slide will often be partially out of focus during scanning - particularly when capturing lower magnification images (x20 objective or less) or tiled images covering large physical areas (often almost $2mm^2$). **(Figure 13)** shows the consequences of scanning an object with an (exaggerated) uneven surface with a thin focal plane, The schematic **(figure 13D)** illustrates that because of the confocal nature of the image, only the portion of the image to the left of the field of view is in focus (and therefore brighter) when scanning at plane z_1, whereas the right of the field is best seen at z_2. Combining images taken at both planes includes all of the information on the section. **(Figure 13A, B)** show a section of control lung scanned with a x20 objective. Five optical slices were taken through the slide - the tissue section is approx 9.6μm thick. The green and red channels (RTI_{40} and MMC_4 staining respectively) illustrate the point above. Combining all layers in image C allows all of the cells present to be seen. This type of approach was employed in obtaining images of frozen lung sections or cells for quantification. It is critically important in order to avoid loss of data from tissue analysis that images at different z-planes through the specimen are obtained for each field of view. Images can then be combined (by linear averaging), or a fully representative image selected if one exists, for use in

analysis.

3D distribution of antibodies in control lung:

Tissue block staining in 3D: In view of the difficulties experienced in obtaining good frozen sections of control lung tissue I decided to investigate whether the distribution of the antibodies used was the same in paraformaldehyde fixed lung that had not been infiltrated with OCT or cut using the cryostat. Lung tissue was obtained from adult rats, fixed using paraformaldehyde and cut into 5mm cubes in the usual way. Cubes could then be stained using minor modifications to the standard immunohistochemistry protocol. Tissue was fixed to the bottom of a small petri dish using cyanoacrylate adhesive (Super Glue, Loctite UK) and immersed in PBS. The specimen was then imaged using a Zeiss LSM 510 scanning head fitted to an upright Axioplan research microscope. A x40 water 'dipping' objective was then used to image the tissue block as deeply as possible under the surface of the specimen, creating an image stack for 3D reconstruction. **(Figure 3)** shows two different views of the same piece of tissue 146μm x146μm in cross-section by 165.8μm deep. This sample of control lung has been stained with anti-RTI_{40} (green), MMC4 (red) and anti-$RTII_{70}$ (blue). Image quality is limited by antibody penetration into the tissue as well as LSCM capture and bleaching. It is clear that the relationships between the apical membranes of ATII cells (pink), surrounded by ATI cells (green) seen in tissue sections is maintained when imaging an intact cube of tissue without frozen sectioning.

Immunophenotyping – staining controls

Auto-fluorescence

Although previous authors have described the lung as prone to auto-fluorescence under examination with the fluorescence microscope (and recommend various measures to overcome this) I found that fixation using the methods employed here resulted in no significant signal when fixed, unstained tissue was viewed using the methods detailed above.

Secondary only negative controls

The presence of well-demarcated areas of staining using the antibody combinations

employed here suggests low levels of 'background' staining. This was confirmed by incubating control and injured tissue with secondary antibody in the absence of a primary. Staining and imaging using the methods detailed above did not result in any significant secondary only signal.

Isotype-specific negative controls

To further ensure that the primary antibody staining demonstrated here was biologically significant, and not non-specific binding, further control staining of control and injured lung was performed using unrelated primary antibodies (having the same isotypes as the primaries in our panel) and the same secondary antibodies (with appropriate isotype specificity) used in the experimental work detailed here **(table 7).** Isotype-specific control antibodies were obtained from Stratech Scientific Ltd. and are purpose made negative controls raised against haptens not normally present in human or animal tissue. Both normal lung tissue, and injured lung sections showing significant inflammatory infiltrate were stained and imaged using the LSCM (following the same protocol as the other experimental work detailed here). Again, no staining was visible either in control lungs or injured lungs with inflammatory infiltrate.

Table 7. Isotype specific primary antibody negative controls

Negative control isotype	Clone	Ref. number
mouse IgG1	NCG01	NC-748
mouse IgG2a	NCG2A.01	NC-1390
mouse IgG2b	NCG2b.01	NC-1391
mouse IgG3	NCG3.01	NC-1357

Results 2: Repairing lung alveolar epithelium

Introduction

Having characterised the normal rat lung alveolar epithelium the next step was to investigate the composition of the epithelium during recovery from an acute injury. A rat model of *S. aureus* induced acute lung injury was used, and compared to a similar model using *S. pneumoniae*. Analysis of the composition of the recovering alveolar epithelium determined by immunohistochemistry was compared to ultrastructural imaging by electron microscopy.

The phenotype of the alveolar epithelium following *S. aureus*-induced lung injury

Instillation of *S. aureus* suspension into the distal airways of the lung causes inflammation and consolidation in the alveolar airspaces. This injury induces a localised inflammatory reaction that is resolving by 3 days. Lungs examined macroscopically at this time point exhibit areas of darker tissue - visible to the naked eye - that correspond to the inflamed regions, (McElroy, Cain et al. 2002). Other parts of the lung appear normal (referred to here as non-inflamed regions). Examination of the morphology of these inflamed regions (by light microscopy on frozen lung sections, or haematoxylin and eosin stained paraffin-fixed sections) reveals three morphologically distinct sub regions of lung tissue: **(figure 14)**. These sub regions exhibited (i) thickened alveolar walls with some inflammatory cells in the airspaces (ii) consolidated regions in which the small airspaces are filled with cells and debris - here the alveolar wall is not distinct from the airspaces or the inflammatory cell influx (iii) regions which are morphologically indistinguishable from control lungs. The panel of antibodies reacted with the alveolar epithelium lining thickened alveolar walls and control-like alveolar walls but not cells in with the consolidated regions.

Alveolar walls in the inflamed regions were lined by RTI_{40}-positive cells (ATI cells) and MMC4/$RTII_{70}$-positive cells (ATII cells) **(figure 15A).** However, the surface area of the alveolar walls covered by MMC4/$RTII_{70}$-positive cells (ATII cells) was increased by over 5-fold in *S. aureus*-injured lungs in comparison with controls **(figure 16B).** In

contrast, the surface area of the alveolar walls covered by RTI_{40}-positive cells (ATI cells) in *S. aureus*-injured lungs was significantly decreased in comparison with control lungs (**figure 16A**). The expression of pro-SP-C and SP-D in MMC4/$RTII_{70}$-positive cells was not uniform. Some groups of MMC4/$RTII_{70}$-positive cells were positive for pro-SP-C and SP-D while other groups of MMC4/$RTII_{70}$-positive appeared to be either negative or express very low levels of pro-SP-C and SP-D **(figure 17)**

In areas of the alveolar epithelium associated with increased numbers of ATII cells I also observed alveolar membranes that co-expressed a unique combination of markers, RTI_{40} and MMC4 **(figure 15A, D)**. Furthermore, three-dimensional analysis of RTI_{40}/MMC4-coexpressing membranes using confocal laser scanning microscopy confirmed co-localization of these markers on the same membrane **(figure 18).** Deconvolution of high magnification images of the epithelial surface in inflamed regions of the lung confirms that in areas of RTI_{40}/MMC4-coexpression, the proteins colocalise at the limits of resolution of the LSCM system i.e. around 0.5μm. **(figure 20)**. Quantitative analysis using Openlab demonstrated that RTI_{40}/MMC4-positive membranes in *S. aureus*-injured lungs accounted for approximately 3% of the alveolar surface in the macroscopically injured region **(figure 16, figure 6).** Approximately one third of RTI_{40}/MMC4-positive membranes also expressed $RTII_{70}$ **(figure 19)**. RTI_{40}/MMC4-positive cells either did not express pro-SP-C, or expressed pro-SP-C at much lower levels, in comparison with $RTII_{70}$/MMC4-positive cells (ATII cells) **(figure 17A)**. The small area of RTI_{40}/MMC4-coexpressing epithelium in control lungs was limited to areas where ATI cells (RTI_{40}-positive) and the apical membrane of ATII cells (MMC4/$RTII_{70}$-positive) were adjacent. These areas are likely to represent the interface of separate red and green staining membranes within the same voxel (the voxel or "volume element" is the 3D conceptual counterpart of the 2D pixel - the smallest non-divisible element in a 3D digital image) rather than true co-expression of proteins on the same membrane **(figure 20, figure 18)**. Quantification of the lengths of continuous RTI_{40}/MMC4 positive membrane gave further evidence that the areas of apparent RTI_{40}/MMC4 colocalisation in control lungs are unlikely to represent intermediate phenotype cells co-expressing these membrane antigens. Measurement of the apical membrane length of ATII cells in control rat lungs in our model gives a mean value of 7μm (1.54-22.8μm), which is in keeping with other investigators' findings (e.g. Hais et

al. measured a mean ATII cell luminal surface area of 62μm per cell - excluding microvilli - which gives a mean cell luminal surface diameter of ~8.9μm if the surface is assumed to be roughly circular (Haies, Gil et al. 1981). (**figure 16**) shows a frequency histogram of the individual lengths of RTI_{40}/MMC4 positive membrane measured in control *vs.* inflamed lungs. In control lungs the majority of RTI_{40}/MMC4 positive segments were tiny, measuring much less than half of the typical diameter of the ATII cell apical membrane (94% of segments were less than 3μm in length). In inflamed lungs, however, these intermediate phenotype segments of membrane were almost all greater than 5μm. This is consistent with the idea that in control lungs apparent RTI_{40}/MMC4 staining represents the limits of the imaging system to resolve adjacent structures rather than intermediate phenotype cells. In inflamed lungs, however, the pattern suggests multiple adjacent cuboidal cells (or fewer numbers of larger flattened cells) expressing RTI_{40}/MMC4 antigens on their surface membranes.

Performing a similar examination of the lengths of epithelial cell membrane with a typical ATII cell phenotype (i.e. $RTII_{70}$/MMC4) in control and inflamed lungs gave expected results. As would be predicted, the bulk of the segments of control epithelium with ATII phenotype were around 7-14μm in length **(figure 21A)**. A number of segments were smaller than a single cell (though less than 1% were shorter than 3μm), reflecting the common situation where the tissue section has cut through the roughly circular apical membrane of the cell along a chord rather than a full diameter. In inflamed lungs, the mean MMC4 segment is ~15μm in length (0.6-84.3μm) with long continuous stretches of ATII phenotype cells **(figure 21B)**. These findings are consistent with the widely reported phenomenon of ATII-cell 'hyperplasia' after alveolar epithelial injury (Adamson and Bowden 1974; Evans, Cabral et al. 1975).

The phenotype of the alveolar epithelium following *S. pneumoniae*-induced lung injury

Using a protocol similar to the *S. aureus* pneumonia model, *S. pneumoniae* was used to cause an injury to the rat lung alveolar epithelium. At 24 hours after bacterial instillation, inflammation and repair were evident in the lungs. Sections were stained using the same panel of antibodies as previously and examined using the LSCM. A significant inflammatory infiltrate was evident in many alveolar airspaces **(figure 22A)**.

Most of the alveolar epithelium was covered by RTI_{40} positive ATI cells, with MMC4 positive ATII cells also visible (NB inflammatory cells in the airspaces are also stained red with MMC4). A population of RTI_{40}/MMC4 positive intermediate phenotype alveolar epithelial cells was also visible.

Ultrastructure of the alveolar epithelium in inflamed lungs

Electron microscopy of lung tissue from control animals showed normal lung ultrastructure **(figure 23)**. Long thin attenuated ATI cells form the majority (~95%) of the surface area. These cells characteristically showing a paucity of organelles with only the prominent nuclei evident **(figure 23B)**. Cuboidal ATII cells were positioned in the corners of the alveoli, flanked by ATI. The *sine qua non* of ATII cells is presence of surfactant containing lamellar bodies that resemble the layers of an onion in cross-section **(figure 23A, D)**. In contrast with control lungs the alveolar walls of inflamed lungs 3 days after *S. aureus*-injury, were covered by mostly cuboidal epithelial cells in **(figure 24)**. Some epithelial cells had more typical ATII cell features (lamellar bodies, apical microvilli) but appeared to be spreading, and had reduced perinuclear cytoplasm **(figure 24A)**. Other cuboidal epithelial cells lacked both microvilli and lamellar bodies **(figure 24 B)**.

In some places ATI cells (or ATI-like cells) were observed overlying ATII cells. Where this occurred, high magnification views of the ATII cell apical surface showed a double membrane **(figure 24C)**.

Some ATI cells also had an occasional microvillus. These ultrastructural studies demonstrated that the alveolar wall in inflamed regions from *S. aureus*-treated lungs was thickened secondary to a relative increase in the numbers of ATII-like cells. Inflamed regions also and contained a population of epithelial cells not found in control lungs with features consistent with an 'intermediate' phenotype.

Results 3: Alveolar epithelial cells in vitro and in development

Introduction

The changes in phenotype of freshly isolated ATII cells with time in a standard submerged cell culture environment were examined. The progression from a ATII phenotype to a ATI-like phenotype in culture was characterised using the same immunophenotyping techniques employed in both the control and injury/repair models above. Alveolar epithelium from rat lungs at various stages of development were also imaged. I sought to determine whether a subset of alveolar epithelial cells displaying the same combination of both ATII and ATI markers seen in repair would be detectable in culture and/or during alveolar development.

Analysis of freshly isolated type II cells - modified Papanicolau staining

Immediately after isolation cells were cytospin and allowed to air dry. Subsequent staining allowed quantification of the proportion of ATII cells isolated, and the numbers of contaminating cells of other lineages. Characterisation was performed initially by modified Papanicolau (Pap) staining of the cytospin cells (**figure 25A**). Cells were counted at high magnification using a x100 oil immersion objective. Cells containing ≥ 4 dark staining inclusion bodies (lamellar bodies) were counted as being ATII cells (Dobbs 1990), other cell types were identified by characteristic morphological features. This method gave a figure of 66% ATII with approximate proportions of contaminants as shown (**figure 25B**). Cell types were identified by light microscopy. A 'running mean' was used to estimate the total number of cells needed to count in order to reach a stable figure for the proportion of ATII cells.

Phenotype of Cultured Alveolar Epithelial Type II cells

Freshly isolated ATII cells co-expressed ATII cell markers, $RTII_{70}$ and MMC4 but not RTI_{40}. By day 5 in culture, all the cells expressed RTI_{40} but not $RTII_{70}$ or MMC4. This change in expression of cell type specific protein expression was also accompanied by a change in morphology as cells flattened, spread, and became confluent (**figure 26, figure 27**). On Day 1 many flattened, spreading cells were weakly positive for RTI_{40} with a sub-population of cells (5.9 % ± 1.4 %, n =3) strongly positive for both RTI_{40} and

MMC4 (**figure 28**). I did not detect $RTII_{70}$ at Day 1 of culture. These data suggest that the kinetics of cells with the RTI_{40}/MMC4-phenotype are consistent with their role as transition cells (*i.e.* not present in isolated ATII cells or when the cells are ATI-like and express RTI_{40}). 3D visualisation of RTI_{40}/MMC4 positive cells revealed that these cells had begun to spread and take on a more flattened shape than the MMC4 expressing ATII (**figure 29**). RTI_{40} signal appeared to be localised to the spreading edge of the cells (**figure 30**).

The alveolar epithelium in development

Developing rat lungs were stained with MMC4 and RTI_{40} to see if MMC4/RTI_{40} positive cells could be detected in the alveolar epithelium. At day 16 (E16) the size of the embryo enabled visualisation of an entire saggital section **(figure 31).** No MMC4 staining was seen at this time point, and no RTI_{40} staining was visible in the lung. The choroid plexus and parts of the central nervous system did stain positively for RTI_{40} as previously described (Williams, Cao et al. 1996) **(figure 31A, B).** At E17 the embryonic lung was dissected out and visualised in section, some tubules were lined by cuboidal cells with RTI40 positive apices, but no significant MMC4 staining was present **(figure 32).** The embryonic lung was beginning to look much more adult by E20 **(figure 33).** RTI_{40} lined 'airspaces' were obvious, with ATII cells staining with both MMC4 and RTI_{40}. Alveolar septae were still very thickened and cellular, with ATII cells grouped in clusters rather than occurring singly as in the mature lung. Non-ciliated cells in the terminal bronchioles could also be identified by MMC4 apical staining (Boylan, Pryde et al. 2001). Lungs from pups at post-natal day 3 (PN3) provided the first evidence of MMC4/RTI_{40} positive cells **(figure 34).** Cells with an intermediate phenotype were visible in the epithelium of the terminal bronchioles, flanked by non-ciliated MMC4 positive cells, occasional cells at the broncho-alveolar junction were $RTII_{70}$ positive in addition to MMC4/RTI_{40} **(figure 34).** The alveoli were lined by RTI_{40} positive ATI cells and MMC4/$RTII_{70}$ positive ATII cells but did not show any intermediate MMC4/RTI_{40} positive cells. Lungs were also surveyed on post-natal days 4 and 5 **(figure 35).** The process of alveolar remodelling continued at these time points, with thinning of the alveolar walls. Despite the appearance of expansion of the alveolar epithelium no MMC4/RTI_{40} positive cells were seen in the alveoli. MMC4/$RTII_{70}$ expressing ATII

cells became more scattered and widely spaced with 3D visualisation showing them protruding markedly into the alveolar airspace - a feature that is less pronounced as the lung matures.

Results 4: Haemorrhagic Shock - a model of indirect acute lung injury

Introduction

Having examined the repairing alveolar epithelium in a model of direct acute lung injury (i.e. bacterial instillation), we developed a model of indirect lung injury with a view to comparing the process of repair after direct versus indirect epithelial insult. The degree of alveolar epithelial injury induced by profound hypotension for 30 minutes followed by positive pressure ventilation for 4 hours was assessed by examining BAL fluid for evidence of lung leak (total protein content), and epithelial cell specific protein markers. These measures have previously been found to correlate with histological measures of epithelial damage in a model of direct lung injury (McElroy, Pittet et al. 1995). A differential cell count was also performed on BAL fluid to quantify the inflammatory response to injury in the lung. The use of epithelial cell type specific markers to assess the severity of alveolar injury offered the advantage of further indicating the degree to which particular epithelial cell populations had been affected (McElroy and Kasper 2004). Although the duration of our protocol was too short to expect detectable epithelial repair, it represents the first step in the process of developing a recovery/repair model.

Alveolar epithelial injury after profound hypotension followed by fluid resuscitation and positive pressure ventilation

Animals were anaesthetised and surgery performed as detailed above (**figure 8**). Blood loss during surgery was minimised, and animals found to have significant acid-base disturbance on ABG sampling at the end of the stabilisation period were excluded from further study. Examination of the BAL fluid of 3 haemorrhaged animals compared to 3 controls (surgery but no haemorrhage) revealed significant differences in measures of pulmonary inflammation, alveolar air-blood barrier integrity and alveolar epithelial cell injury (**figure 8**). Cell counts showed a similar total number of cells in the lavage fluid from haemorrhaged and control animals (86.2 *vs* 97.3 $x10^4$cells/ml respectively) (**figure 38B**). Differential counts, however revealed a significantly larger proportion of neutrophils in the BAL from haemorrhaged animals (12.7% *vs* <1%, $p<0.05$), with no significant difference in the proportion of macrophages or 'other' cell types between the

two groups. Quantification of epithelial cell type-specific integral membrane proteins in BAL fluid showed significantly more RTI_{40} protein after haemorrhage (14.6 RDU *vs* 108.0 RDU, $p<0.05$), and an increase in MMC4 protein compared to controls though this did not reach statistical significance (63.3 RDU *vs* 124.7 RDU, $p=0.16$) **(figure 38C and D)**. The presence of alveolar epithelial injury in the haemorrhaged animals was also confirmed by the retrieval of significantly more protein in the BAL fluid of these animals (13.1 mg *vs* 2.7 mg, $p<0.05$) **(figure 38A)**.

Discussion

Overview

This study has successfully used an immunotargeting approach to obtaining information about the phenotypes of lung alveolar epithelial cells in primary cell culture, after injury and in development.

In order to gather information about local repair processes at the alveolar epithelium it is not possible to rely on 'global' measures of tissue biochemistry. Using Laser Scanning Confocal Microscopy I have developed a system to extract quantitative data about epithelial cell populations as well as qualitative information about antigen expression on novel intermediate cell phenotypes.

After evaluating the available methodologies, a robust and reproducible primary rat ATII cell culture system was implemented, allowing investigation of cultured ATII cells under controlled conditions. Immortalised transformed cell-lines were unlikely to be adequate for this task given that the *in vitro* biological feature of interest is the transformation in phenotype of ATII cells in culture.

In order to translate between the *in vitro* and *in vivo* settings this study employed a clinically authentic disease model of bacterial pneumonia and has attempted to generalise the cell culture and animal model findings by examining the lung alveolar epithelium in development, seeking common features.

Imaging the lung alveolar epithelium.

Determining cell phenotype: Investigation of alveolar epithelial cell phenotype after *S. aureus* induced lung injury presents particular problems. By 3 days after bacterial instillation injured lungs are inflamed, the alveolar septae thickened and cellular. The air spaces themselves become filled with inflammatory cells, oedema fluid and other debris. Light microscopy allows a useful survey of the gross histology of the lung parenchyma, but provides too little information to be relied upon to discriminate between cell types **(figure 14)**. Electron microscopy is information rich, but will only provide morphological data about a very small sample of tissue, with no straightforward additional means of characterising cells **(figure 24)**. Immunohistochemistry provides a

useful tool for phenotyping cells - providing that antibodies to appropriate cell-specific markers are available (Funkhouser and Peterson 1989). In this study I have employed a novel combination of antibodies to proteins specific to ATI and ATII cells in the alveolar epithelium **(table 4)**. MMC4 (anti-aminopeptidase-N) and anti-$RTII_{70}$ are both monoclonal antibodies that are, in the context of the rat lung alveolus, specific to ATII cell membrane proteins (ref Boylan 2001, Dobbs, Pian 1997). The monoclonal antibody anti-RTI_{40} is also specific to the apical cell membrane, though only in ATI cells. This cell membrane specificity is particularly useful after injury, where antibodies to other ATII cell specific proteins that are not membrane associated can be much less informative for the following reasons:

1. **Loss of specificity after injury:** Antibodies against ATII cell specific proteins SP-D and pro-SP-C were also used in this study to phenotype lung epithelial cells. In control lungs, staining was neatly confined to the cytoplasm of ATII cells as expected, and provided corroboration of the specificity of the other ATII cell antibodies **(figure 9, figure 9)**. After injury, however, the picture was much less clear. The lung parenchymal changes after injury and during repair remove a lot of the morphological cues for the identification of cells. ATII cells are no longer confined to the 'corners' of the alveoli flanked by ATI, and alveolar septae no longer consist of only the attenuated cytoplasmic processes of ATI cells. The thickened, cellular alveolar walls in the repairing lung stain much less crisply for cytoplasmic markers, with more 'background' staining, and some weak staining of inflammatory cells with anti-pro-SPC and anti-SPD **(figure 17)**. There are a number of possible reasons for this apparent loss of specificity; inflammatory cells may express surfactant proteins when activated - SP-D is known to be an opsonin and may be present on the surfaces of alveolar macrophages in areas of inflammation. Increased surfactant secretion or loss of surfactant from damaged ATII cells may contribute to the smearing of the pro-SP-C and SP-D signals after injury. In contrast to the situation with cytoplasmic markers, the antibodies to membrane associated proteins continued to provide useful information about the phenotype of cells at the alveolar epithelial surface after injury - though also appeared to stain some inflammatory cells in the alveolar airspaces **(figure 17, figure 15, figure 18)**.

2. **Sectioning artifact:** Cytoplasmic stains are much more vulnerable to the problems of sectioning - whether the physical sectioning of tissue using a cryostat or optical sectioning with the LSCM - because the cytoplasm is not stained uniformly, a positively stained cell can appear negative if cut and imaged through an area containing no antigen. Membrane staining is affected by this problem to a much lesser extent **(figure 4)**.

3. **Colocalisation difficulties:** Determining whether an area of cytoplasmic staining and apparently corresponding section of stained epithelial membrane belong to the same cell is relatively straightforward in control lung alveolar epithelium, but much less reliable in the injured and inflamed lung **(figure 9, figure 10 compared with figure 17). (Figure 24)** shows that after *S. aureus* injury ATI cells may overlie cuboidal cells. Given both the thinness of the ATI cell cytoplasm (approximately 0.2μm) and the tendency of ATI cells overlay ATII cells in repairing lungs (Faulkner and Esterly 1971; Greenberg, Gyorkey et al. 1971; Evans, Stephens et al. 1972) it is unlikely that the co-expression of cell-type specific membrane and cytoplasmic markers will discriminate between co-expression and overlay.

The combination of ATI cell specific marker anti-RTI_{40} and the ATII cell specific markers MMC4 and anti-$RTII_{70}$ were the most useful for examining alveolar epithelium in both control and injured lungs. This group of membrane staining antibodies then defined the scope of the other markers available: MMC4 will only stain frozen lung sections fixed in paraformaldehyde. Other epithelial cell markers I attempted to add to the panel of antibodies (e.g. anti-Aquaporin-5 and surfactant protein A) would not stain tissue or cells fixed with paraformaldehyde, and could not therefore be used to investigate colocalisation with MMC4.

Demonstration of staining pattern in control lungs

Imaging control lungs stained with the panel of antibodies described above showed the expected colocalisation of ATII cell markers MMC4, $RTII_{70}$, pro-SP-C and SPD to ATII cells, and RTI_{40} to the apical membrane of ATI cells **(figure 8, figure 10, figure 9, figure 37)**. Imaging control lung in 3D also demonstrated the structure of the alveolar surface in a manner consistent with other published findings using from scanning

electron microscopy **(figure 3)**, (Fehrenbach 2001).

Quantification of epithelial staining

In order to allow quantitative as well as qualitative assessment of the alveolar epithelium I developed a method of imaging large areas of frozen tissue sections, or cells growing in primary cell culture, using immunofluorescence and LSCM, and then analysing the images obtained. Images were captured and the areas of positive staining measured as described in *Methods*. The simplicity of the path-tracing technique employed allows a simple comparison of the areas covered by cells of a given phenotype in different lung tissue sections. Comparing the figures obtained for the relative alveolar epithelial surface area covered by ATI and ATII cells in control tissue with those obtained from conventional morphometric analysis of the lung parenchyma gives good agreement. Haies et al. (Haies, Gil et al. 1981) found that ATI cells occupied 97.5% of the alveolar surface leaving 2.5% for ATII cells, a surface area ratio of 39:1. Analysis of the relative areas occupied by ATII and ATI cell luminal surfaces using the imaging system employed in this study gives a ratio of 40:1. The literature describing methods of extracting more complex morphometric information from 2D images (usually electron micrographs) is substantial (reviewed in (Cruz-Orive and Weibel 1990)). In this study my aim was not to quantify the numbers or surface area of a particular cell type in the whole lung, or even the entire inflamed portion of the injured lung. Rather, quantification was used to compare the composition of the largely homogeneous control lung alveolar epithelium with the repair process in small local areas of epithelium after a very patchy lung injury. Given the strengths of our approach, however, it would be straightforward to employ the same imaging and measuring techniques, coupled with an appropriate sampling methodology, as the basis for more complex morphometric studies of the lung.

Demonstration of lung inflammation and injury caused by *S. aureus* and *S. pneumoniae*

S. aureus instillation into the distal airways induces a localized inflammatory reaction that is resolving by 72 hours (McElroy, Cain et al. 2002). We analyzed the alveolar epithelium in the inflamed region using membrane protein markers of ATII and ATI

phenotype, combined with LSCM and image analysis (Dobbs, Williams et al. 1988; Dobbs, Pian et al. 1997; Boylan, Pryde et al. 2001). The data presented here indicate that *S. aureus*-inoculation leads to a focal increase in the numbers of ATII cells and a corresponding decrease in the surface area covered by ATI cells in comparison with control lungs. Ultrastructural studies confirmed the decrease in ATI cell numbers, or surface area, in inflamed regions of *S. aureus*-injured lungs **(figure 24).** However, the increase in ATII cell numbers (as indicated by ATII cell membrane-protein staining) was not reflected in the biochemical analysis of inflamed lung for surfactant proteins (see below).

In alveolar regions associated with increased area covered by ATII cells, I detected alveolar epithelial membranes in which the ATI and ATII cell proteins were co-expressed in unique combinations. The most abundant mixed phenotype were membranes that co-expressed RTI_{40} and MMC4. Moreover, RTI_{40}/MMC4-positive cells appeared to define a group of cells that were not uniformly positive for other ATII cell markers (*i.e.* pro-SP-C or $RTII_{70}$). Ultrastructural studies in other models of lung injury demonstrate that intermediate cell types are a heterogeneous group with variable ATII- or ATI-like characteristics (Adamson and Bowden 1974; Evans, Cabral et al. 1975; Hirai, Yamauchi et al. 1983). It is possible that RTI_{40}/MMC4-positive cells are the phenotypic equivalent, or some subset, of these ultrastructural intermediate cells. RTI_{40}/MMC4-positive cells that also express $RTII_{70}$ or pro-SP-C may represent early intermediates. Imaging the alveolar epithelium 24 hours after *S. pneumoniae* instillation using the same antibodies to cell type specific membrane proteins showed an inflammatory infiltrate in the air spaces, and similar population of RTI_{40}/MMC4 positive cells **(figure 22)**. The appearance of RTI_{40}/MMC4 positive intermediate phenotype cells is not a phenomenon specific to *S. aureus* induced lung injury.

Lung tissue biochemistry

Because the injury caused by the *S. aureus* model of bacterial pneumonia used in this study appears macroscopically well circumscribed, it has been possible to examine the concentrations of ATI and ATII cell proteins in macroscopically inflamed and macroscopically normal regions of the lungs of treated animals. These measurements have also been compared to control lungs. Biochemical analysis of the rat lungs used in

this study was carried out in collaboration with Christine Tyrrell using standard methodology (Clegg, Tyrrell et al. 2005)

Macroscopically damaged lobes (greyish areas) were homogenized separately from the macroscopically normal lobes (pink areas). Control lungs were normal in appearance and homogenized whole. The protein concentration of homogenized lungs was determined using a Bio-Rad Protein assay.

MMC4 and RTI_{40} proteins were quantified using an ELISA-based dot blot assay as previously described (McElroy, Pittet et al. 1995; Boylan, Pryde et al. 2001).

Western Blot Analysis - Monoclonal antibodies were detected using an anti-mouse IgG horseradish peroxoxdiase (Rockland Immunochemicals Inc., PA, USA). Polyclonal antibodies anti-aquaporin 5 (Chemicon International), anti-pro-SP-C (Beers, Kim et al. 1994) and anti-SP-D (Cao, Tao et al. 2004) were detected with anti-rabbit IgG horseradish peroxidase (Rockland Immunochemicals Inc.). The optical density of Western blot bands was determined in the usual way using a gel documentation and analysis system.

Biochemistry - ATI cell markers:

The concentration of RTI_{40} was decreased by over 18-fold in the inflamed region of *S. aureus*-inoculated lungs in comparison with control lungs as assessed in an ELISA-based dot-blot and by Western blot analysis (**figure 38A**). Similarly, the concentration of aquaporin 5, expressed by ATI cells and non-ciliated bronchiolar epithelial cells (Nielsen, King et al. 1997), was decreased by 5-fold in *S. aureus*-inoculated lungs (inflamed region) in comparison with control lungs (**figure 38A**). However, RTI_{40} was not significantly different from control values, while aquaporin 5 was upregulated, in lung tissue from the macroscopically normal regions from *S. aureus*-treated rats. In combination with the morphologic data, these biochemical data suggest that the reduction in ATI cell numbers or surface area is restricted to the macroscopically inflamed regions of *S. aureus*-treated lungs.

Biochemistry - ATII cell markers

In macroscopically inflamed regions from *S. aureus*-treated rats, only the concentration of MMC4 was selectively increased in the lung homogenates (**figure 38B**) though this

result must be interpreted cautiously in the light of the staining of inflammatory cells with MMC4 observable with LSCM (**figure 15, figure 17**). The concentration of SP-D was significantly elevated, in comparison to control values, in both the inflamed and non-inflamed lung homogenates in *S. aureus*-treated lungs while the concentration of pro-SP-C was not significantly different in the three groups. Therefore the increased ATII cell numbers, as indicated by an increase in the surface area of $RTII_{70}$/MMC4-positive cells seen by immunofluorescence, was not specifically reflected in an increase in surfactant protein concentration.

Overall, the biochemistry results are broadly consistent with the picture seen using microscopy, but appear to give a much less detailed view. Possible reasons why biochemical analysis does not specifically reflect the increase in ATII phenotype seen at microscopy include:

1. **Reduced surfactant synthesis:** Cells with a ATII cell phenotype (as defined using membrane associated markers MMC4 and RTII70) may have a reduced surfactant synthesising capacity during a hyperplastic response to lung injury, and not be represented in surfactant protein assays. This loss of surfactant production could reflect an early stage in the process of transformation to a ATI phenotype. (Fehrenbach, Kasper et al. 1999; Yano, Mason et al. 2000).
2. **Tissue biochemistry not a sensitive enough tool:** Even within a lobe of the lung that is macroscopically inflamed, there is a huge variation in morphology at the alveolar level (**figure 14**) that is simply 'averaged out' by biochemical analysis. Examining the concentration of cell specific markers in homogenised tissue can be likened to holding a microphone above a football stadium to hear what the fans' are saying. It is not difficult to tell when a goal has been scored, but the technique loses its usefulness when trying to ascertain information about an individual supporter.

Primary ATII cell culture - in vitro corroboration of the *in vivo* findings

Isolation of ATII cells: In 1974 Kikkawa and Yoneda published a method for the isolation of ATII cells, to facilitate the investigation of surfactant biochemistry. Since then it has become possible to isolate ATII cells from a variety of species to facilitate

the investigation of epithelial cell biology (reviewed in (Dobbs 1990)) (Kikkawa and Smith 1983; Richards, Davies et al. 1987; Murphy, Dinsdale et al. 1999). Methods of ATII cell isolation can be placed into two broad categories, defined by the technique used to separate ATII cells from the initial cell suspension obtained by mechanical disruption and enzymatic digestion of the lung parenchyma.

I initially used the *discontinuous density gradient* technique described by Richards et al (Richards, Davies et al. 1987). The lung vasculature is first perfused to remove blood, this is then followed by repeated broncho-alveolar lavage to wash out alveolar macrophages. The lungs are then digested using proteolytic enzymes to free ATII cells. The technique described by Richards uses trypsin to achieve this, which was added to minced lung tissue. DNAase is also added to reduce cell clumping. In order to separate ATII cells from other contaminating lung cells the principle of *differential sedimentation* was used by centrifuging the filtered crude cell suspension in a tube containing a discontinuous Percoll gradient. The sedimentation velocity of a cell is proportional to its density and the square of the cell diameter (Boone, Harell et al. 1968), which causes cells of similar size and density to accumulate in a band at the same level within the centrifugation tube. The fundamental problem with this method is that ATII cells overlap with other lung cell types in size and shape. In order to obtain a relatively pure sample of ATII cells it is therefore necessary to reject a significant proportion of the ATII yield along with contaminant cells. The resulting subset of ATII cells may be less than 10% of the total number in the lungs and therefore may not be representative of the rest of the ATII population (Dobbs 1990).

Because of the problem of obtaining large enough numbers of sufficiently pure ATII cells I abandoned this differential sedimentation approach in favour of the *differential adherence* based method favoured by Dobbs (Dobbs 1990) (see *Materials and Methods* section above). Dobbs' method is very similar to Richards' in the initial stages, though enzyme digestion is accomplished by instilling intra-tracheal elastase rather than adding trypsin to minced tissue. The crude cell suspension obtained contains mainly macrophages and leukocytes as contaminants, which are removed by 'panning' the mixture over culture plates coated with non-specific rat Immunoglobulin G (IgG). By binding to the IgG via the leukocyte common antigen or to Fc receptors, the majority of macrophages and leukocytes can be removed leaving ATII cells in suspension. This

method improved the yield and purity of ATII cells obtained.

Examination of ATII cells in culture: The phenotype of isolated ATII cells as they transform to ATI-like cells confirmed the presence of MMC4/RTI_{40} positive cells at a time point in culture before epithelial cells were defined as ATI-like cells *(i.e.* RTI_{40}-positive attenuated cells) **(figure 30, figure 29)**. Importantly, the presence of MMC4/RTI_{40}-positive cells in culture also demonstrated that co-expression was not a specific response to bacterial pneumonia but more likely to be generalized to alveolar epithelial repair. It is not known whether MMC4 co-expression with RTI_{40} has any functional significance or whether co-expression reflects the possibility that the MMC4 protein has a longer half-life than other ATII cell-selective proteins.

3D imaging of MMC4/RTI_{40} positive cells showed the concentration of RTI_{40} at the spreading edge of flattening cells **(figure 30)**. The function of RTI_{40} is not known, though data from RTI_{40} null mice suggest that it is required for ATI cell differentiation, and normal alveolar development. Mice lacking RTI_{40} die at birth from respiratory failure, and are found to have lung markedly abnormal lung histology, with thickened alveolar septae and tortuous alveolar lumens (Ramirez, Millien et al. 2003). The study of RTI_{40} in other systems sheds some light on possible functions in the lung. Scholl et al found that RTI_{40} (PA2.26) is associated with the organisation of the actin cytoskeleton and migration in cultured keratinocytes, concentrating in actin rich vili, filopodia, lamellipodia and ruffles (Scholl, Gamallo et al. 1999). Similarly, in cultured lymphatic endothelial cells, over expression of RTI40 enhanced cell migration and filopodia formation (Schacht, Ramirez et al. 2003). It seems likely that RTI_{40} has an important role in facilitating the flattening, spreading and migration of differentiating intermediate cells.

Development

Immunofluorescence and imaging using the LSCM were used to ascertain whether MMC4/RTI_{40} intermediate cells are part of the process of rat lung development. RTI_{40} has been detected in the foetal rat lung as early as embryonic day 15 (E15), but is not easily detectable until E17 becoming more abundant thereafter (Williams and Dobbs 1990). I was able to detect RTI40 in the central nervous system of the foetus at E16 as previously described (Williams, Cao et al. 1996), but did not see lung expression until

E17 **(figure 31, figure 32).** The MMC4 antigen was detected at E16 by Boylan et al. using ELISA based dot-blot, but immunofluorescence was not attempted in this study until E21 (Boylan, Pryde et al. 2001). Lung staining with MMC4 was not detectable in this study by immunofluorescence at E16 or E17 **(figure 31, figure 32)**, but was present at E20, colocalised on ATII cells with $RTII_{70}$ **(figure 33).** Although morphologically intermediate cells have been described in foetal sheep (Flecknoe, Wallace et al. 2003), and cells colocalising ATI (RTI_{40}) and ATII (MPA) specific markers in foetal rats (Williams and Dobbs 1990) I did not detect cells with a RTI_{40}/MMC4 phenotype in the foetal rat lung. Lungs were examined postnatally, however, as extensive alveolar remodelling occurs in rat pups - as evidenced biochemically by continued changes in RTI_{40} and MMC4 protein concentrations (Boylan, Pryde et al. 2001). No intermediate phenotype cells were seen in the alveolar epithelium at postnatal days 3, 4 or 5 **(figure 34, figure 35)**. At post-natal day 3 (PN3), RTI_{40}/MMC4 positive cells were seen in the epithelium of the terminal bronchiole, with occasional epithelial cells expressing $RTII_{70}$ in addition to RTI_{40}/MMC4 at the broncho-alveolar junction **(figure 34)**. The significance of this finding is unclear, although the epithelium of the terminal bronchiole is known to contain a variety of progenitor cell-types (Giangreco, Reynolds et al. 2002; Hong, Reynolds et al. 2004).

A current scheme for epithelial repair

It is likely that in the normal adult lung the vast majority of cells exist in a quiescent state (i.e. G_0) **(figure 1B a.)**. (Uhal 1997). After injury the progenitor ATII cell is somehow stimulated to divide, enters S phase and then undergoes mitosis leading to relatively undifferentiated cuboidal daughter cells, possessing some ATII cell characteristics (e.g. microvilli), but lacking others (e.g. lamellar bodies) **(figure 1B b.)**. Morphological intermediates consistent with this suggestion have been observed in models of alveolar epithelial injury, including (Adamson and Bowden 1974) and (Evans, Cabral et al. 1975). In our *S. aureus* pneumonia model, these cells appear as MMC4/$RTII_{70}$ positive – still having a ATII cell immunophenotype, but occurring contiguously along the alveolar epithelium, and covering a much greater area than in control lungs. These cells may represent what Hirai et al describes as 'early intermediates' (Hirai, Yamauchi et al. 1983). Daughter cells may then assume a ATI or

ATII cell phenotype. As they differentiate towards the ATI phenotype early intermediate cells are likely to shed ATII phenotypic markers **(figure 1B c.)**. The finding that in the *S. aureus* injured lungs some MMC4/$RTII_{70}$ cells are pro-SP-C negative is consistent with this, but may also simply represent the down regulation of surfactant synthesis after injury induced hyperplasia (Fehrenbach, Kasper et al. 1999; Yano, Mason et al. 2000). RTI_{40}/MMC4 positive cells **(figure 1B d.)** can be described as 'late intermediates' (Hirai, Yamauchi et al. 1983). Expression of RTI_{40} by intermediate cells may facilitate migration and spreading as part of epithelial repair, RTI_{40}/MMC4 positive cells in our culture system become flattened and attenuated consistent with this suggestion. Finally, the intermediate becomes a fully differentiated ATI-cell, losing MMC4 expression **(figure 1B e.).**

The ATI cell has often been regarded as terminally differentiated, but evidence exists that foetal ATI cells (Flecknoe, Wallace et al. 2002) and ATI-like cells in culture (Shannon, Jennings et al. 1992) can be induced to transdifferentiate to a ATII cell phenotype, though this phenomenon has not been demonstrated experimentally in an adult lung. In addition, it seems from the weight of evidence derived largely from in vivo stathmokinetic studies (i.e. induction of metaphase arrest) that only the ATII cell phenotype is able to re-enter the cell cycle for further division (Adamson and Bowden 1974; Evans, Cabral et al. 1975).

After a more severe injury to the alveolar epithelium, it is possible that progenitors from the terminal bronchioles or even circulating bone marrow derived cells contribute to repair **(figure 1B f.)**.

Alveolar epithelial repair in the context of other tissues

Consideration of the process of healing in other tissues offers a framework with which to consider factors affecting the repair process in the alveolar epithelium. Generic mechanisms of tissue repair are usefully summarised by Mutsaers et al. who offer a summary of the 'highly orchestrated sequence of events' (Mutsaers, Bishop et al. 1997). This complex multistage process involves several overlapping stages that occur broadly sequentially. Initially haemostasis is achieved by platelet aggregation, clot formation and local vasoconstriction. This is followed by hyperaemia and increased permeability of nearby blood vessels facilitating an inflammatory infiltrate. Provisional matrix

composed largely of fibrin, fibronectin provides a scaffold for the inflammatory process, becoming granulation tissue as fibroblasts lay down matrix in which new vessels are forming. Remodelling by the rapid synthesis and degradation of connective tissue proteins leads to scar formation initially as production exceeds removal. The final phase of the normal repair process involves resolution of scar tissue.

Mutsaers details the important categories of interactions involved in the coordination of wound healing (Mutsaers, Bishop et al. 1997):

1. Cell-cell and cell-matrix interactions: These interactions trigger migration, growth and differentiation and can be categorised as cell-matrix adhesion interactions at the cell basal surface (e.g. integrins and their ligands), cell-cell interactions between adjacent cells (e.g. cadherins, intercellular adhesion molecules), and luminal cell–cell adhesion molecules (e.g. platelet-endothelial cell adhesion molecule, granule-associated membrane protein 140).

2. Extracellular Matrix (ECM) Turnover: In addition to the action of matrix components via integrins ECM can also bind and later present other bioactive factors. Fibroblasts are involved not only in the synthesis of ECM components, but also in their degradation by production of enzymes such as matrix metalloproteinases (MMPs). Regulation of the balance of these processes is by a variety of mechanisms (autocrine, paracrine and endocrine).

Key mediators of wound healing and fibrosis are also identified as locally released peptide growth factors and cytokines (e.g. platelet derived growth factor (PDGF), transforming growth factor beta (TGF-β), fibroblast growth factor (FGF), epidermal growth factor (EGF)), blood-derived proteins (e.g. fibrinogen and fibronectin), and the mechanical environment.

Healing in the lung – avenues for further work

In the context of the lung, the pathological process in ALI/ARDS has been similarly characterised as a series of stereotypical stages that reflect the failure of normal repair and resolution (see earlier: page 16). Detailed morphological and morphometric studies as early as the 1970s characterised the generic response of the lung to injury (Bachofen and Weibel 1974). Bachofen and Weibel carefully describe the appearances under the

electron microscope of human lung tissue with established ARDS fixed within 30 minutes of the patients' death. The 'basic feature' common to all of the injured lungs examined was the 'transformation of alveolar epithelium into a cuboidal epithelial lining, together with interstitial oedema and a proliferative reaction of the connective tissue...". This connective tissue proliferation led to lung fibrosis, worsening gas exchange and death after a disease duration of between 21 and 60 days in the patients studied (Bachofen and Weibel 1974). Recent examination of the onset of the fibroproliferative response after acute lung injury has shown some unexpected results. In contrast to the traditional characterisation of the pathogenesis ARDS where fibrosis is a late event in the disease process, Marshall et al. have found evidence of fibroproliferation after 24 hours, implying that fibrosis begins in parallel with initial exudative and inflammatory events (Marshall, Bellingan et al. 2000). Many of the factors which are highlighted as important modulators of tissue repair in other organ systems have been examined in the context of lung injury and suggest avenues of investigation for future work:

1. Integrin and matrix interactions: White et al. examined monolayer wound repair in a series of studies using a cultured human non-secretory central airway epithelial cell line (16HBE14o). Monolayers were grown on a variety of ECMs (collagen-IV, laminin-1, or laminin-2 matrix) and wounded. Wound closure was blocked by monoclonal antibodies to β1-integrin or agglutinins preventing the binding of alpha-dystroglycan to laminin indicating that these interactions are required for airway epithelial cell spreading and migration (refs) (White, Dorscheid et al. 1999; White, Wojcik et al. 2001). The β6-integrin subunit has also been implicated as important in distal airway epithelial repair and resolution of inflammation (Breuss, Gallo et al. 1995; Huang, Wu et al. 1998). It would be potentially very useful to delineate the effect of disruption of these integrin/matrix interactions on the transdifferentiation of ATII cells during alveolar epithelial repair.

2. Mechanical environment: It is clear that the lung is very sensitive to mechanical stress, particularly that induced by positive pressure ventilation in the context of lung injury. The adverse effects of non-physiological mechanical distension on the lung have been demonstrated cell culture, animal models and in clinical studies, with a variety of putative mechanisms cited for these findings (Lecuona, Saldias et al. 1999; Vlahakis

and Hubmayr 2000; Matthay, Bhattacharya et al. 2002; Gajic, Lee et al. 2003; Vlahakis and Hubmayr 2005) (2000). Stretch modulates the proportion of ATII cells in the lung alveolar epithelium during both development and maturation of the lung and following lung injury and has been shown to affect the ATII to ATI cell transdifferentiation process studied in this thesis directly (Gutierrez, Gonzalez et al. 1998), (Stuart McKechnie unpublished data). Translating these findings into the clinical context, it would be useful to examine the effect of positive pressure ventilation on the alveolar epithelium in the context of injury. The so-called 'two-hit' model reflects the clinical reality for many critically ill patients. Both hypoxia (Vuichard, Ganter et al. 2005) and resuscitated haemorrhagic shock (Fan, Marshall et al. 1998) have been shown to 'prime' rodent lungs leading to a greater severity of injury when exposed to a 'second hit' (in these studies LPS induced ALI). It is likely that mechanical ventilation will act synergistically with other pathological insults to damage the lung in the context of illness/injury and resuscitation. It would be profitable to elucidate the mechanisms for this and find ways of ameliorating the effect since no practicable alternative to positive pressure ventilation is currently available to the critically ill patient requiring ventilatory support.

Summary

This work has shown that characterized ATI and ATII cell membrane markers can be used to identify and quantify the alveolar surface area covered by ATI and ATII cells at localized regions of repair following lung injury. Some cells in repairing alveolar epithelium co-express ATI and ATII cell markers, not seen in other regions of the inoculated lung or control lungs. Our data suggest that RTI_{40}/MMC4-positive cells are intermediates in the ATII to ATI cell transition, this is further corroborated by the appearance of RTI_{40}/MMC4 positive cells during the transformation of ATII cells to ATI-like cell *in vitro*. This is the first study to identify alveolar epithelial intermediate cells based on the expression of membrane protein markers. It is not possible in the lung to easily determine the progeny relationships because cells can migrate in three dimensions. Markers that define the phenotype of epithelial cells in transition represent a unique method to address fundamental issues regarding the role and regulation of ATII cell transdifferentiation in different models of lung injury including fibrosis.

Unravelling the process of lung alveolar epithelial repair is crucial to understanding a wide range of lung pathologies, from acute lung injury to chronic fibrosis. The ATII cell appears to have a central role in this, though the factors that modulate its proliferation and differentiation *in vivo* remain obscure. It would be informative to compare the effects of indirect lung injury (e.g. haemorrhagic shock) with the repair process after the direct injury used in this study. A more homogeneous lung injury may facilitate investigation into the effects of a clinically relevant 'second-hit' (like hypoxia or the mechanical stress of ventilation) on alveolar epithelial repair.

Figures

figure 1

A: 'The model circa 1980'

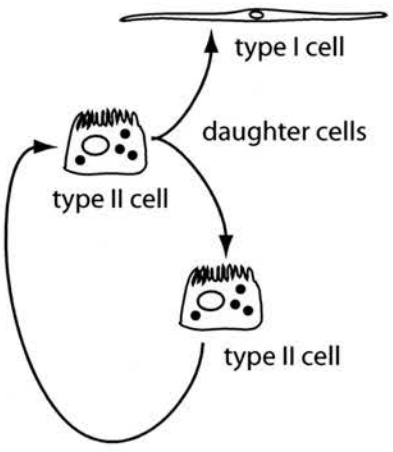

B: A current model

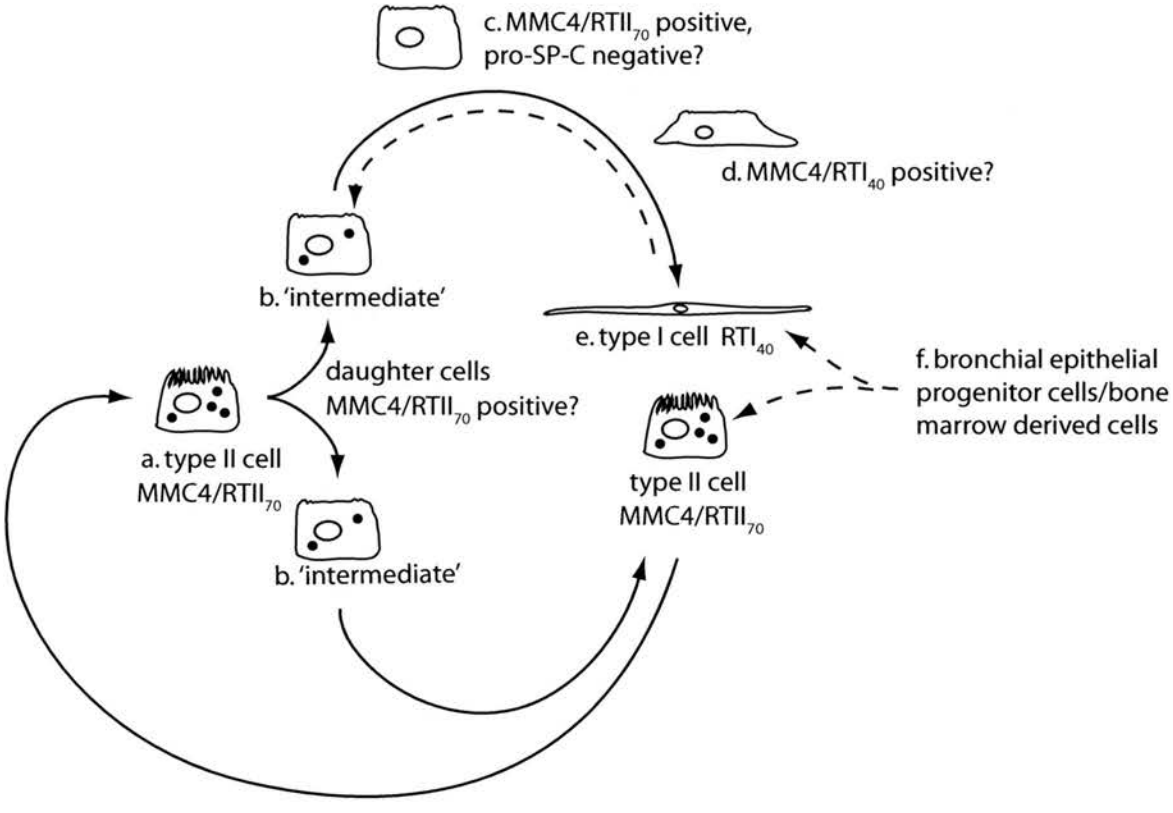

(A) In this model the ATII cell is the progenitor of ATI and ATII cell types. Division of an ATII cell porduces daughter cells, one of which becomes a terminally differentiated ATI, the other retains the ATII phenotype and replenishes the ATII cell population. (B) Here, the ATII cell is the usual progenitor of ATI and ATII cell types. Cell division gives rise to two undifferentiated daughter cells that can assume either ATI or ATII cell mature phenotype. Transformation from ATII cell to ATI cell phenotype is potentially reversible, but only ATII cells can re-enter the cell cycle. After severe epithelail injury, cells from outside the alveolus may contribute to repair. Adapted from Uhal (1997).

figure 2

A: simplified optics of a laser scanning confocal microscope (LSCM)

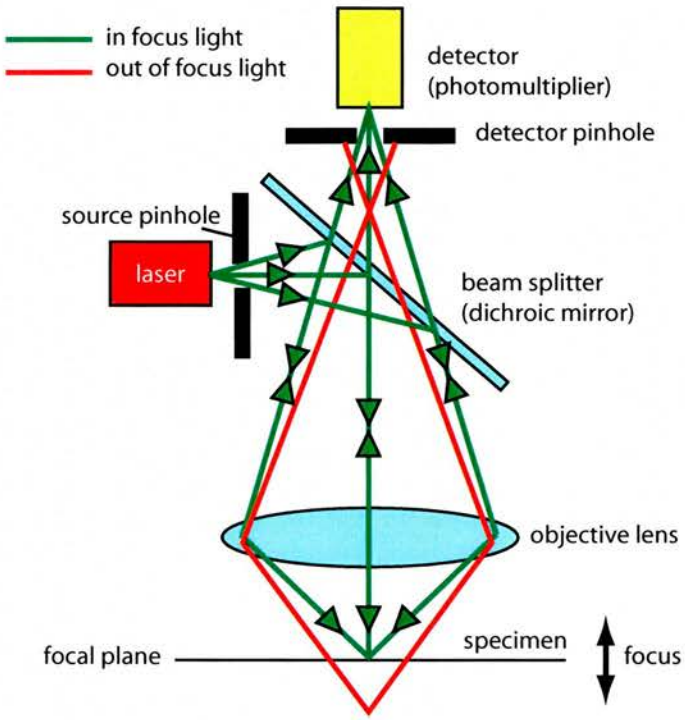

B: schematic showing typical LSCM set up

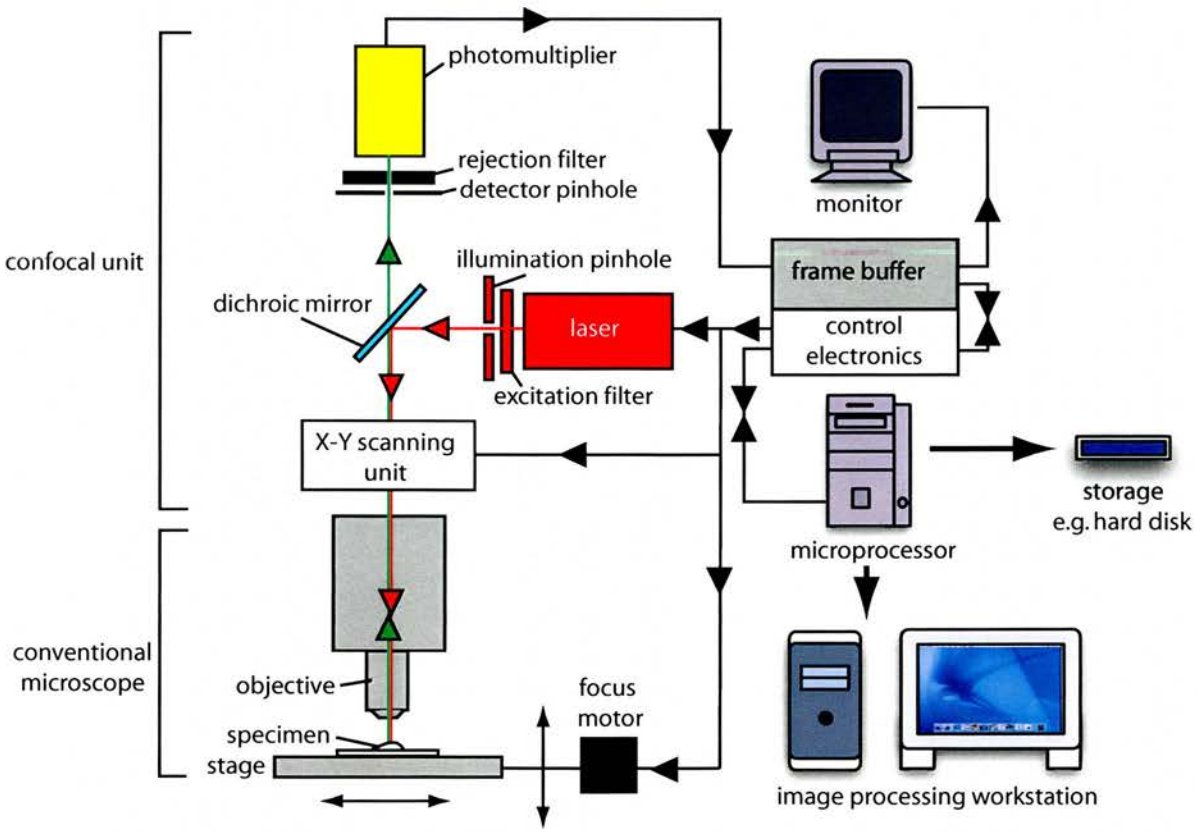

figure 3

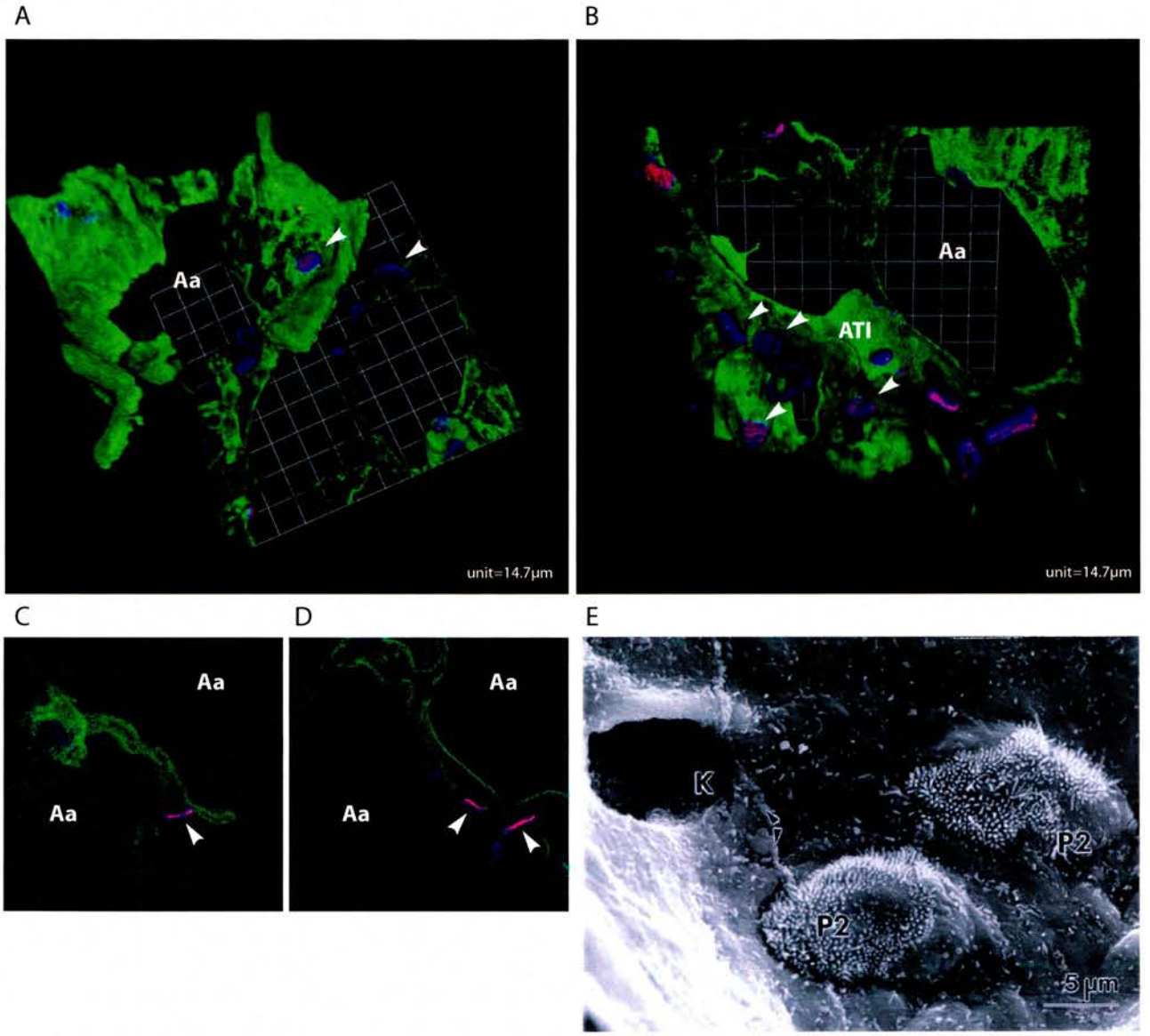

Tissue blocks approximately 5mm^3 stained with anti-RTI$_{40}$ (green 488), MMC4 (red 546) and RTII$_{70}$ (blue 647). The three dimensional structure of the alveolus is clearly visible in the tissue blocks (A) and (B) with the purple MMC4/RTII$_{70}$ positive apical membranes of ATII cells protruding from the RTI$_{40}$ positive ATI cells lining the alveolar airspace (Aa). Selecting single optical sections (C) and (D) from the 3D stacks reveals the internal structure of the tissue - the familiar 2D appearance of RTI$_{40}$ positive ATI cell 'tram lines' flanking ATII cells.

For comparison, (E) shows a scanning electron micrograph of human lung taken from Fehrenbach (2001). Two ATII cells (P2) protrude above the largely smooth alveolar epithelial surface. A pore of Kohn (K) and the cell–cell junction (arrowheads) between two ATI cells are indicated.

figure 4

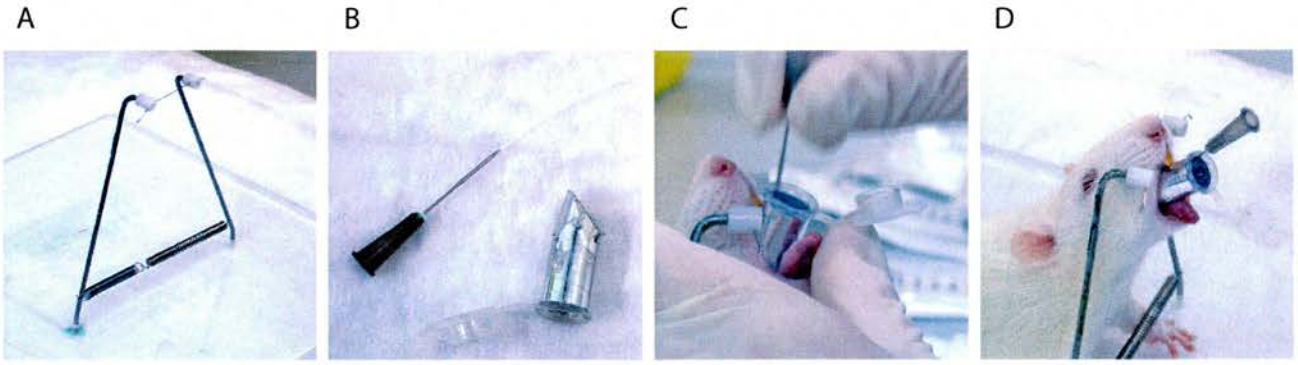

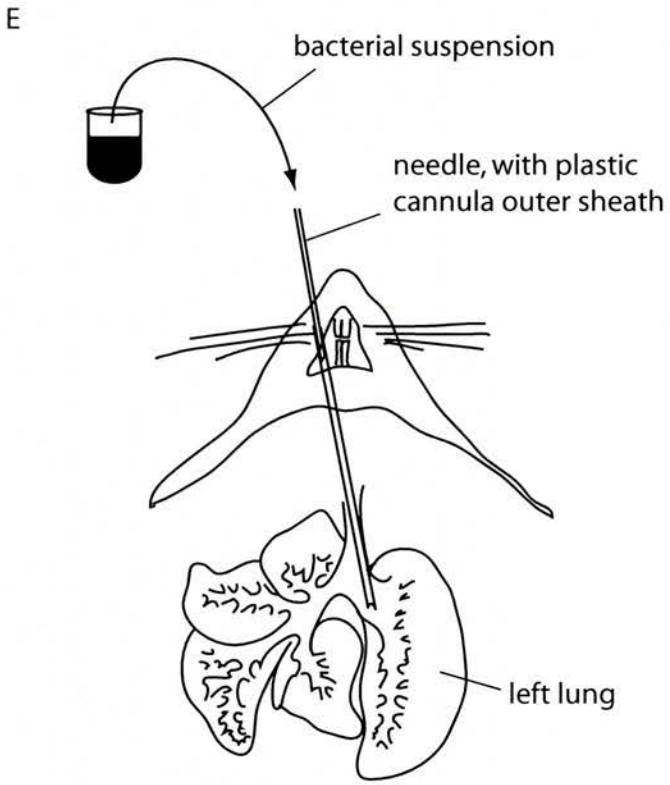

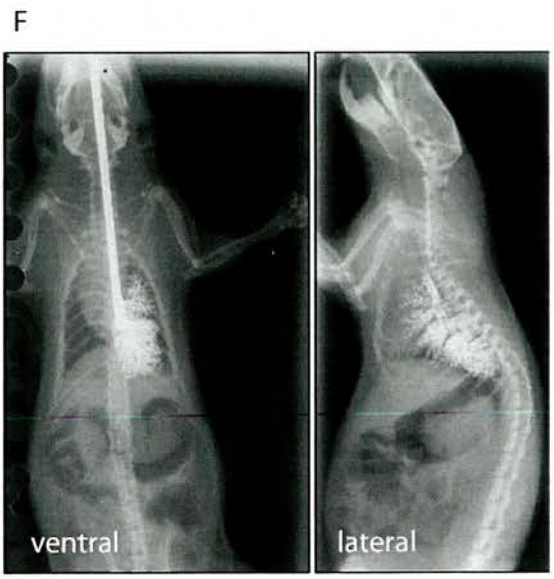

Rats are maintained in a vertical position by suspension on a horizontal wire by the front upper incisors (A). The intubation wedge is placed in the mouth and tracheal tube inserted (B-D). Bacterial suspension or PBS control is instilled resulting in a reproducible left lower lobe pneumonia (E, F). (E) and (F) adapted from Bakker-Woudenberg IA (2003) *Experimental models of pulmonary infection.* J Microbiol Methods 54(3):295-313

figure 5

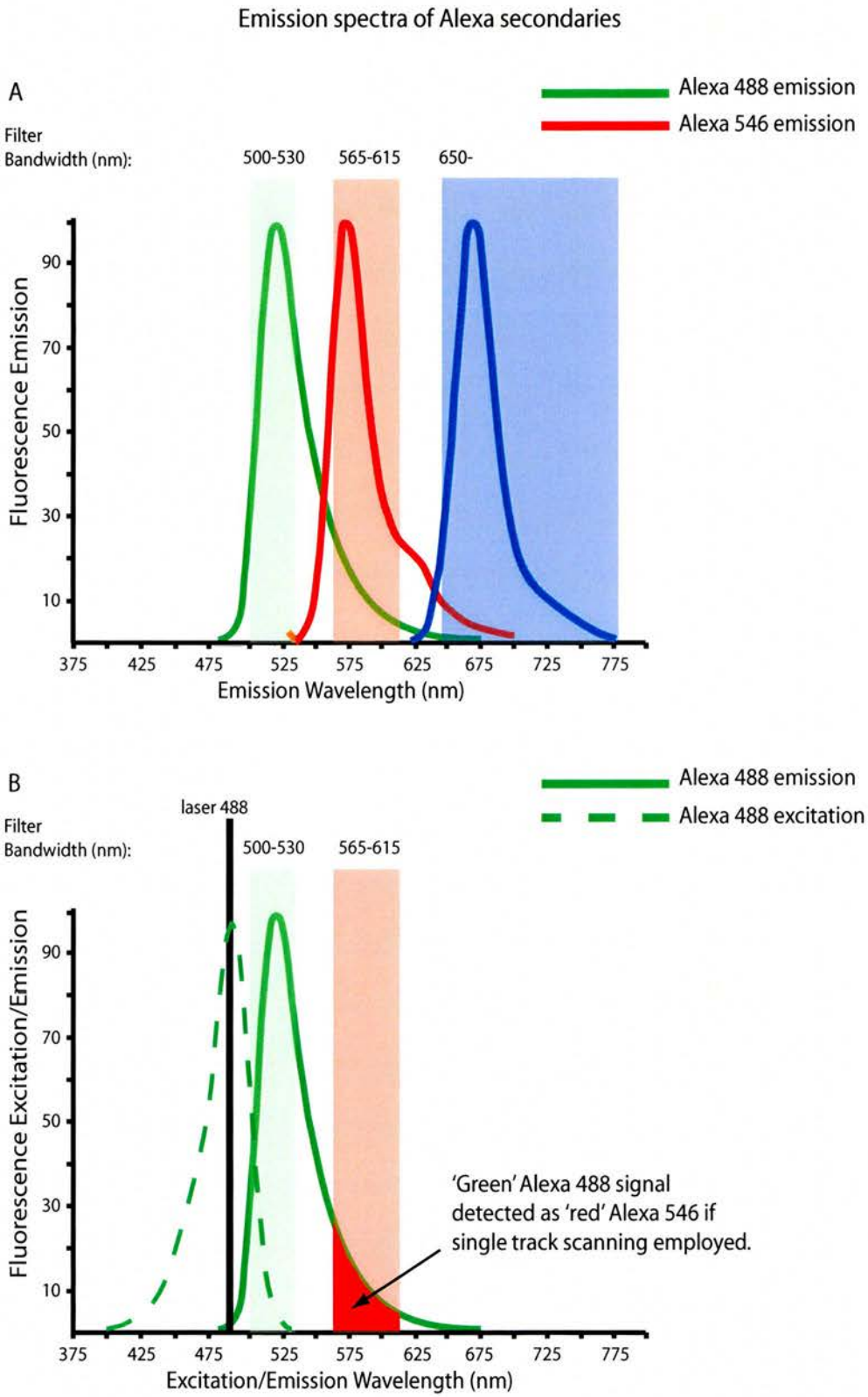

Diagram shows (A) the emission spectra of the Alexa secondary antibodies used for staining. Alexa 647 emissions were filtered through a Low Pass 650nm filter, Alexa 488 emissions through a Band Pass 500-530nm filter, and Alexa 546 emissions through a Band Pass 565-615 filter. (B) The excitation spectra for the red and green flourophores overlap. If they are detected simultaneously, then the tail of the green emission may be erroneously recorded as red (red shaded area).

figure 6

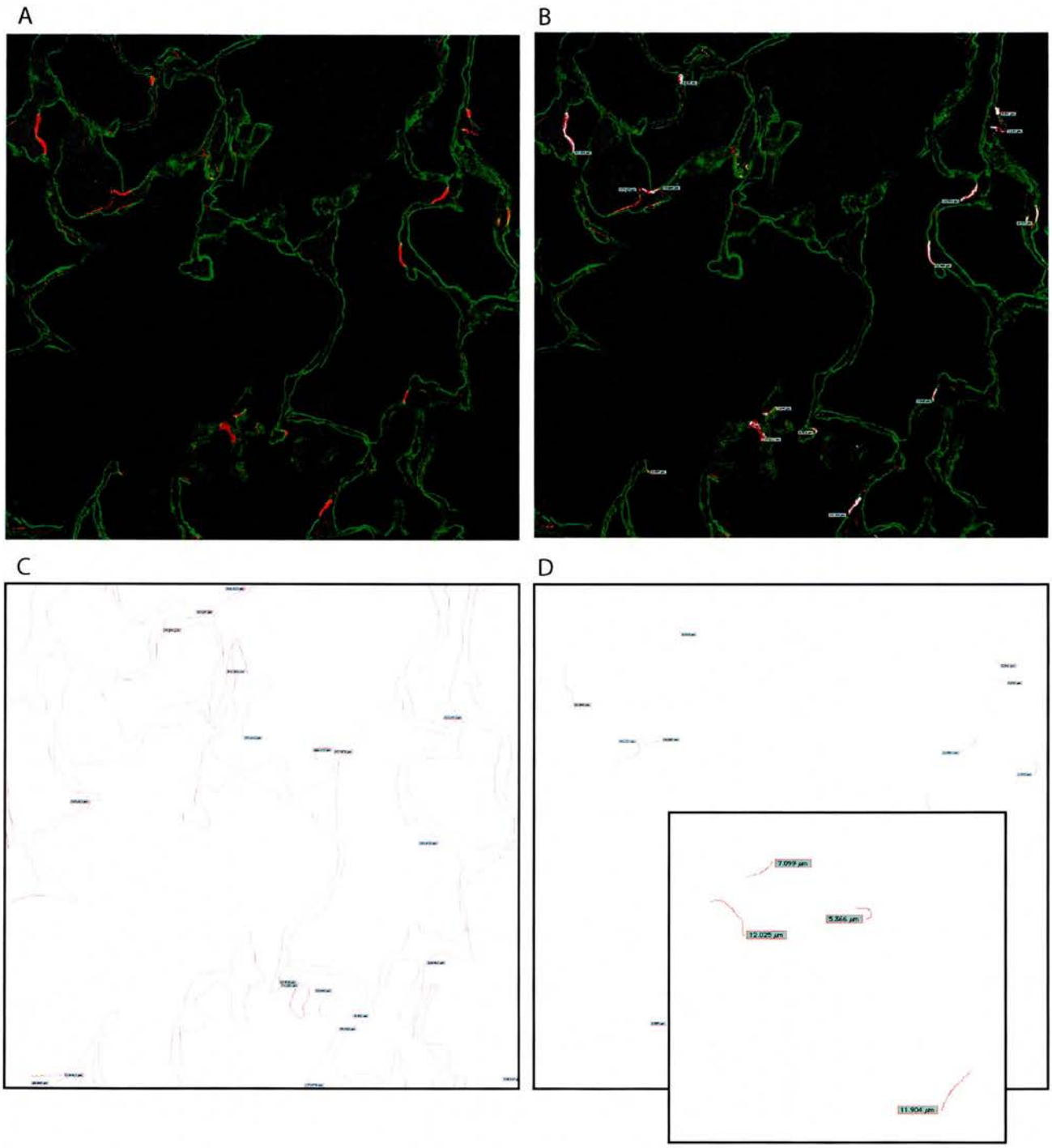

Quantification of an image of a control lung section otained by confocal microscopy. The area of interest (e.g. the MMC4 (red 546) positive ATII apical membrane) is highlighted by creating a binary map of the areas of positive fluorescence staining. Here a white map has been created for the MMC4 positive areas and overlaid on the original image (B). The the lengths of the regions of interest are then traced using a graphics tablet, after image calibration (D). The lengths obtained in this way can be expressed as a fraction of the entire epithelial surface in the image, by tracing the whole epithelium (C).

Haemorrhagic shock model

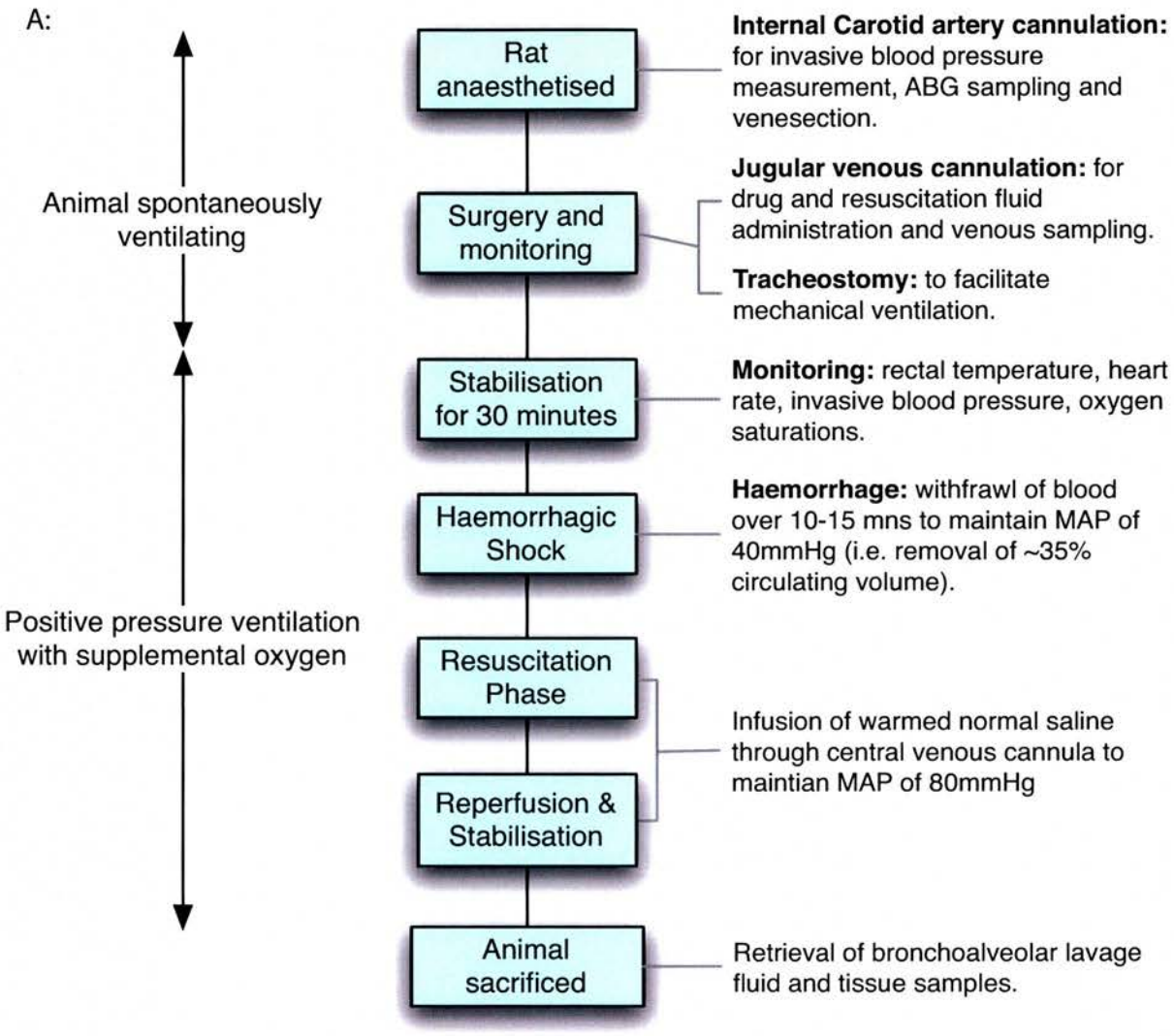

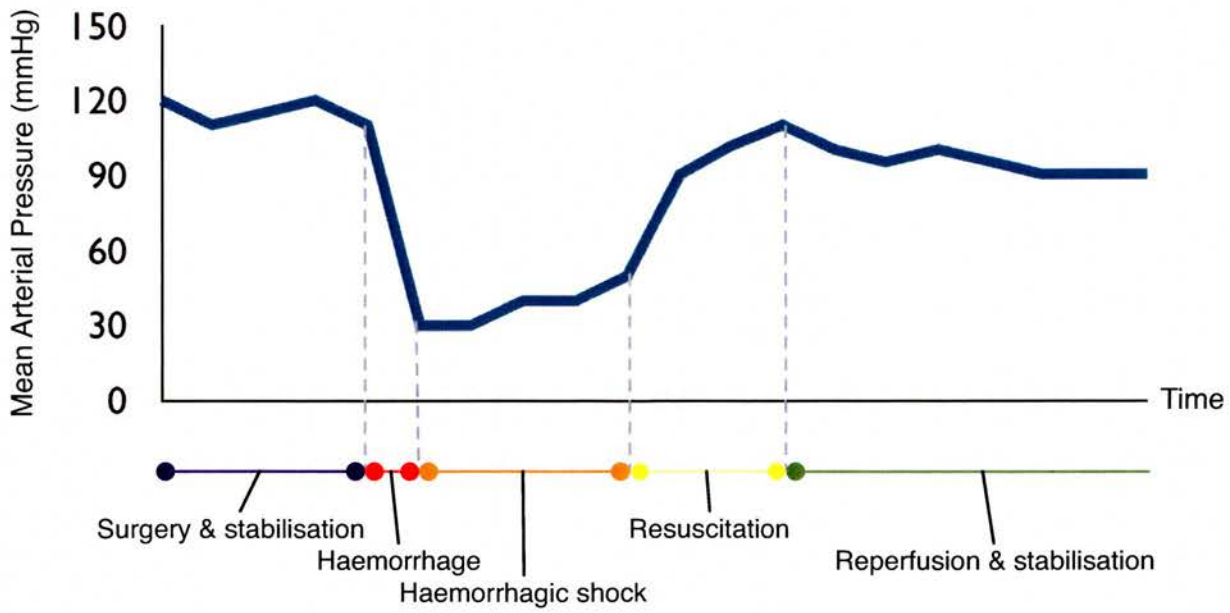

A: Diagram showing the prcedure for the rat model of haemorrhagic shock.
B: The invasive mean arterial pressure trace from a representative experiment.

figure 8

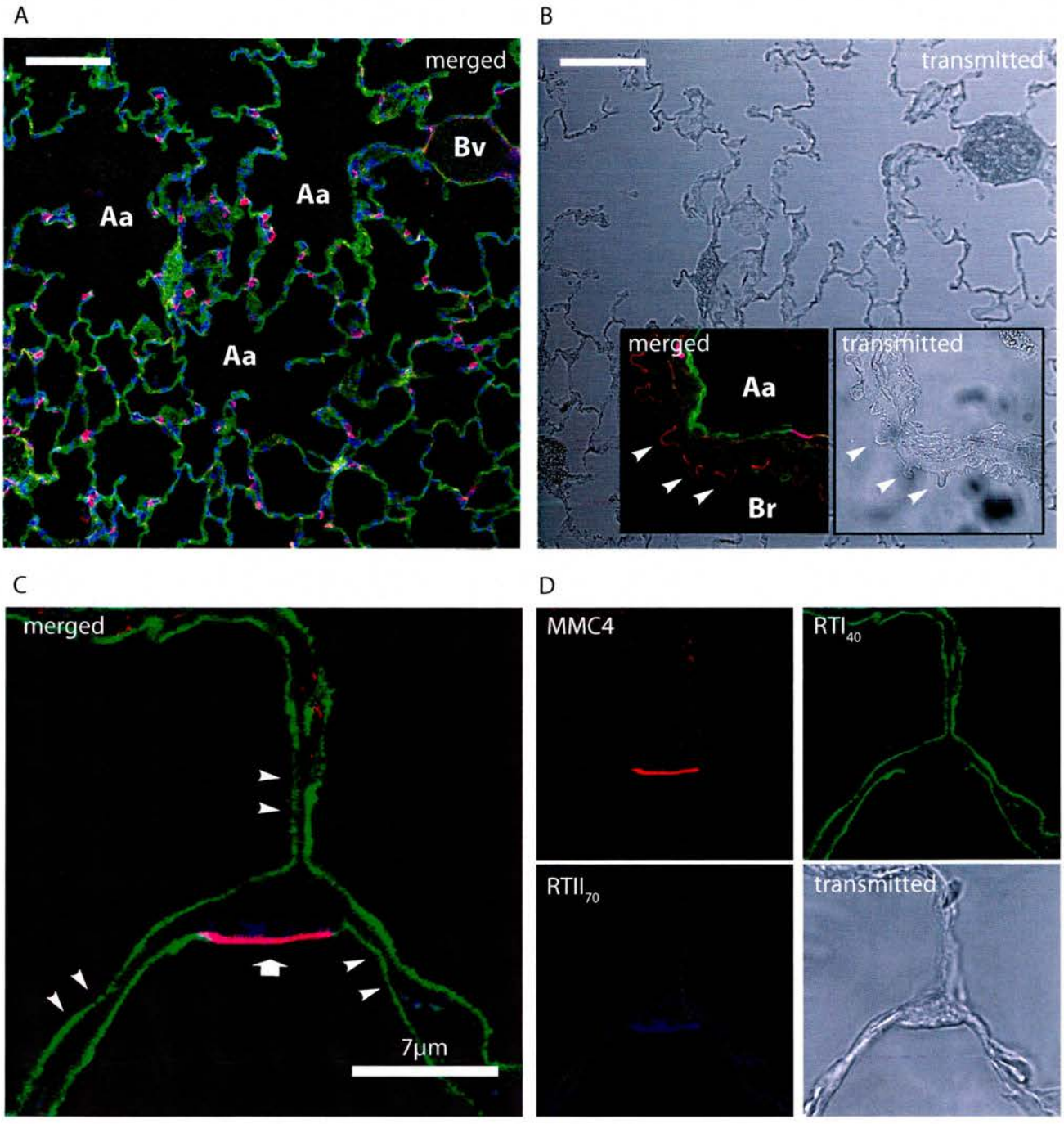

Control lung stained with MMC4 (546 red), RTI_{40} (488 green), and $RTII_{70}$ (647 blue). Alveolar airspaces (Aa) are lined by RTI_{40} positive ATI cells with MMC4/$RTII_{70}$ positive ATII cells (short broad arrow) in the corners of the alveoli. A blood vessel (Bv) is also visble in the low magnification view (A). A high magnification view of terminal bronchiolar epithelium (B, inset) shows MMC4 positive/$RTII_{70}$ negative Clara cells (arrowheads).

figure 9

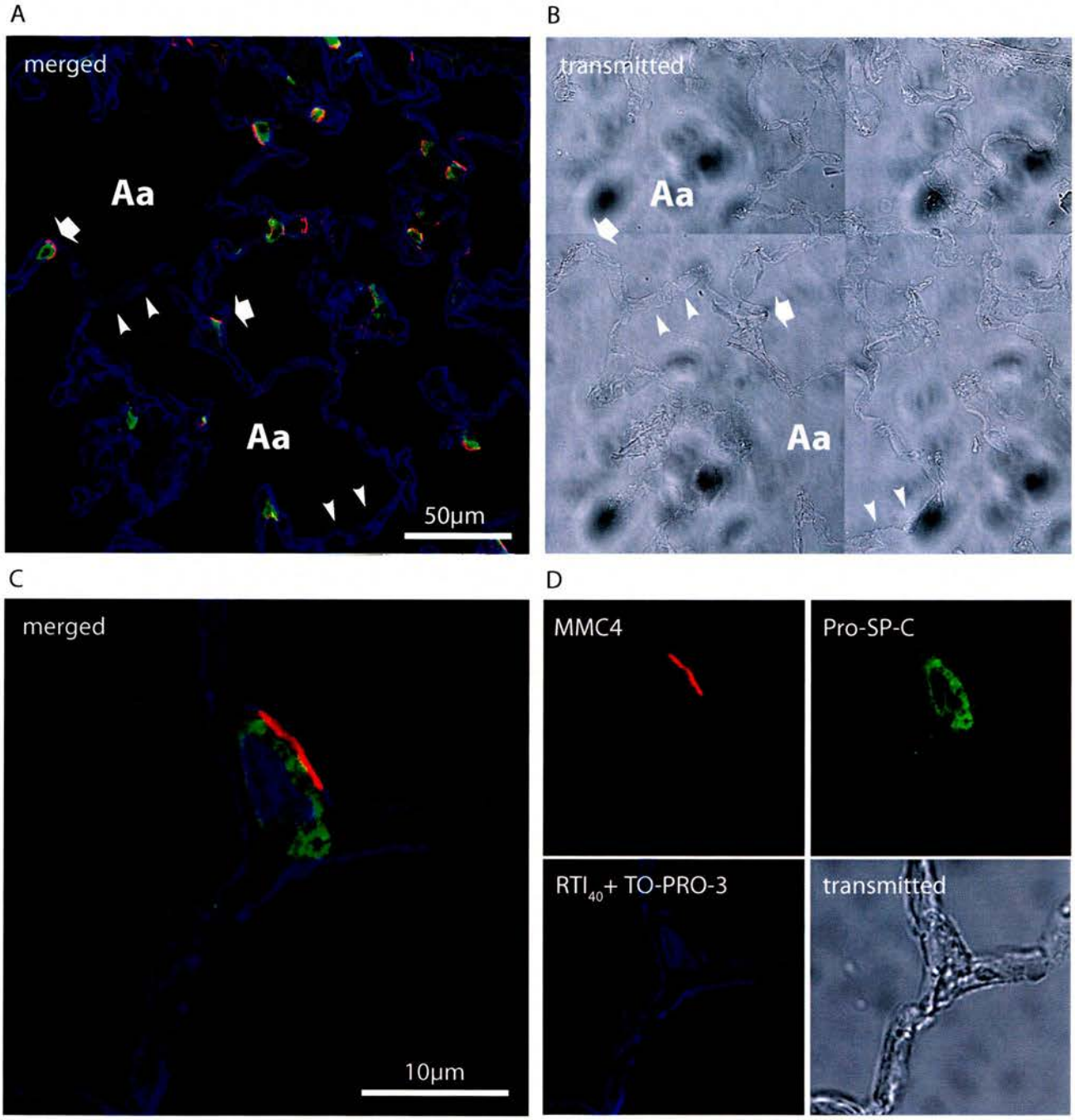

Control lung stained with anti-RTI_{40} (647 blue), MMC4 (546 red), anti-pro-SP-C (488 green) and DNA dye TO-PRO-3 (647 blue). RTI_{40} positive ATI cells form most of the alveolar wall (double arrows) with ATII cells (broad arrow) at the corners of the alveoli. ATII cells stain with MMC4 at the apical membrane and anti-pro-SP-C in the cytoplasm.

figure 10

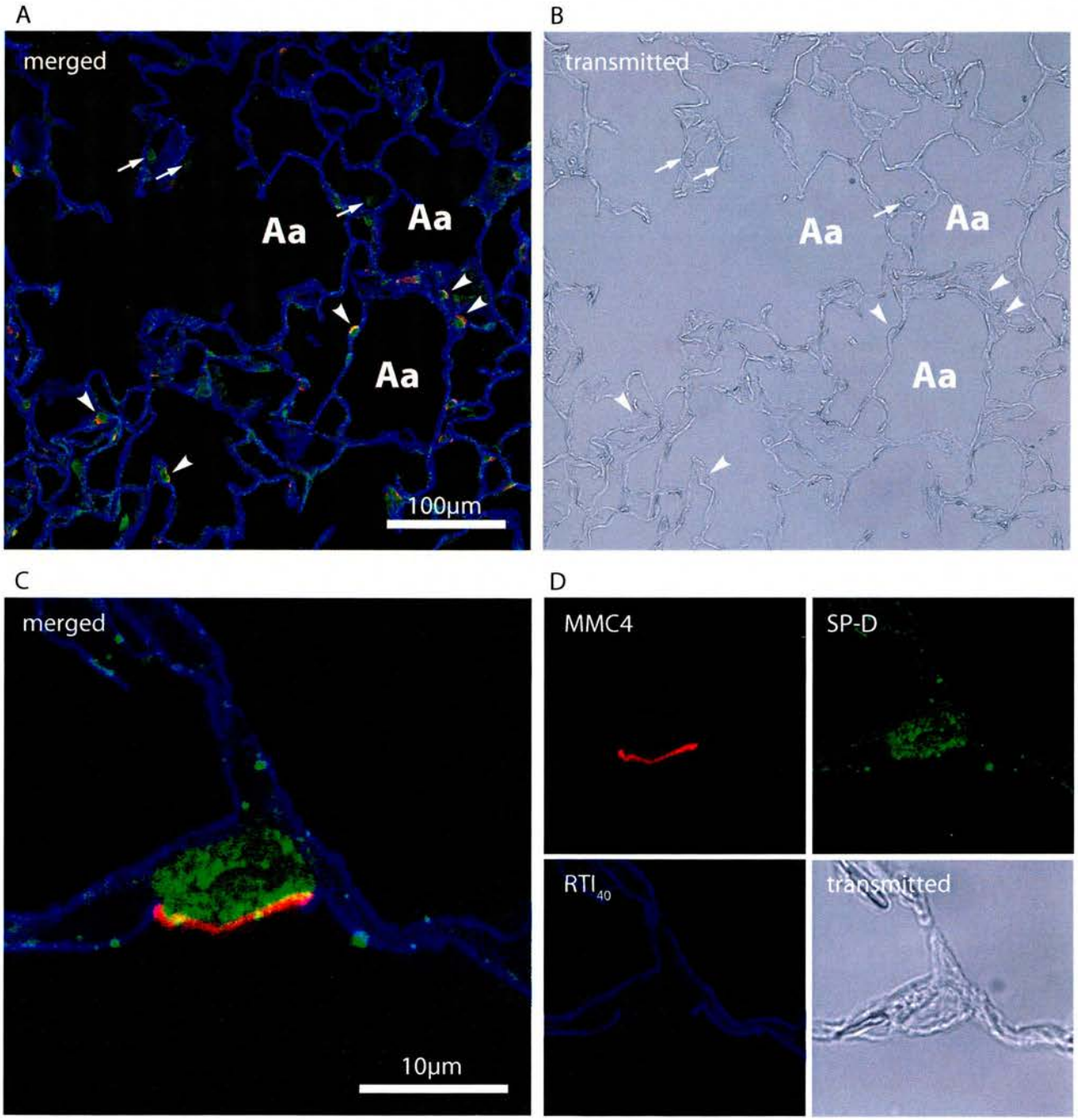

Control rat lung stained with anti-SP-D (green 488), anti-RTI_{40} (blue 647), and MMC4 (red 546). RTI_{40} positive ATI cells line the alveolar airspaces (Aa). ATII cells are easily identifiable by their MMC4 positive apical membranes (arrowheads). The cytoplasm of ATII cells also stains strongly positive for SP-D. Some alveolar macrophages also stain weakly positive for SP-D (white arrows).

figure 11

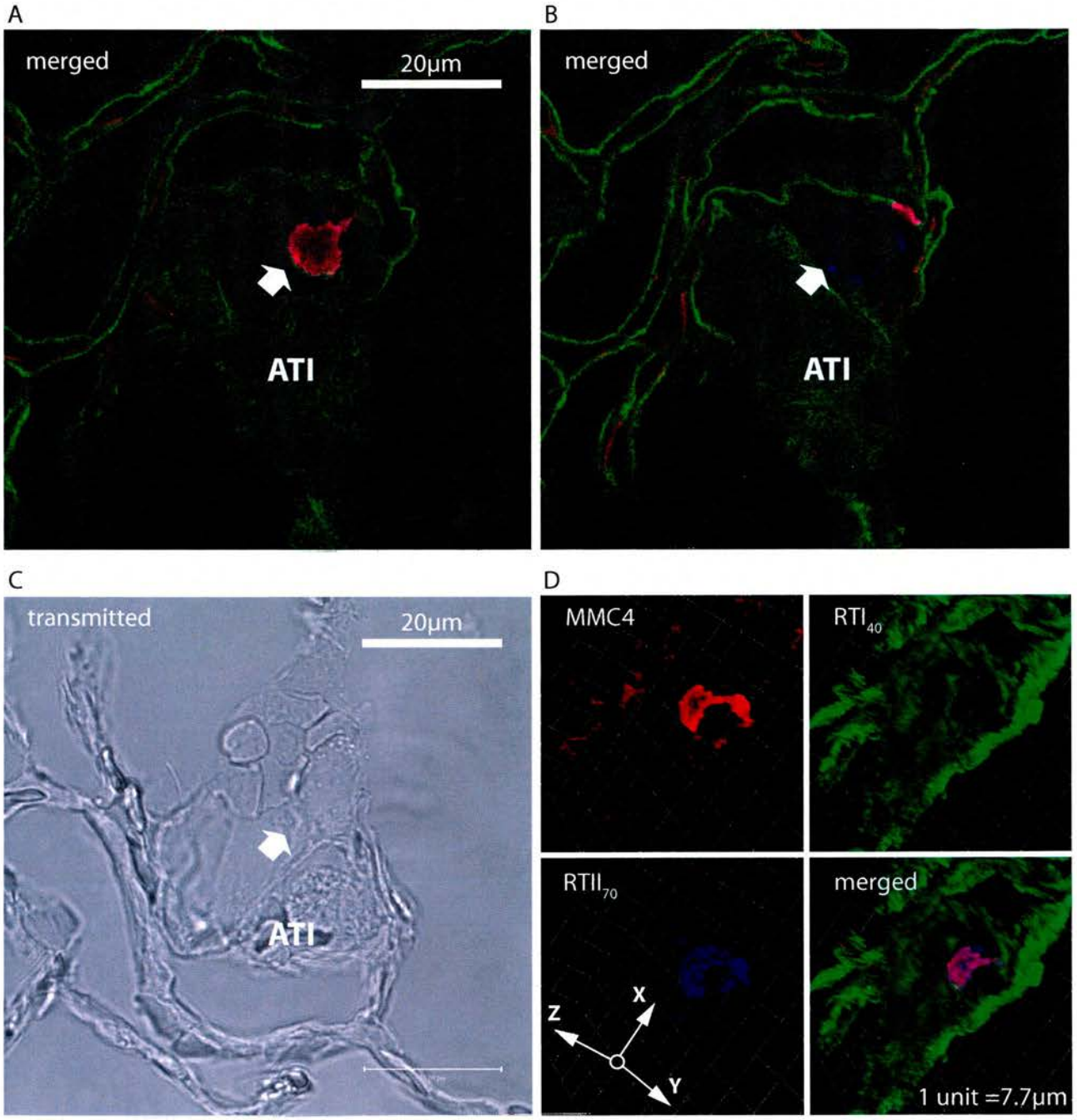

Control lung stained with anti-RTI_{40} (green 488), MMC4 (red 546), and anti $RTII_{70}$-(blue 647). The image shows a ATI cell sectioned *en face* (ATI) surrounding a ATII cell (broad arrow). Images (A) and (B) are taken in different vertical planes, from the top and bottom of the section. The MMC4/$RTII_{70}$ positive apical membrane of the ATII cell is clearly visible in (A), but disappears almost completely in B. The 3D reconstruction in (D) shows the actual positions of the cells relative to one another.

figure 12

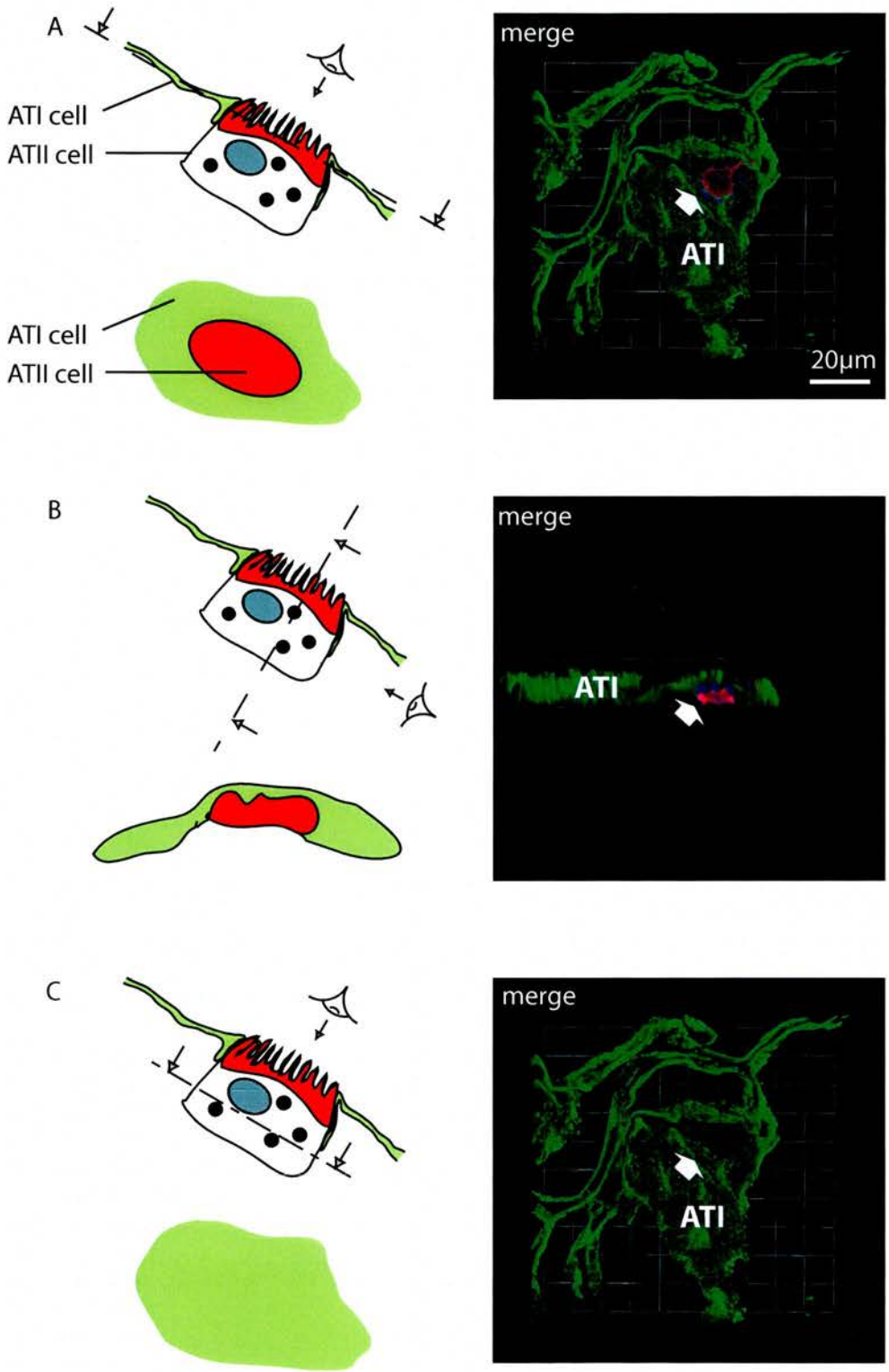

Control lung stained with anti-RTI_{40} (green 488), MMC4 (red 546), and anti $RTII_{70}$ (blue 647). The image shows a ATI cell sectioned *en face* (ATI) surrounding a ATII cell (broad arrow). The 3D reconstruction of a stack of optical sections can be interrogated to show the top (A), botttom (C) or section through the specimen (B).

figure 13

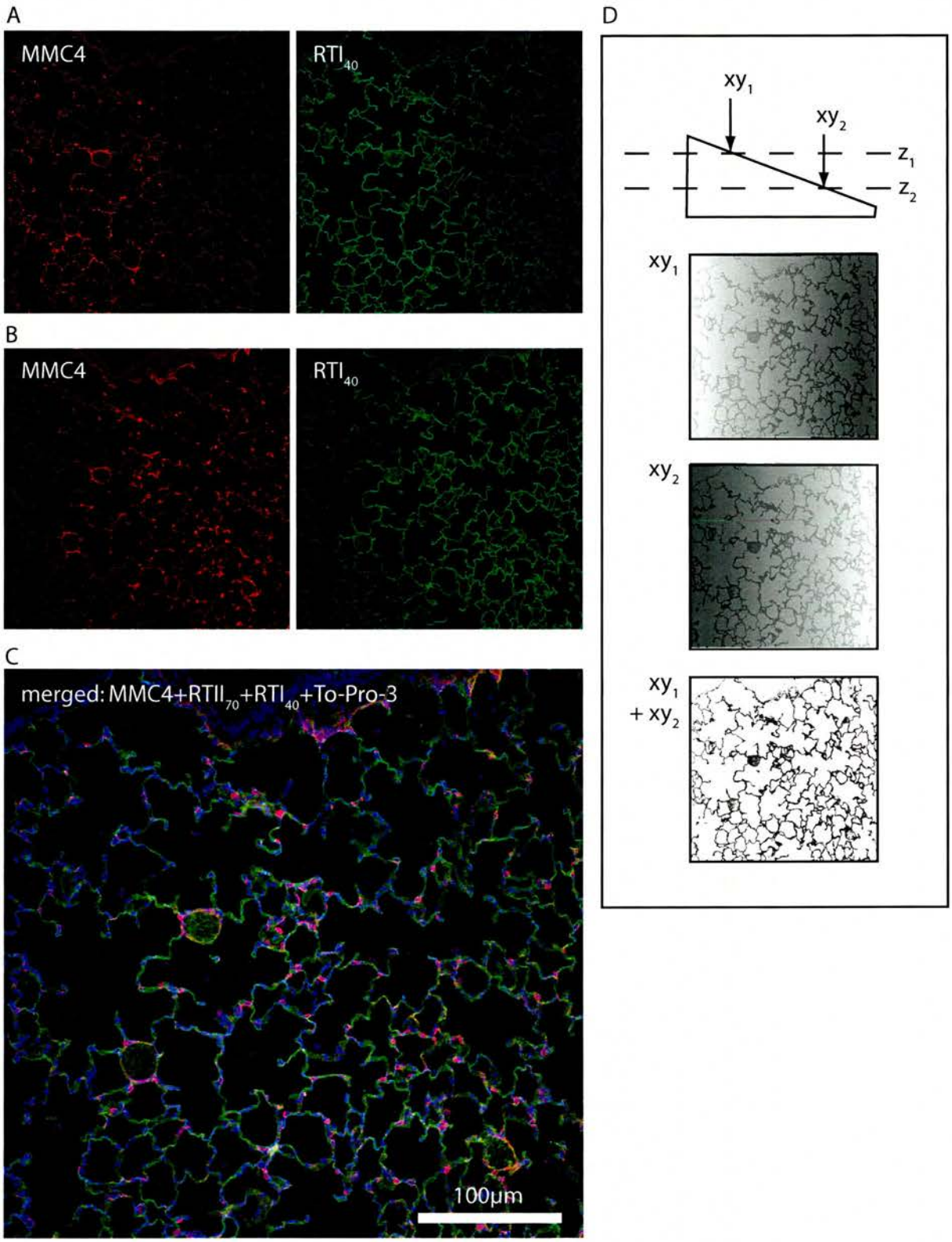

Schematic (D) shows the consequences of imaging a thin optical section through a thin but uneven specimen. Only the portion of the image to the left of the field of view is in focus (and therefore brighter) when scanning at plane z1 (A), whereas the right of the field is best seen at z2 (B). Combining images taken at both planes includes all of the information on the section. green and red channels (RTI_{40} and MMC4 staining respectively) illustrate the point above. Combining layers (C) allows all of the cells present to be seen.

figure 14

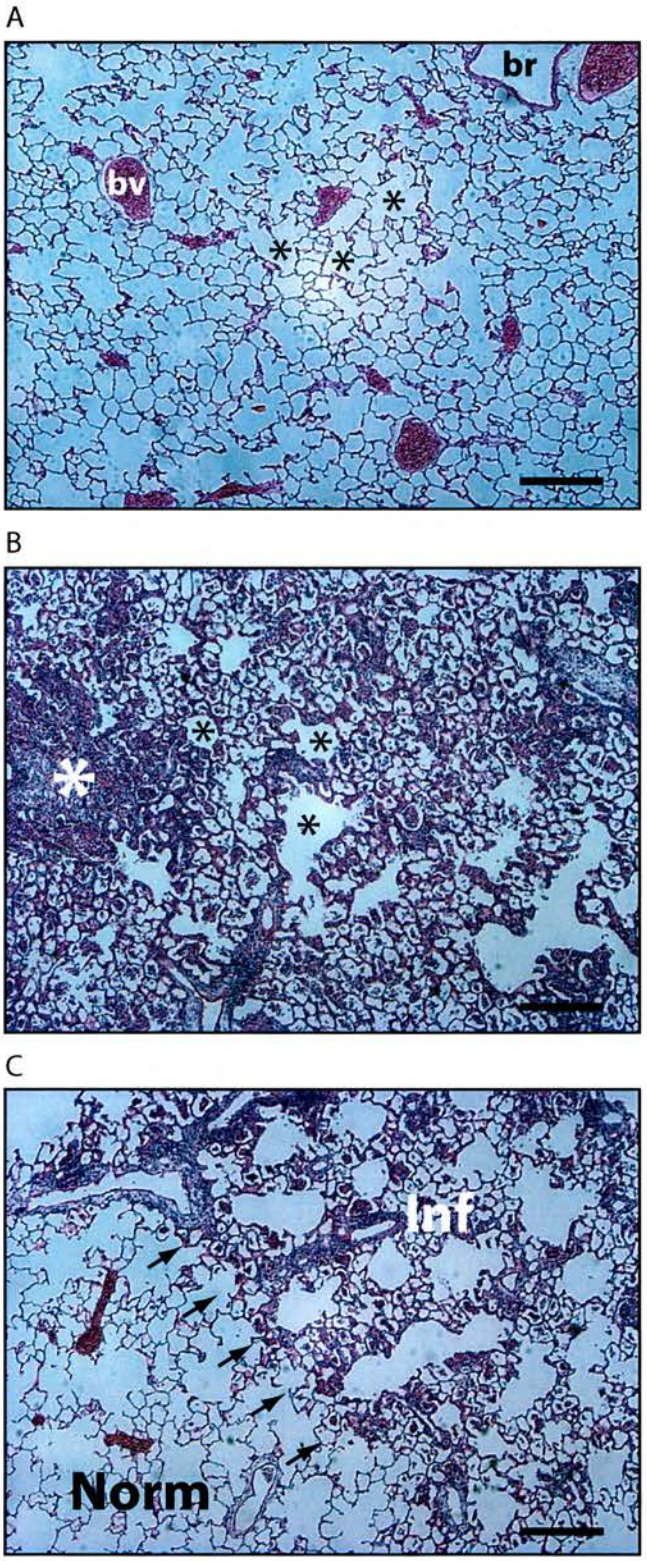

The morphology of rat lung sections demonstrated on haematoxylin and eosin stained paraffin-fixed sections. Control lung section (A) shows alveolar air spaces (asterisks), blood vessels filled with red cells (Bv), and a terminal bronchiole (Br). (B) shows an area of consolidation in which the small airspaces are filled with cells and debris (asterisks). In some areas the alveolar wall is not distinct from the airspaces or the inflammatory cell influx (white asterisk). (C) shows the boundary (arrows) between obviously inflamed tissue with thickened alveolar walls and inflammatory cells in the airspaces (Inf) and a region which is morphologically indistinguishable from control lung (Norm). Bar=100μm.

figure 15

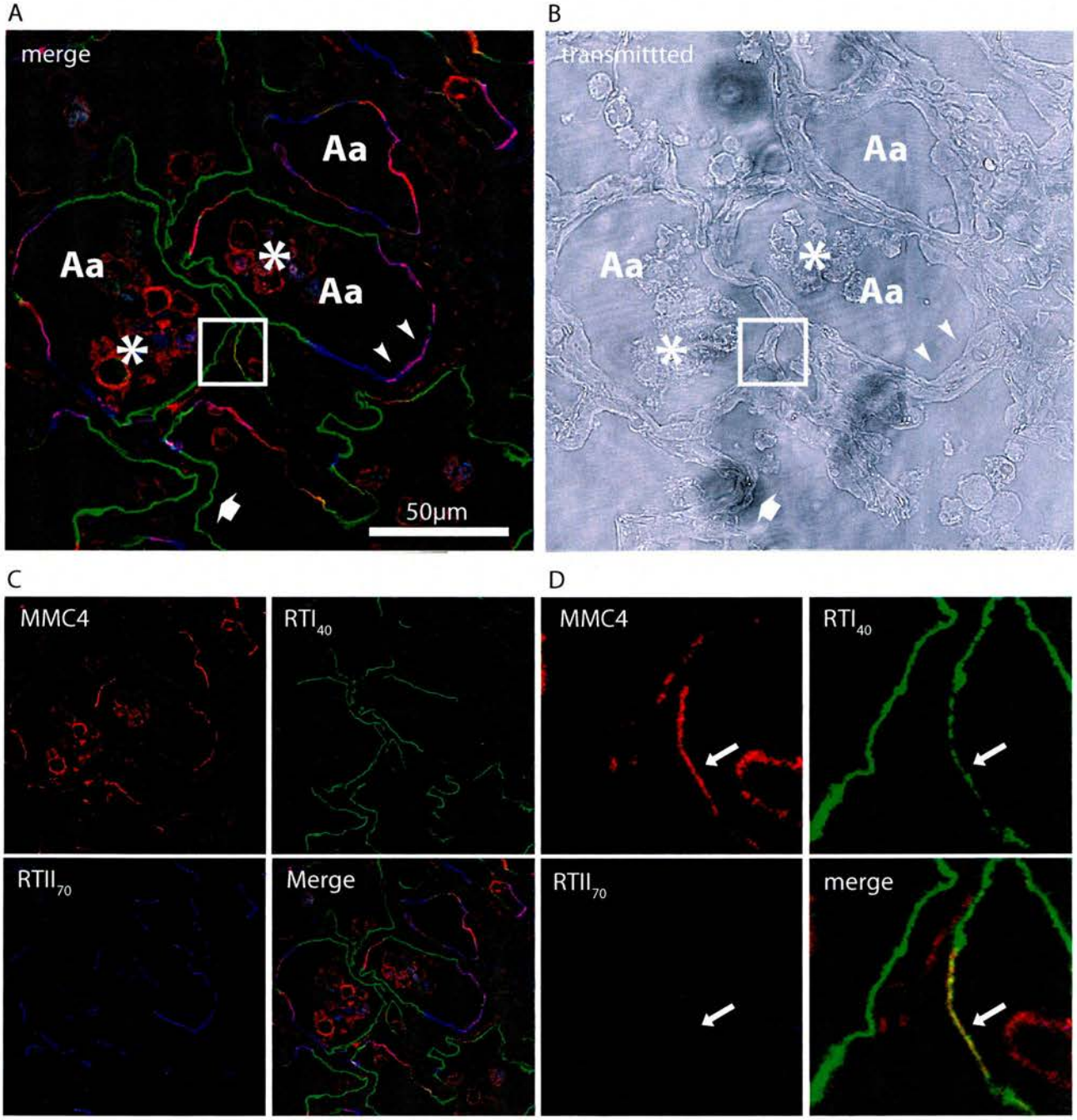

Inflamed rat lung sections stained with MMC4 (red 546), RTI_{40} (green 488) and $RTII_{70}$ (blue 647). Images demonstrate that the surface area of alveolar walls co-expressing the ATII cell markers MMC4/$RTII_{70}$ is increased in comparison to control lungs (purple cells, small arrowheads). While the alveolar surface covered by the ATI cell marker, RTI_{40} is decreased in comparison to control lungs (green, broad arrow). Some alveolar membranes are stained with a new combination of MMC4 (red) and RTI_{40} (green) to generate yellow membranes (inset magnified in (D) longer arrow indicates MMC4/RTI_{40} positive area). Image also demonstrates that monocytes/macrophages in the airspaces express MMC4 (asterisks).

figure 16

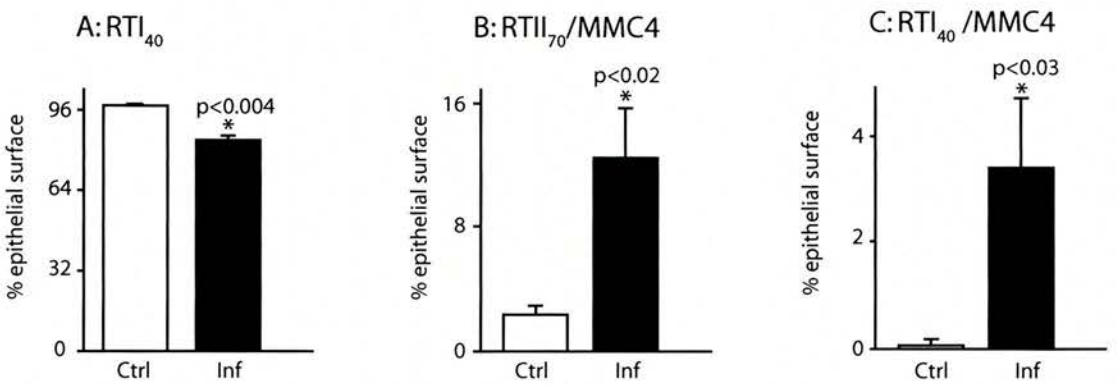

Percentage of the alveolar wall covered by ATI and ATII cell-markers in S. aureus-injured (n=3) and control (n=5) lungs. Images captured and analyzed as detailed in Methods. The total epithelial surface measured in control and S. aureus-treated lungs was 16,063 ± 3,058 µm and 15,783 ± 1,203 µm, respectively. A: ATI cells (RTI_{40}-positive membranes), B: ATII cells ($RTII_{70}$/MMC4-coexpressing membranes). C: Alveolar Intermediate cells (RTI_{40}/MMC4-coexpressing membranes). (Error bars show SEM).

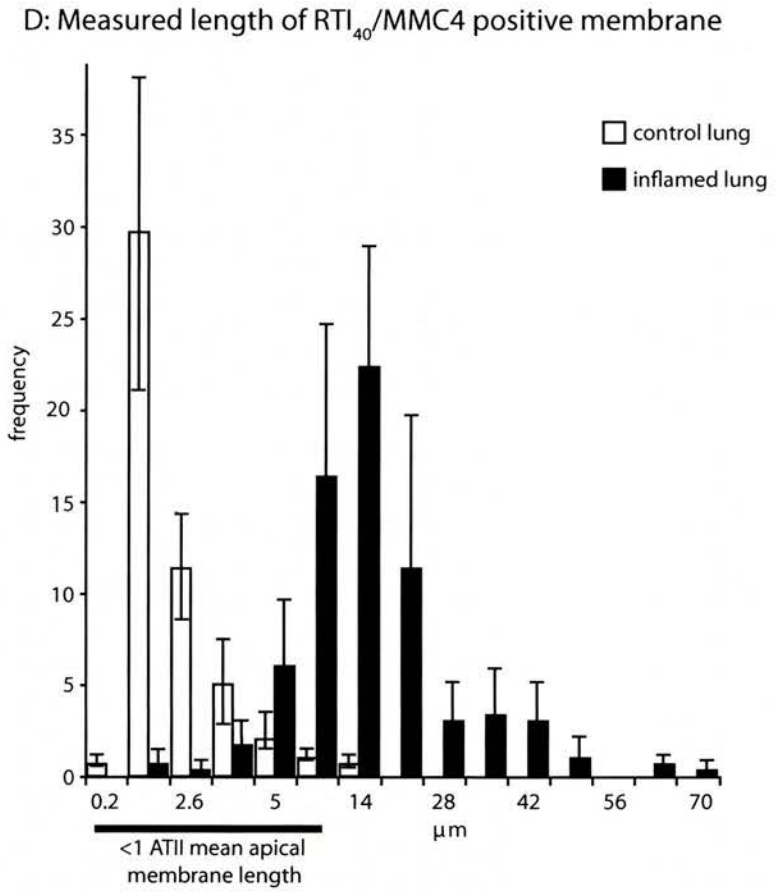

D: Frequency histogram shows the distribution of the measured lengths of alveolar epithelium that co-expressed MMC4 and RTI_{40} in control lungs (n=5), and inflamed lungs (3 days post injury, n=3). Almost all of the segments of epithelial surface expressing MMC4/RTI_{40} in the control lung were less than the mean apical membrane length for a ATII cell (i.e. < 7µm). In contrast to this, most of the MMC4/RTI_{40} expressing areas in repairing lung were more than one cell in length - the majority being more than 7µm long. (Error bars show SEM).

figure 17

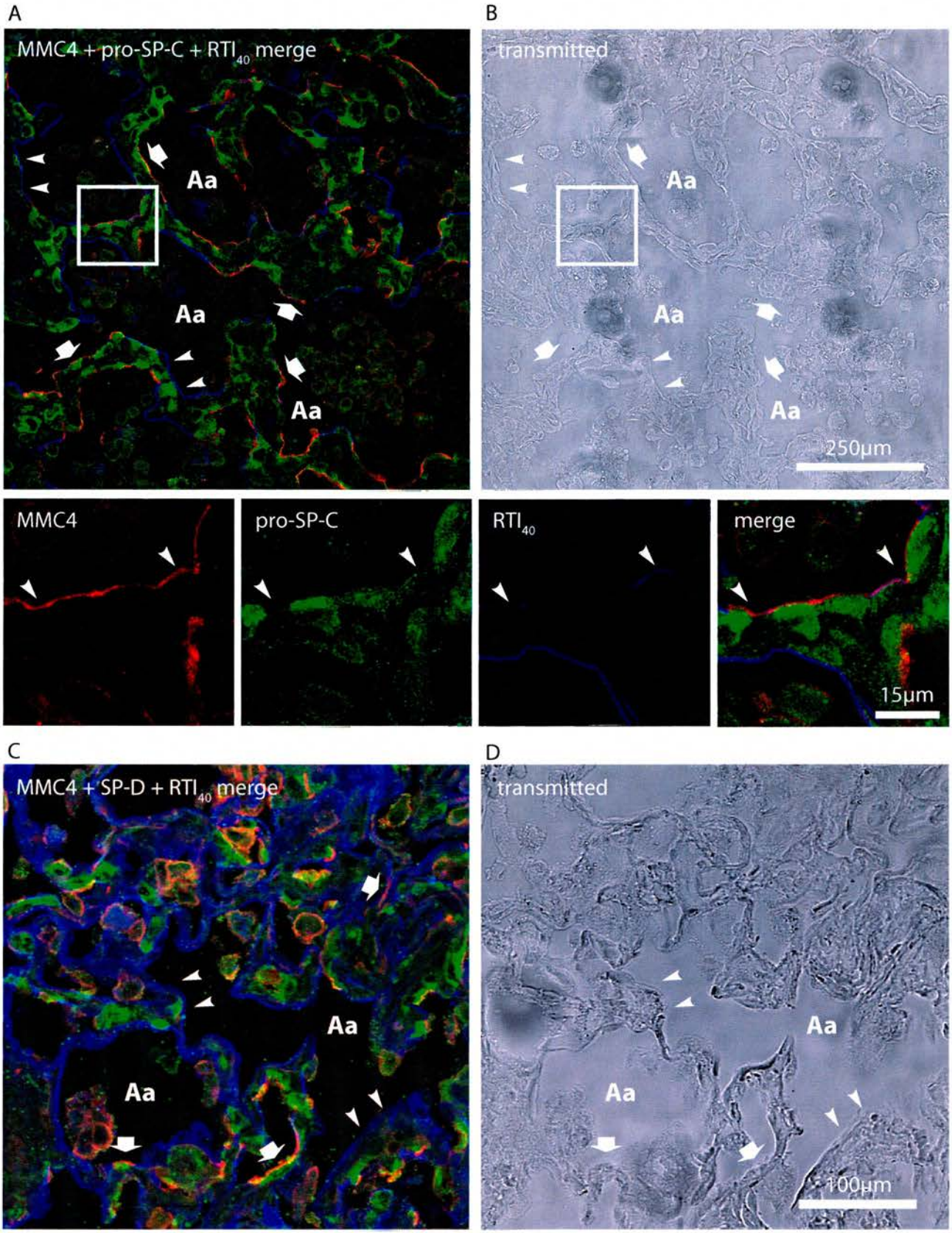

Inflamed rat lung day 3 after infection is stained with MMC4 (red 546), anti-RTI_{40} (blue 647) and anti-pro-SP-C (green 488) or anti-SP-D (green 488). Alveolar walls are lined by RTI_{40} positive cells double arrows, and MMC4 positive cells (broad arrows). Cells with MMC4 positive apical membrane do not universally stain positive for pro-SP-C or SP-D. MMC4/RTI_{40} positive cells are also visible in (A) which do not consistently stain positive for pro-SP-C (inset in (A) and separations - single arrowheads).

figure 18

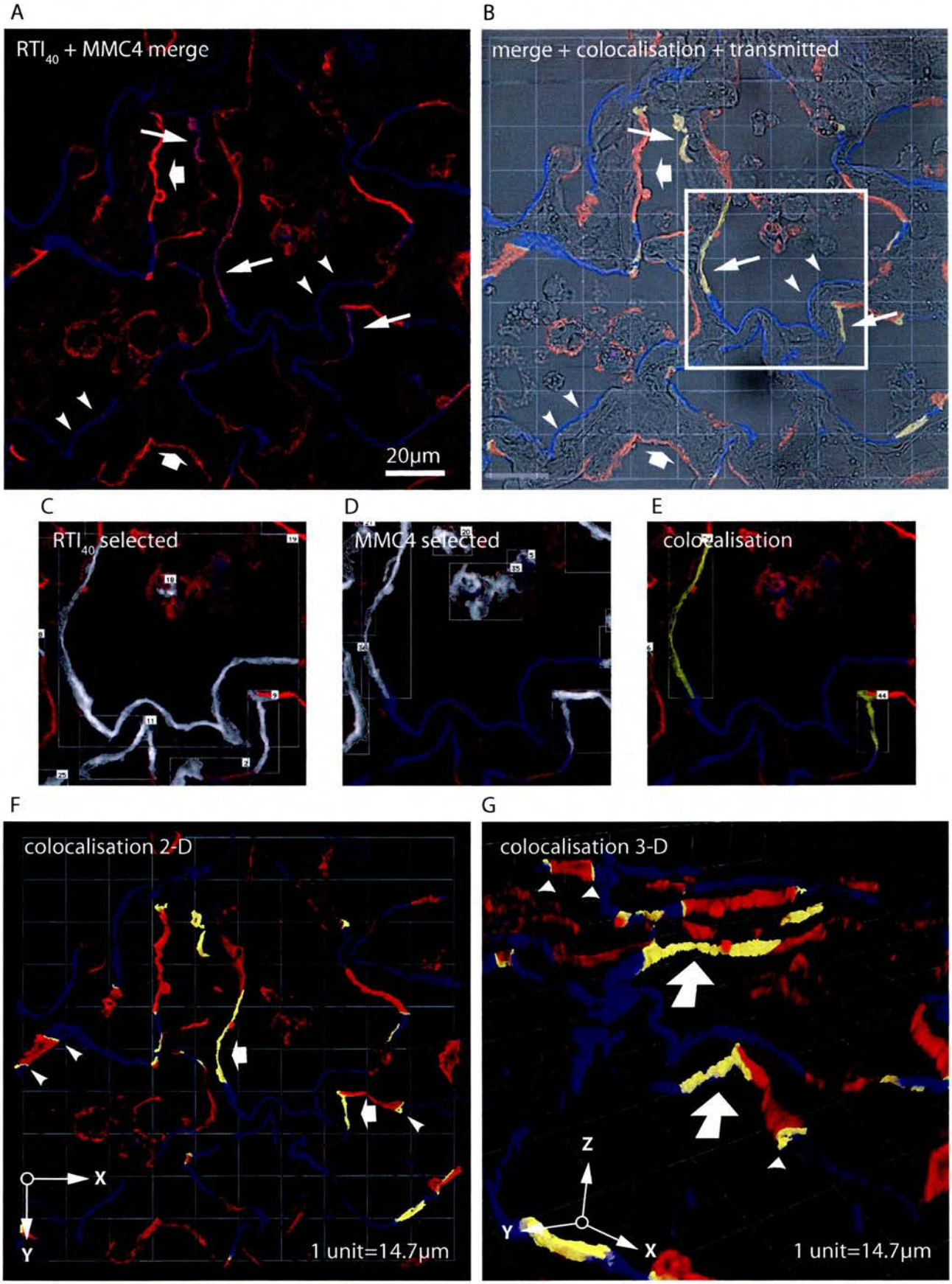

Repairing rat lung alveolar epithelium 3 days after injury stained with MMC4 (red 546), and RTI_{40} (blue 647). In (A) Most of the epithelial surface is RTI_{40} positive (double arrows), but a significant proportion is MMC4 positive (broad arrows). Some areas are MMC4/RTI_{40} positive (purple staining, longer arrows). Using image analysis software, the areas colocalising MMC4/RTI_{40} can be identified and superimposed on the transmitted image (B). Areas of interest (i.e. not inflammatory cells) can be isolated and the colocalisation viewed in 2D (yellow areas in (F)). Using image stacks from the LSCM, the pattern of colocalisation through the entire depth of the section can be viewed in 3D (G). It is easily seen in (G) where colocalisation is merely a ATI-ATII cell junction (arrowheads), and where severel cells are co-expressing RTI and MMC4 at their apical membranes (large arrows).

figure 19

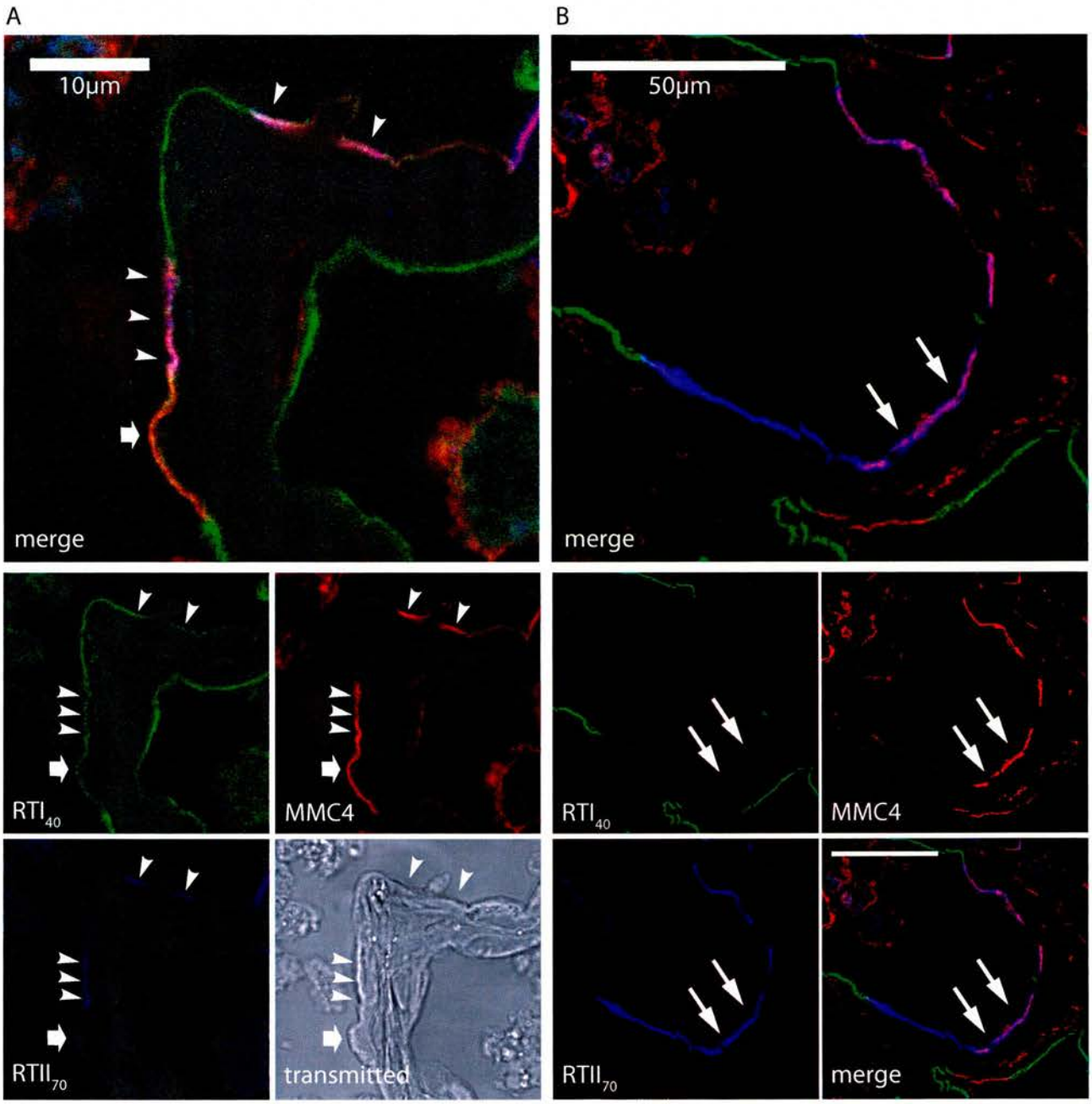

Repairing rat lung stained with MMC4 (red 546), RTI_{40} (green 488) and $RTII_{70}$ (blue 647). The epithelium in (A) shows an area of MMC4/RTI_{40} staining (broad arrow), but also other areas which are positive for both ATII markers MMC4 and $RTII_{70}$ in addition to RTI_{40} (arrowheads). (B) Shows an area of epithelium where several adjacent cells have a ATII cell MMC4/$RTII_{70}$ phenotype (double arrows).

figure 20

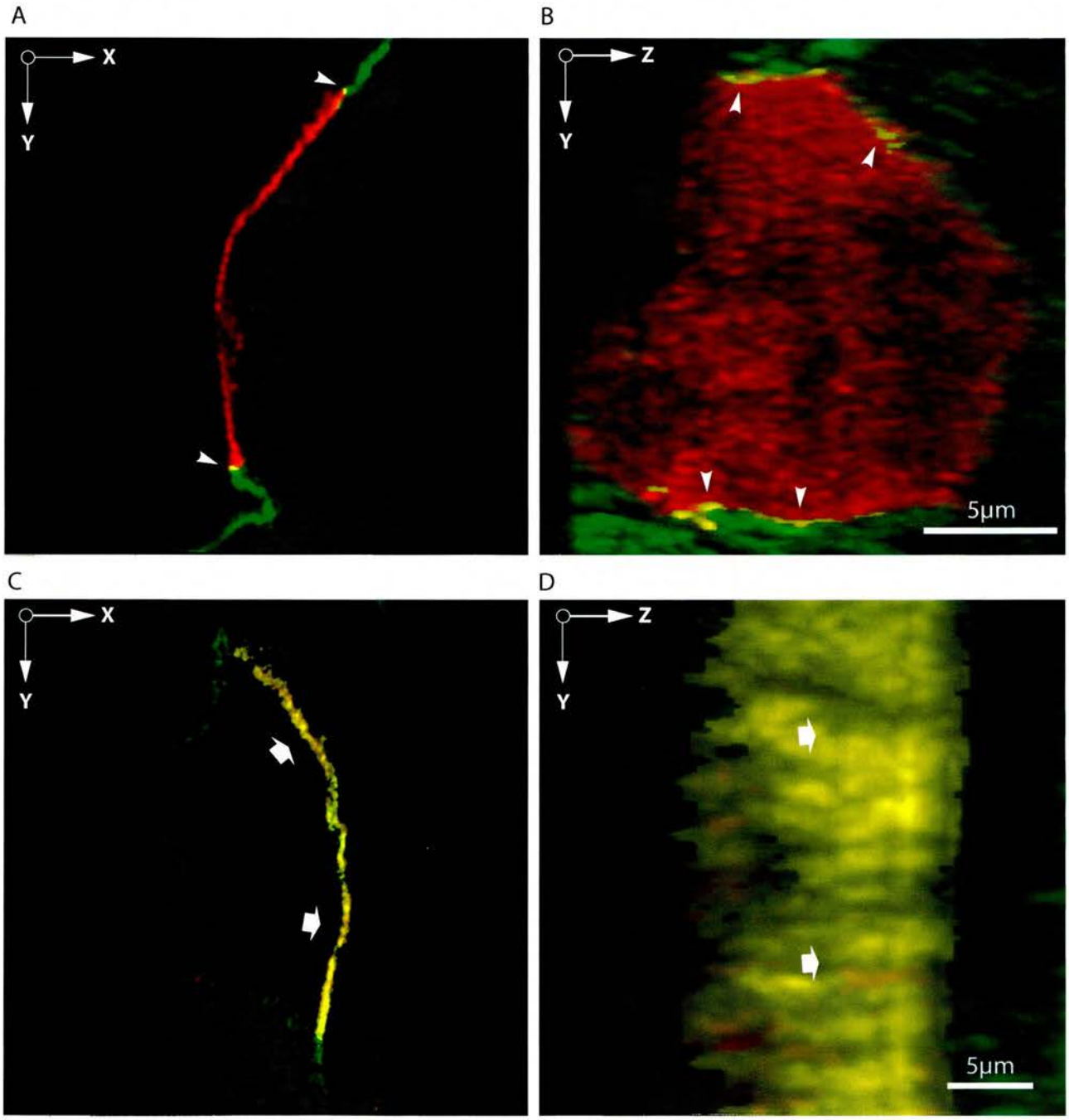

(A) and (B) show perpendicular views of a small segment of rat control lung alveolar epithelium stained with MMC4 (red 546) and RTI_{40} (green 488). The MMC4 positive apical membrane of a ATII cell is visible, flanked by RTI_{40} positive ATI cells. After image deconvolution there is a small area of yellow where the green and yellow signal occupy the same voxel (single arrowheads) - this represents the limits of this imaging system in resolving the junction between ATI and ATII cells.

In (C) and (D) a segment of repairing rat lung alveolar epithelium has been similarly stained. the membrane shows colocalisation of red and green signal across the whole depth of the section (broad arrows), indicating that this area of epithelium is uniformly expressing both MMC4 and RTI_{40}.

figure 21

Measured length of ATII cell (MMC4/RTII$_{70}$ positive) membrane in control and inflamed lungs

A: control lungs

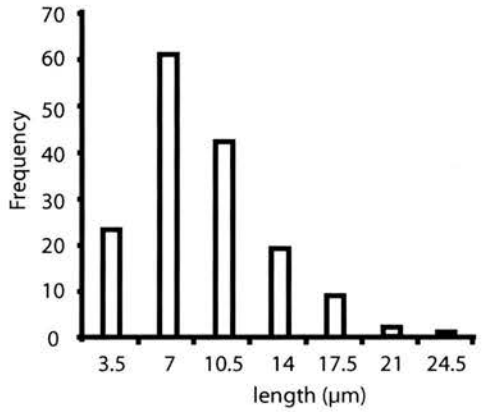

B: inflamed lungs

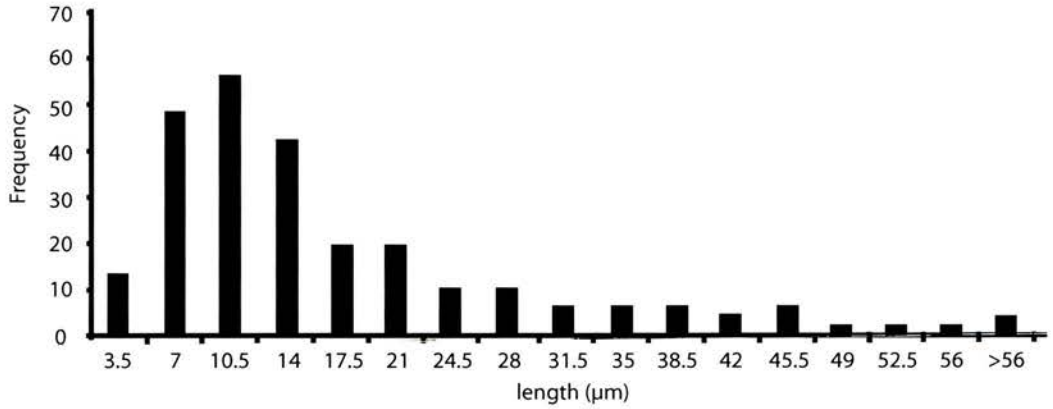

The lengths of individual segents of epithelial membrane expressing ATII cell markers MMC4 and RTII$_{70}$ have been plotted in the form of a frequency histogram for control (n=5) and inflamed (n=3) lungs. The mean value for the length of ATII celll apical membrane is ~7μm, and the majority of control ATII cells were measured at around this length. Inflamed lungs had a mean segment length of ~15μm, with many segments of ATII cell phenotype epithelim which were significantly longer than this.

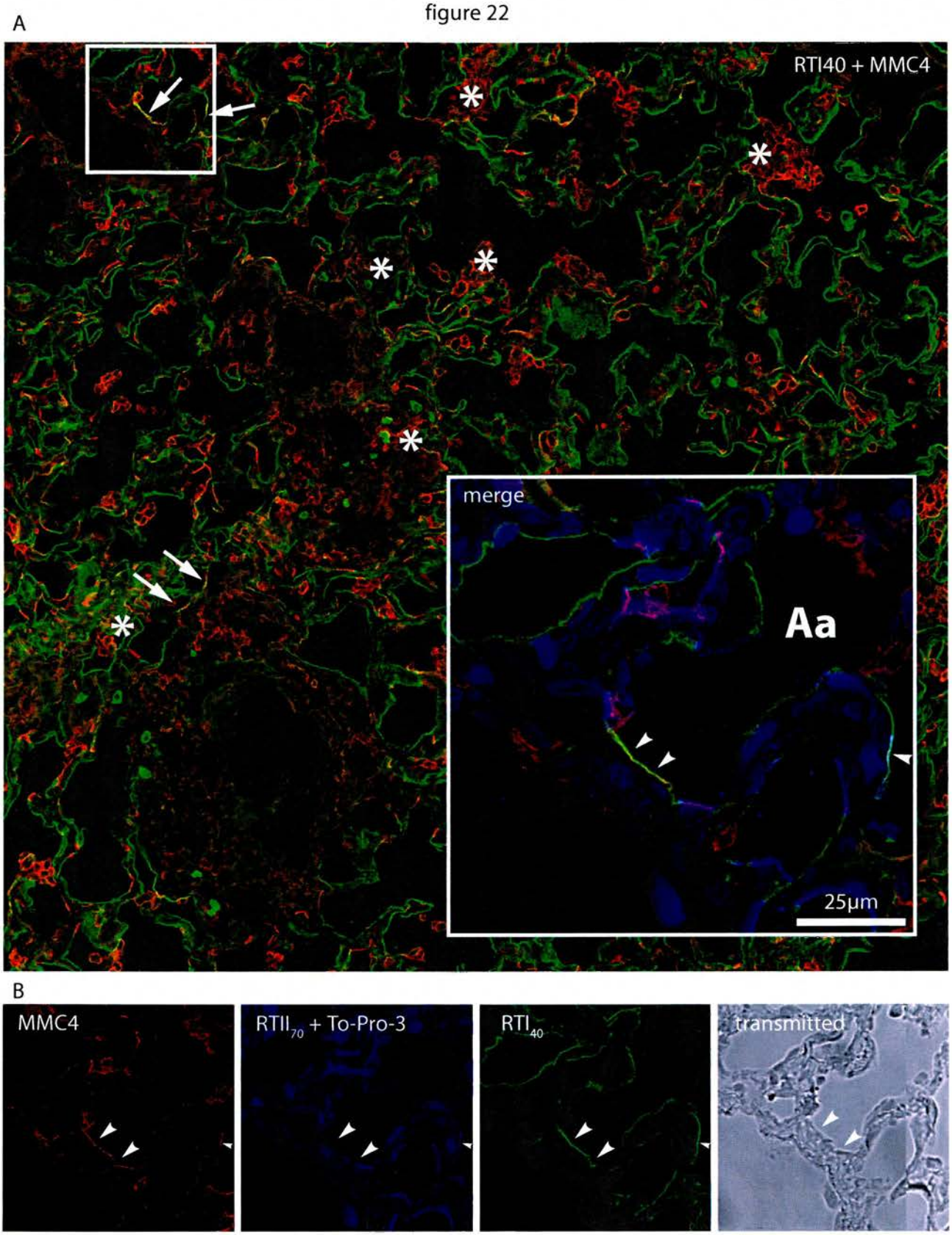

Rat lung 24 hours after instillation of *S pneumoniae*, stained with MMC4 (red 546), RTI_{40} (green 488), $RTII_{70}$ and DNA dye TO-PRO-3 (blue 647). The lower power view (A) shows a significant inflammatory infiltrate in many alveolar airspaces (asterisks). Most of the alveolar epithelium is covered by RTI40 positive ATI cells, with MMC4 positive ATII cells also visible (NB inflammatory cells in the airspaces are also stained red with MMC4). A population of MMC4/RTI_{40} positive intermediate phenotype alveolar epithelial cells is also visible (white arrows). The higher magnification inset in (A) and seperate colour channel images in B show an area of MMC4/RTI_{40} positive epithelium (arrowheads).

figure 23

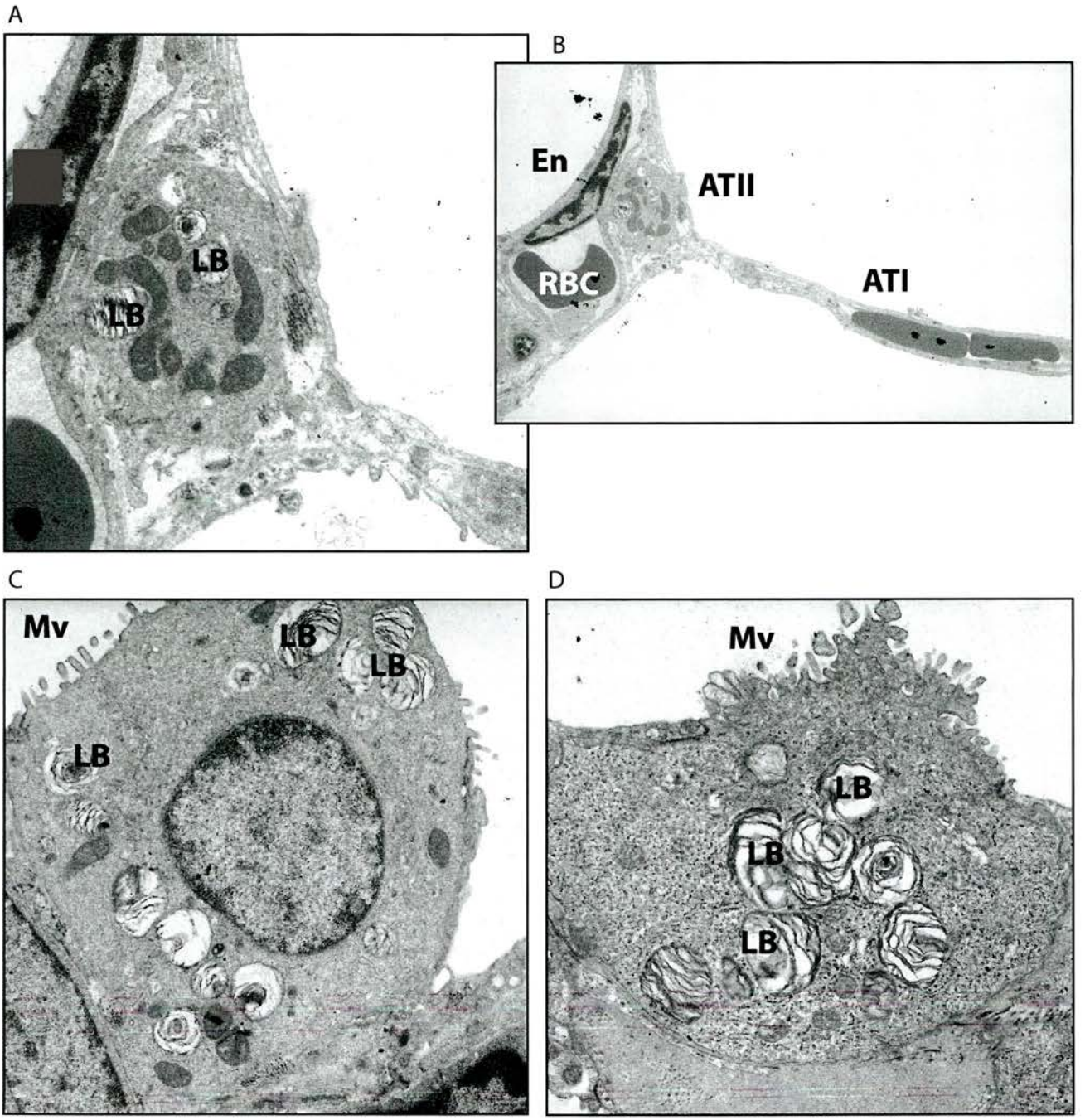

Long thin attenuated ATI cells characteristically showing a paucity of organelles with only the prominent nuclei evident - (B). Cuboidal ATII are positioned in the corners of the alveoli, flanked by ATI (B) and closeup in (A). (B) also shows an endothelial cell (En) and erythrocyte (RBC) making up the other components of the alveolar air-blood barrier. The *sine qua non* of ATII cells is presence of surfactant containing lamellar bodies (LB) which resemble the layers of an onion in cross-section (C) and (D). ATII also have microvilli (Mv) at their apical surface.

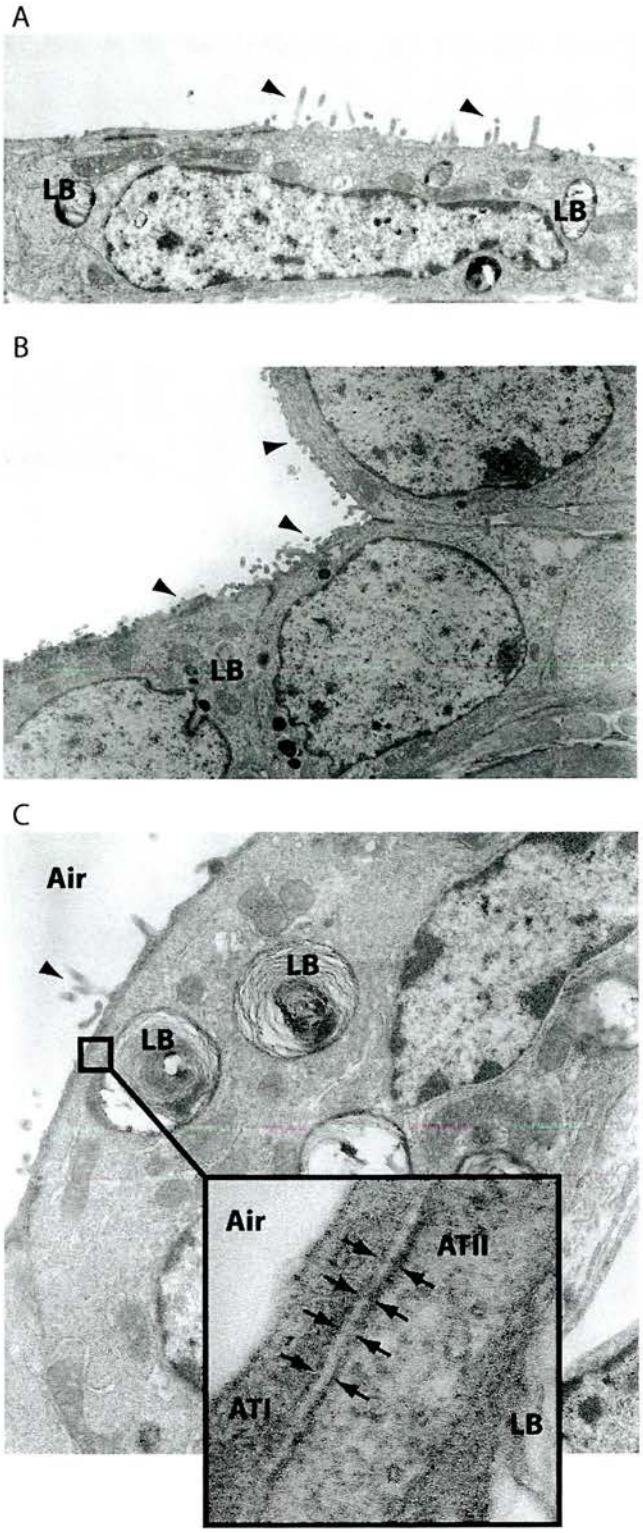

Electron microscopic examination of the rat alveolar epithelium during repair. Some epithelial cells had more typical ATII cell features lamellar bodies (LB), apical microvilli (arrowheads) but appeared to be spreading, and had reduced perinuclear cytoplasm (A). Other cuboidal epithelial cells lacked both microvilli and lamellar bodies (B). In some places ATI cells (or ATI-like cells) were observed overlying ATII cells (C), inset shows a high magnification view of one cell membrane overlying another (arrows).

figure 25

A Pap stain of ATII cell cytospin

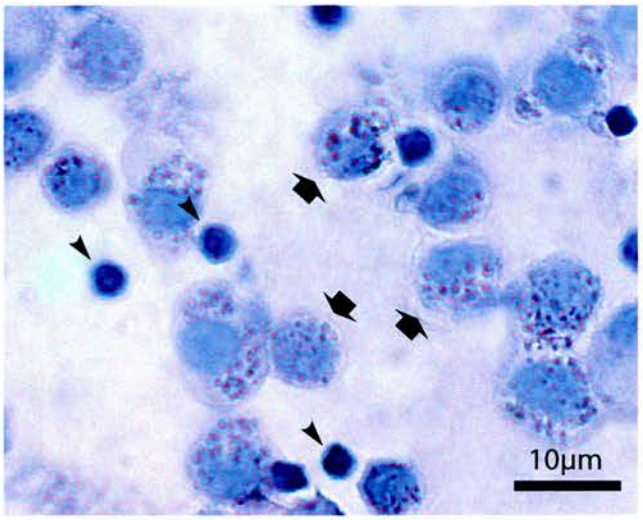

B Cytospin cell counts (pap staining)

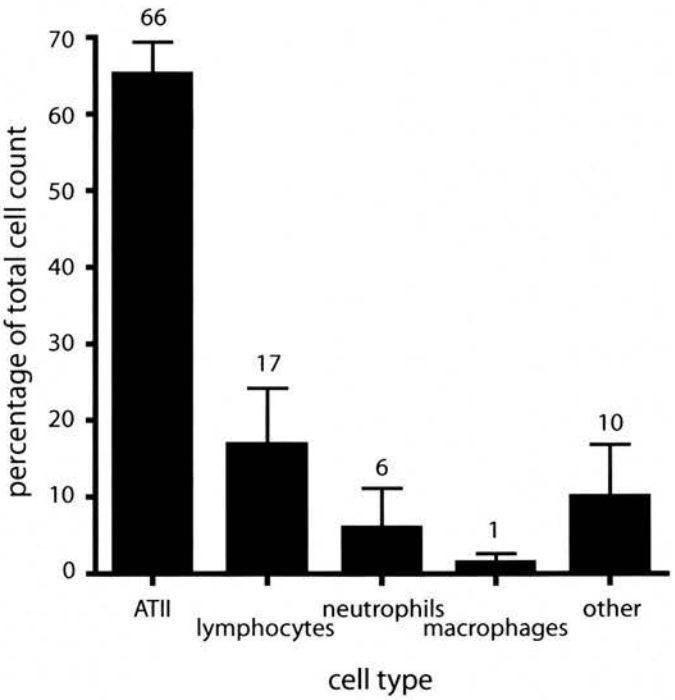

Cytospin preparations of freshly isolated rat ATII cells (n=3) were Pap stained and differential cell counts performed. ATII cells with characteristic lamellar bodies staining dark purple can be seen in (A) (broad arrows), contaminating lymphocytes are also visible (arrowheads). (B) Shows the types and quantities of contaminants routinely present in the ATII cell preparations. (Error bars show SEM).

figure 26

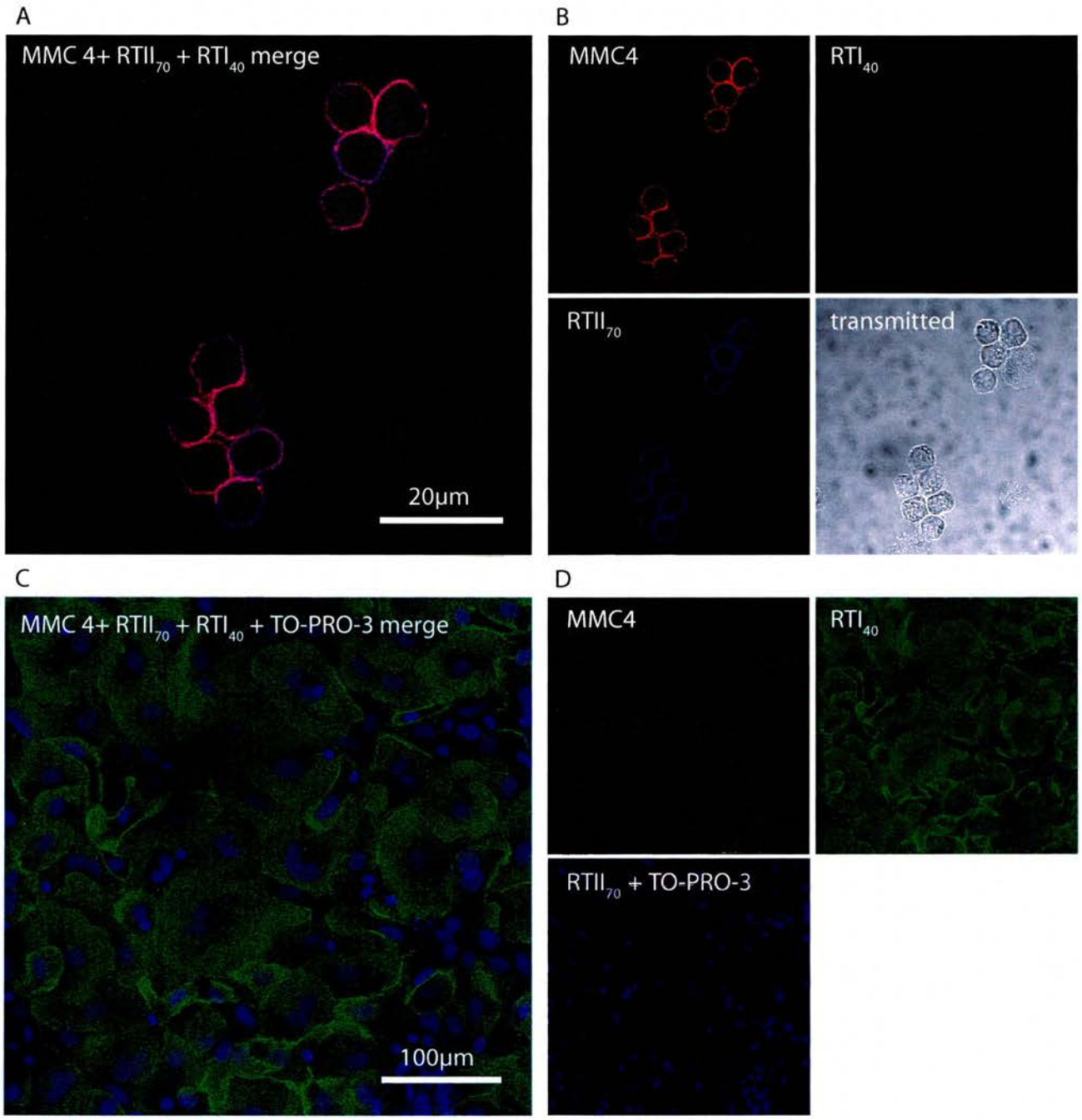

Rat alveolar epithelial cells in primary cell culture stained with MMC4 (red 546), anti-RTI_{40} (green 488), and anti-$RTII_{70}$ (blue 647). Freshly isolated ATII cells are stain positively with MMC4 and anti-$RTII_{70}$, but not anti-RTI_{40} (A) and (B). After five days in culture, the ATII cells have acquired some characteristics associated with the mature ATI cell type - they become flattened, no longer stain with MMC4 or anti-$RTII_{70}$, and are positive for anti-RTI_{40} (C) and (D).

figure 27

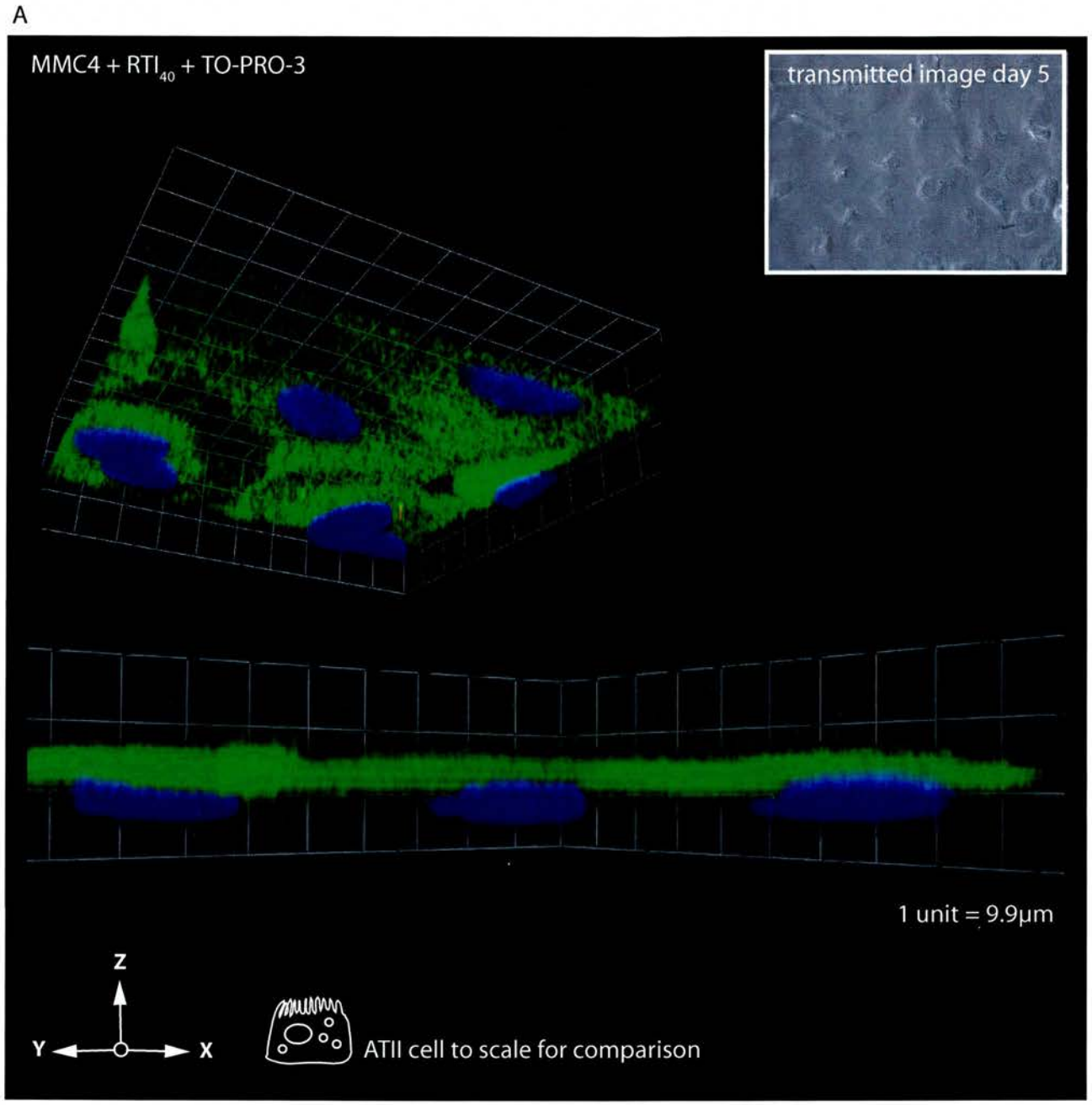

Rat ATII cells after five days in culture stained with MMC4 (red 546), anti RTI_{40} (green 488) and TO-PRO-3 (blue 647). ATII in culture at this time point have acquired some of the characteristics of mature ATI cells - they are flattened and attenuated, with large nuclei. Cells no longer stain positively with MMC4 but are positive for RTI_{40}, a ATI cell specific antibody. (A) Is a 3D image of cells in culture demonstrating the change in morphology - a schematic of a freshly isolated ATII cell is drawn to scale for comparison. (B) Shows traditional 2D immunofluoresence images showing MMC4 negative/RTI_{40} positive staining.

figure 28

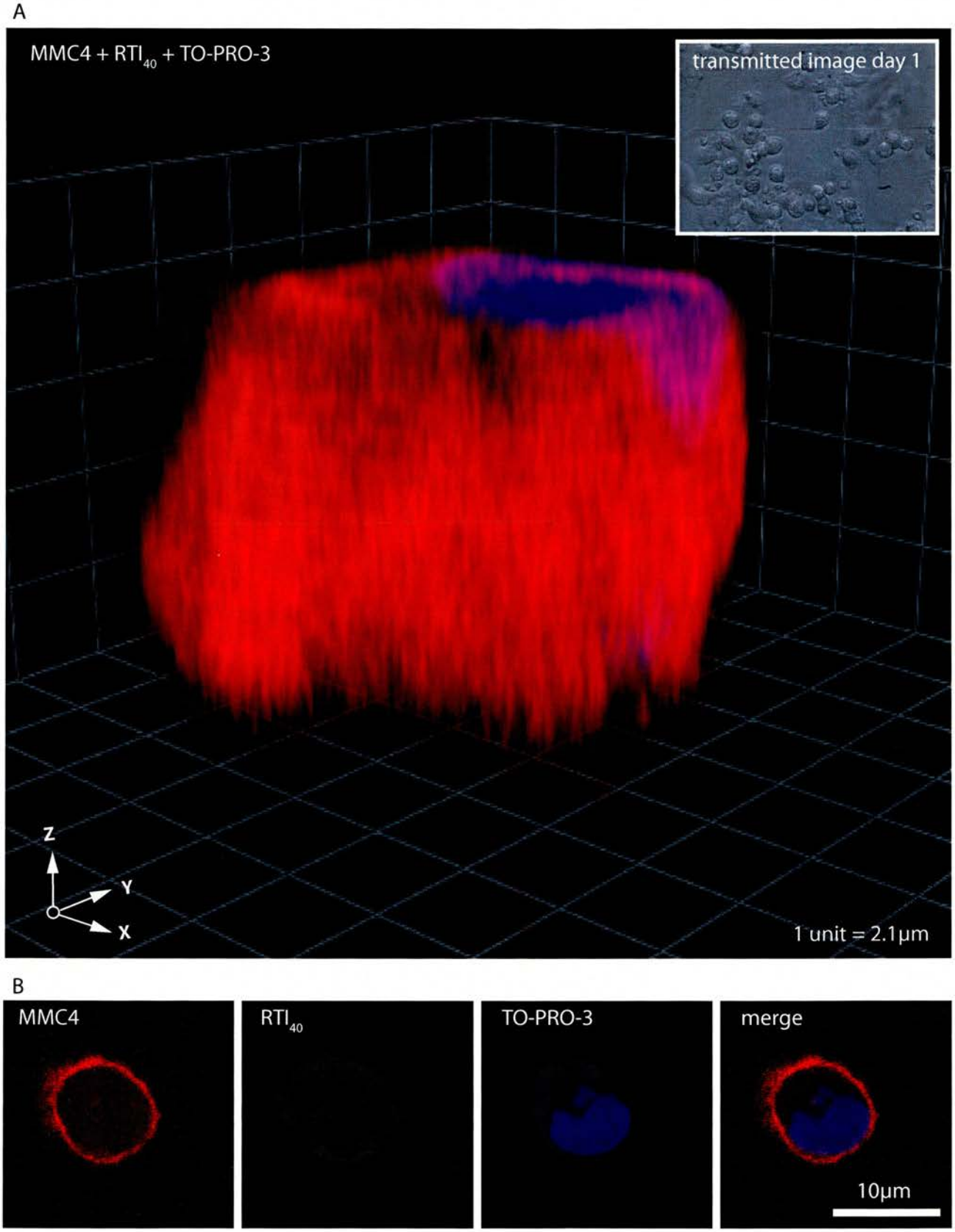

Rat ATII cell in primary culture stained with MMC4 (red 546), anti-RTI_{40} (green 488) and TO-PRO-3 (blue 647). The 3D image in (A) shows the typical cuboidal shape, (B) is a set of traditional 2D immunofluorescence images demonstrating positive staining with the ATII-cell specific marker MMC4. The cell is negative for RTI_{40}.

figure 29

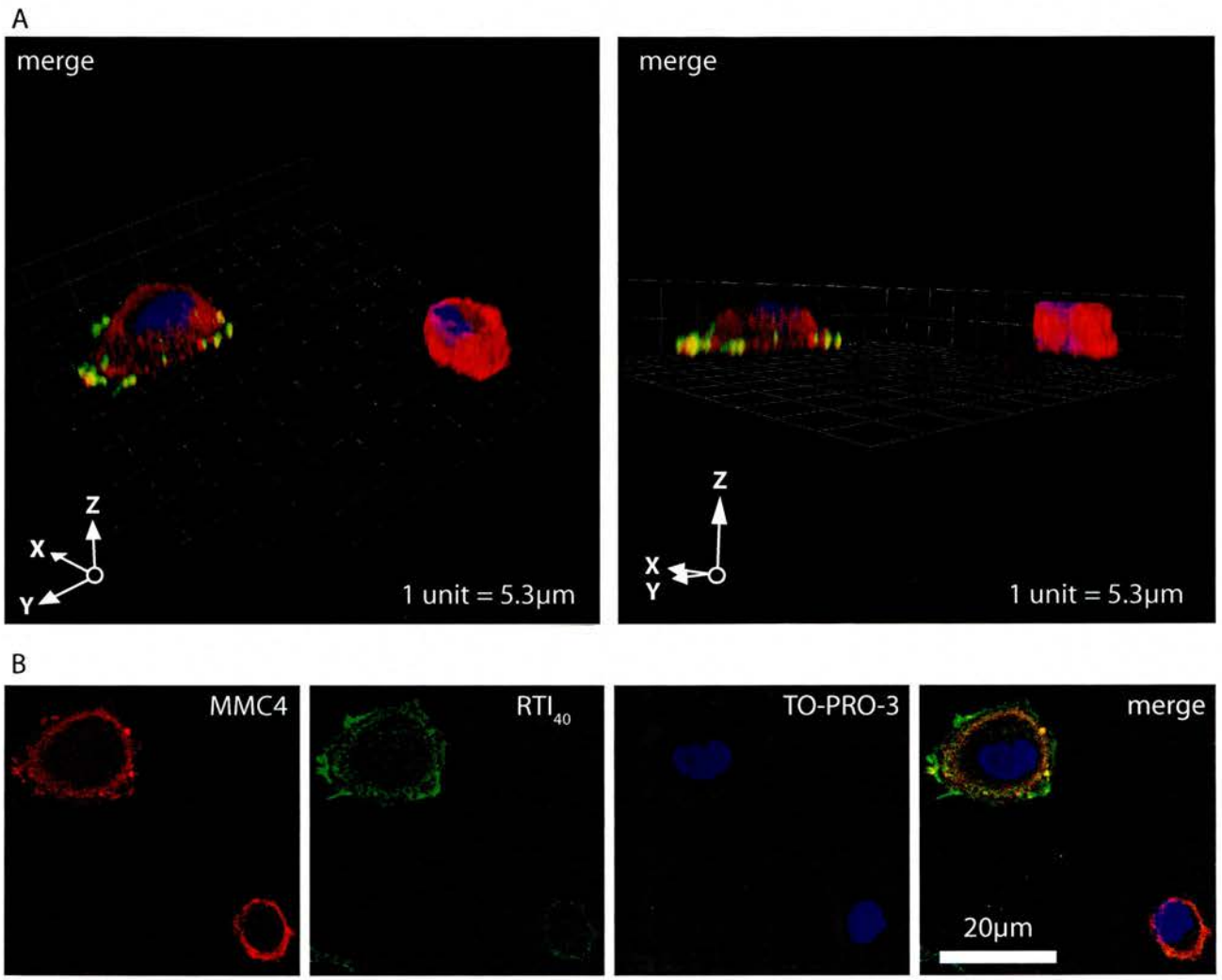

Rat ATII cell in primary culture stained with MMC4 (red 546), RTI_{40} (green 488) and TO-PRO-3 (blue 647). After 1 day in culture some cells have begun to spread and flatten, with a sub-population staining positive for both MMC4 and RTI_{40} (B). 3D visualisation of these cells (A) shows that RTI_{40} is localised to the periphery of the cell at the basal surface.

figure 30

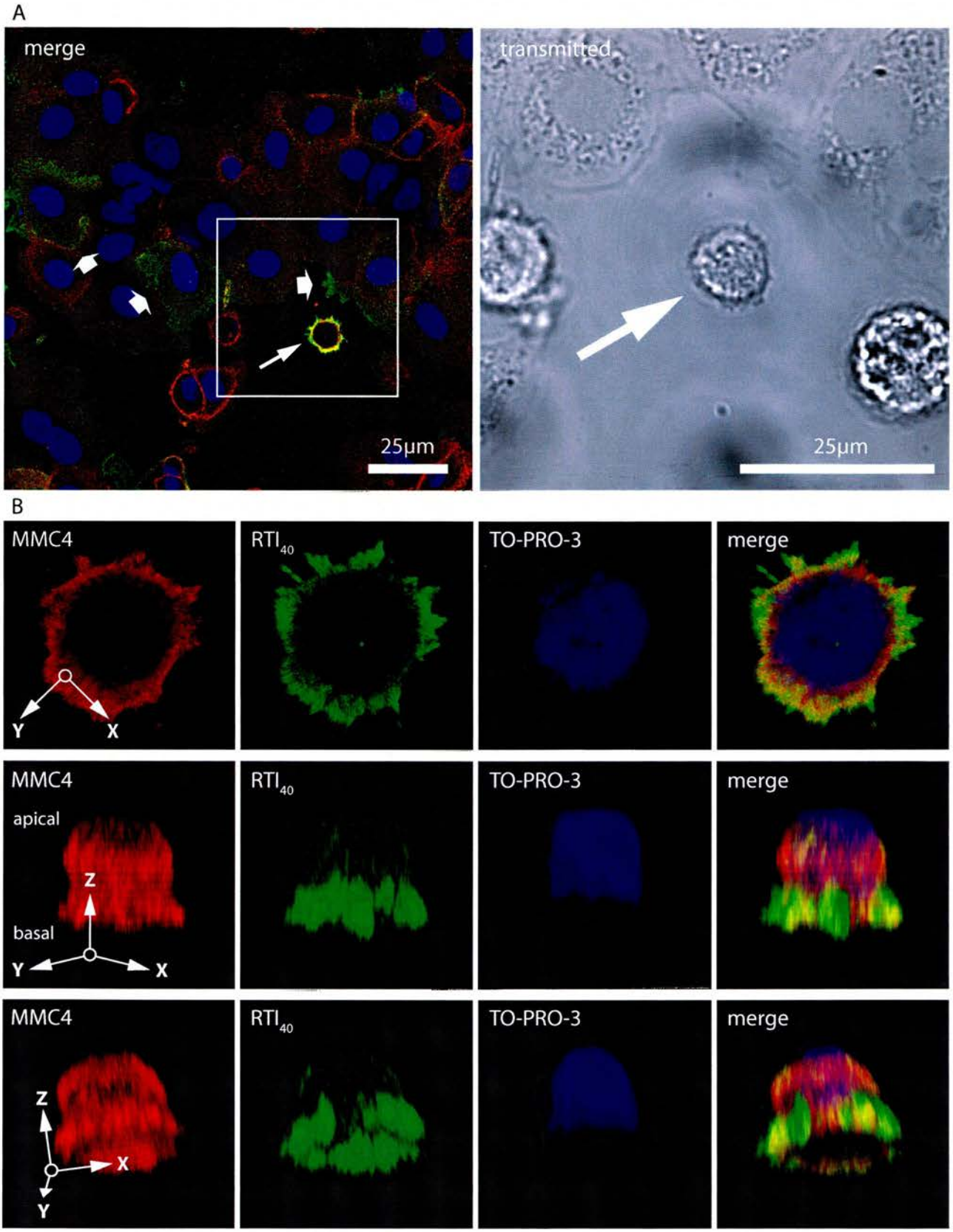

Rat ATII cells in primary culture at day 1 stained with MMC4 (red 546), RTI_{40} (green 488), TO-PRO-3 (blue 647). Many cells can be seen flattening and taking on a more ATI-like morphology. Some cells are beginning to stain positively for RTI_{40} (broad arrow). A small population of cells stains strongly for MMC4 and RTI_{40} (longer arrow). (B) 3D imaging of the co-expressing cell highlighted in (A) (longer arrow) reveals that RTI_{40} is localised to the spreading basal surface of the cell.

figure 31

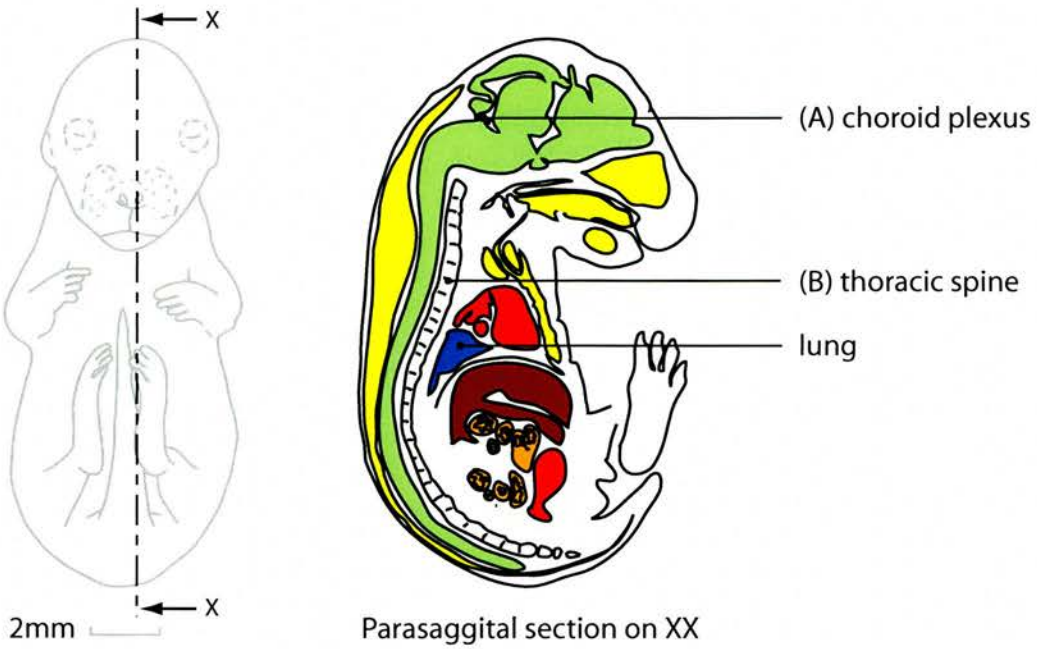

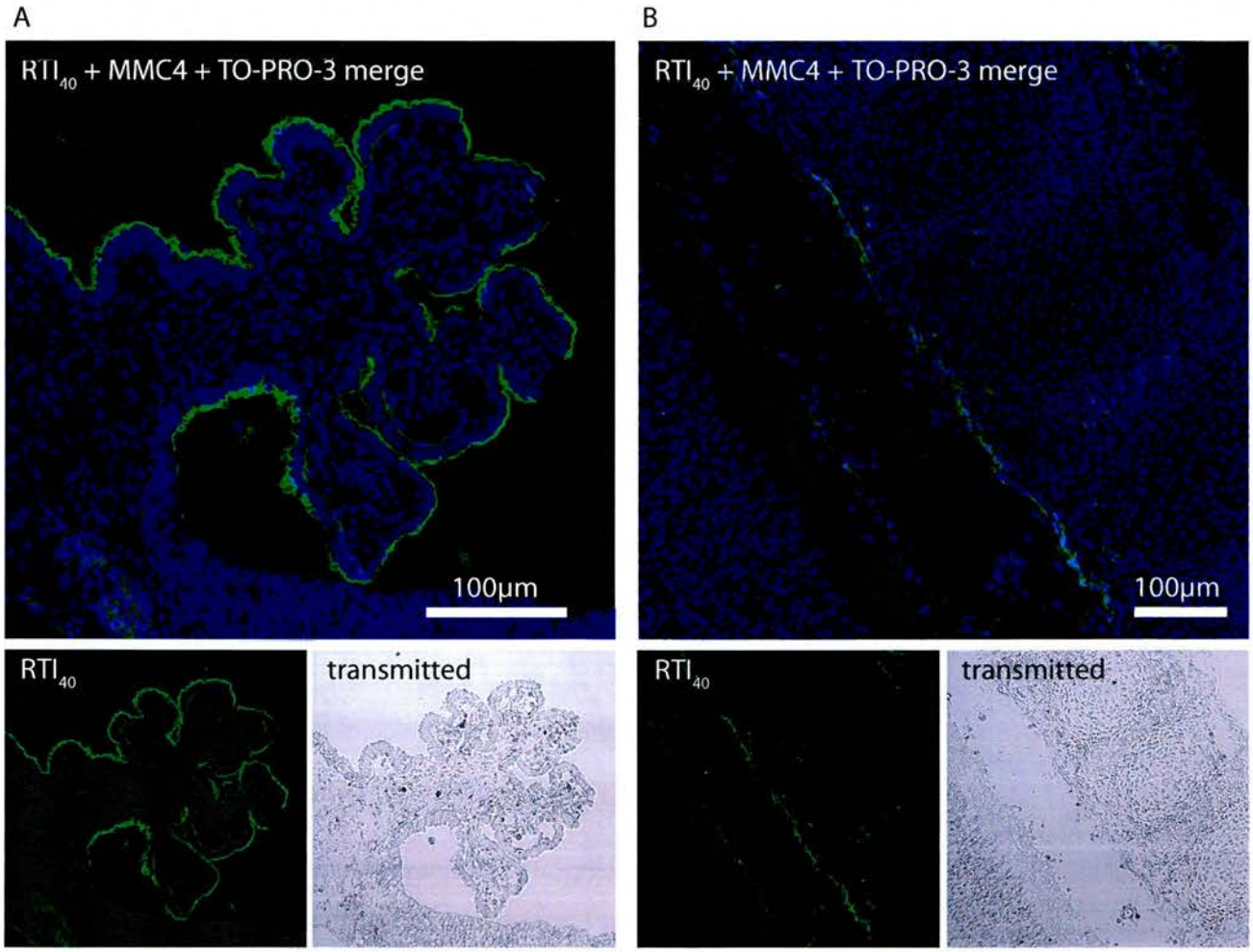

Schematic shows the gross anatomy of the developing rat at embryonic day 16/21 (E16). A parasaggital section stained with MMC4 (red 546), RTI_{40} (green 488) and TO-PRO-3 (blue 647) showed positive RTI_{40} staining in the choroid plexus (A) and around the spinal canal (B) at the level of the thoracic spine. No staining was seen in the embryonic lung at this stage. (Schematic diagram redrawn using comparative information from *The Atlas of Mouse Development* MH Kaufman (Editor), Academic Press 1992).

figure 32

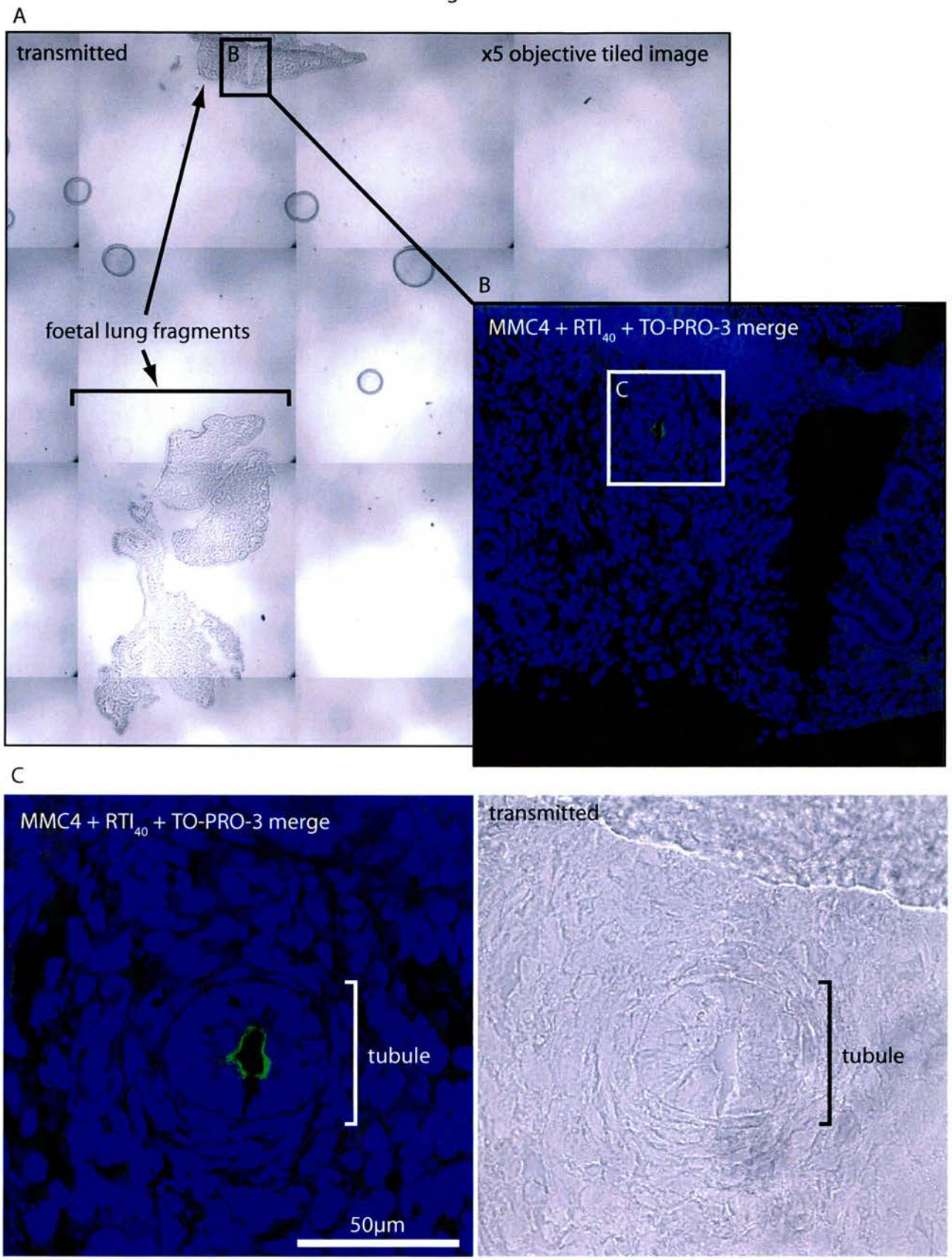

Foetal rat lung at embryonic day 17/21 (E17) stained with MMC4 (red 546), RTI_{40} (green 488) and TO-PRO-3 (blue 647). (A) Shows a 'tiled' image of several fields of view obtained using the x5 objective and includes two tissue fragments. Higher power views in (B) & (C) show an example of the occasional tubules lined with RTI_{40} positive airway epithelial cells.

figure 33

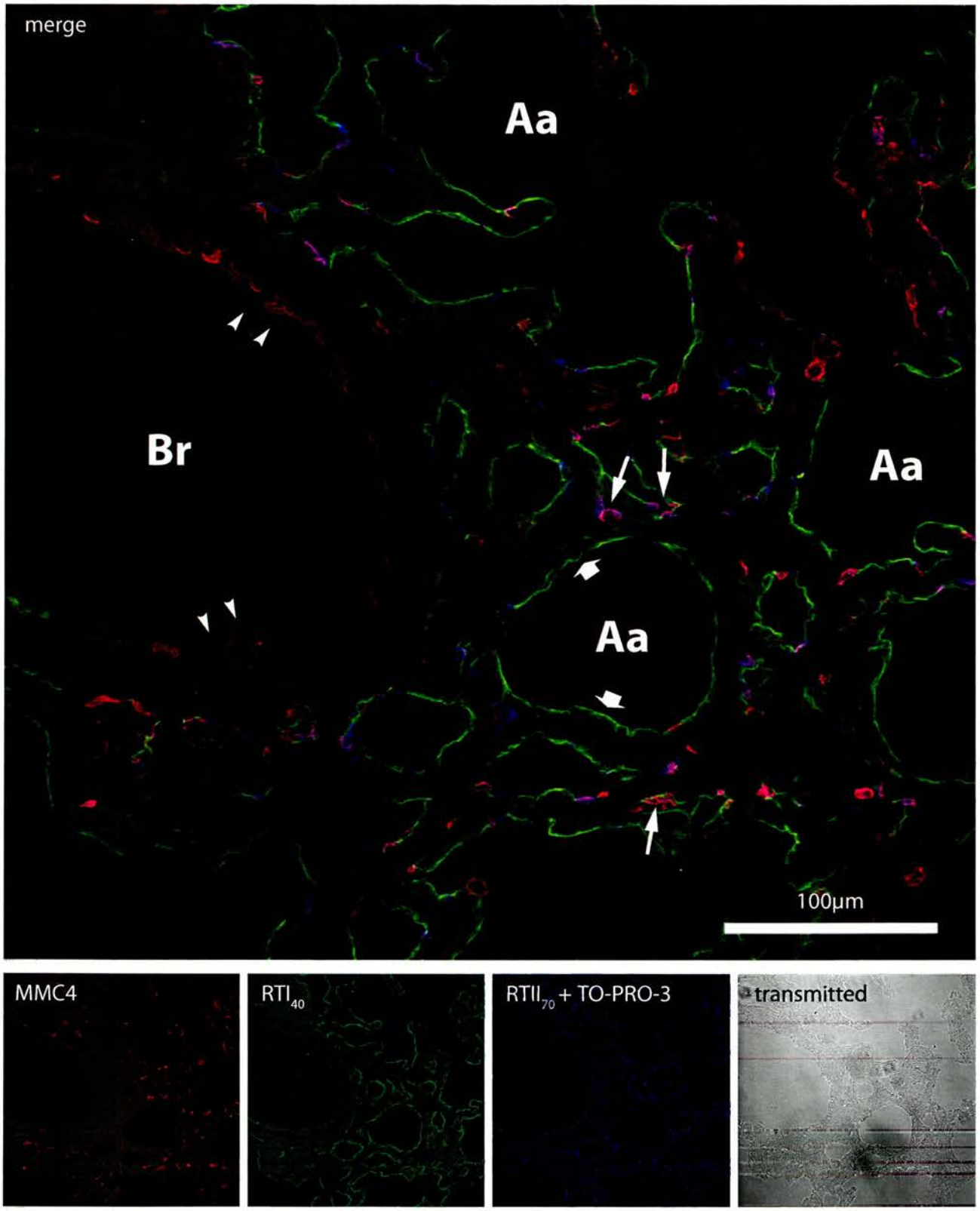

Foetal rat lung at embryonic day 20/21 (E20) stained with MMC4 (red 546), RTI_{40} (green 488), $RTII_{70}$ (blue 647) and TO-PRO-3 (blue 647). Alveolar airspaces (Aa) are separated by thickened cellular septae, lined with RTI_{40} positive epithelial cells (broad arrows). Putative ATII cells expressing MMC4 and $RTII_{70}$ appear in clusters (long arrows). A bronchiole is visible (Br) lined by epithelium containing many MMC4 positive, $RTII_{70}$ negative Clara cells (double arrowheads).

figure 34

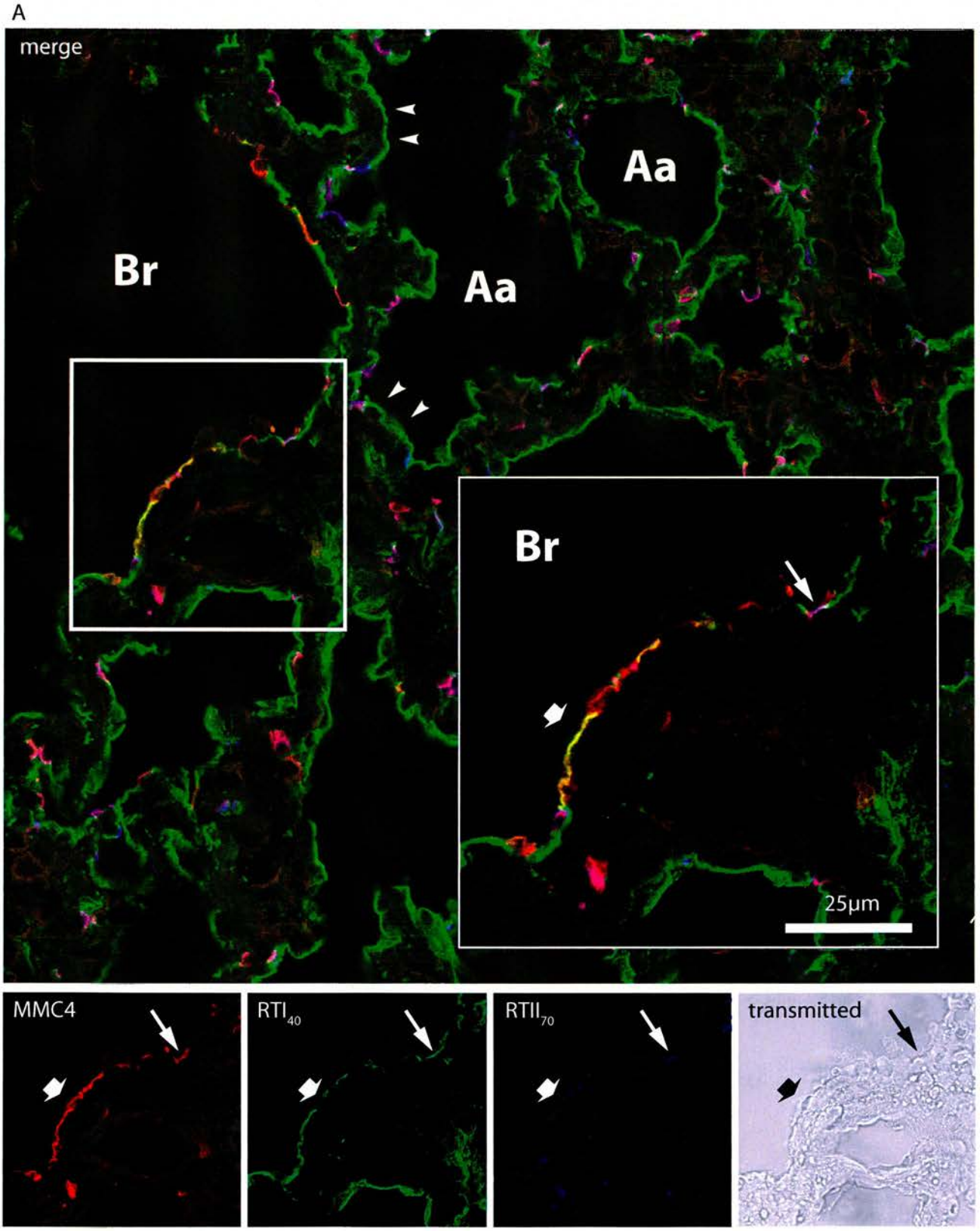

Rat lung at post-natal day 3 stained with MMC4 (red 546), RTI_{40} (green 488) and $RTII_{70}$ (blue 647). The alveolar airspaces are lined by RTI_{40} positive cells, with cells expressing both MMC4 and $RTII_{70}$ scattered throughout. MMC4/RTI_{40} co-expressing cells were not seen in the alveolar epithelium, but were evident in the bronchiolar epithelium (broad arrow) along with occasional cells around the broncho-alveolar junction which expressed MMC4/RTI_{40} and $RTII_{70}$ (long arrows).

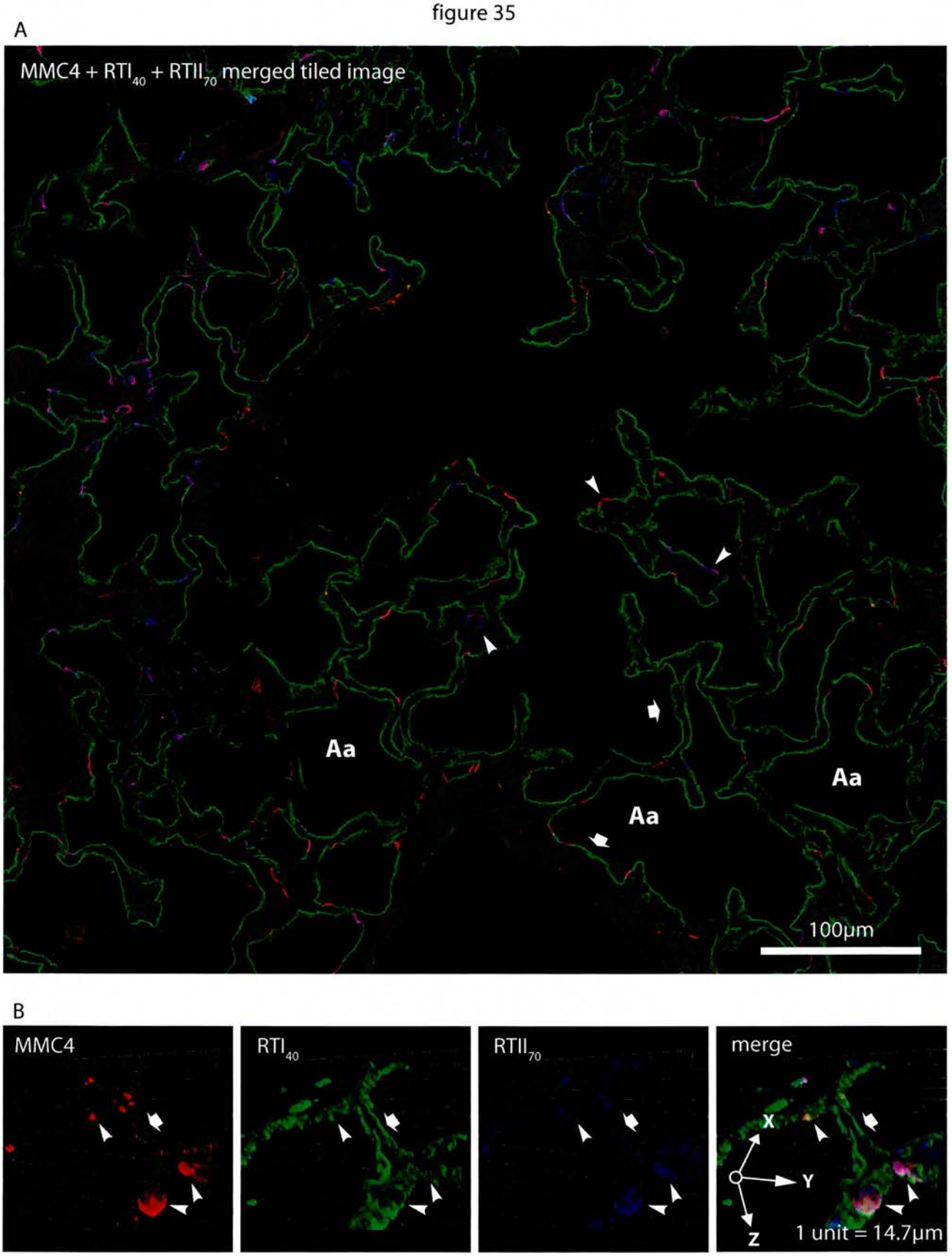

Rat lung sectioned at postnatal days 4 (A) and 5 (B), stained with MMC4 (red 546), RTI_{40} (green 488) and $RTII_{70}$ (blue 647). Alveolar airspaces resemble adult lung lined predominantly by RTI_{40} positive ATI cells (broad arrows), with MMC4/$RTII_{70}$ positive ATII cells at the corners of alveoli (arrowheads). (B) Shows the colocalisation of staining in 3D with the RTI_{40} positive apical membranes of ATI showing a 'tram-line' appearance (broad arrow) and the MMC4/RTII positive apical membranes of ATII cells protruding into the alveolar air space (arrowheads).

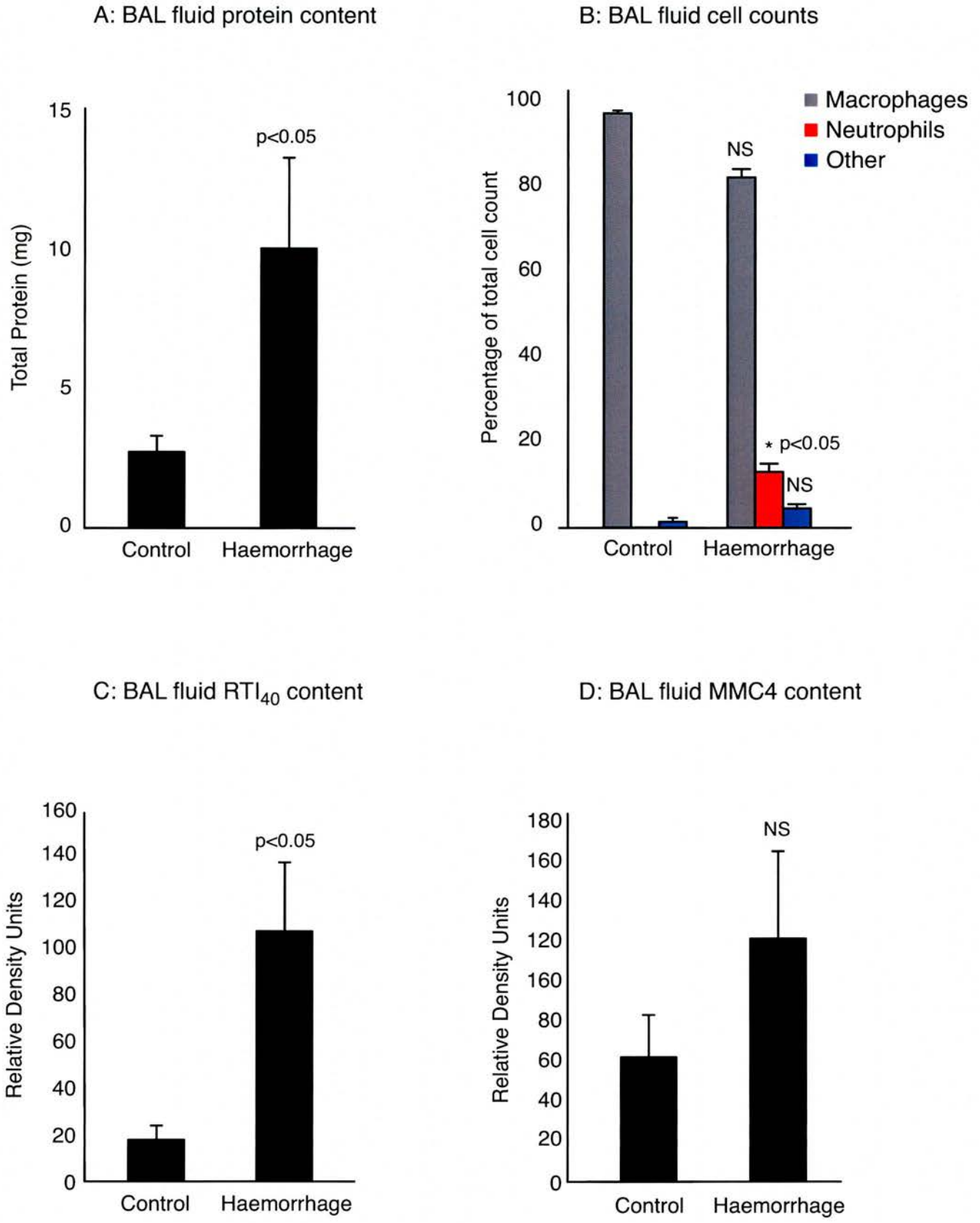

Graphs showing analysis of BAL fluid from rats undergoing haemorrhagic shock and resuscitation (n=3), and control rats that underwent surgery but no haemorrhage (n=3). (Error bars show SEM).

figure 37

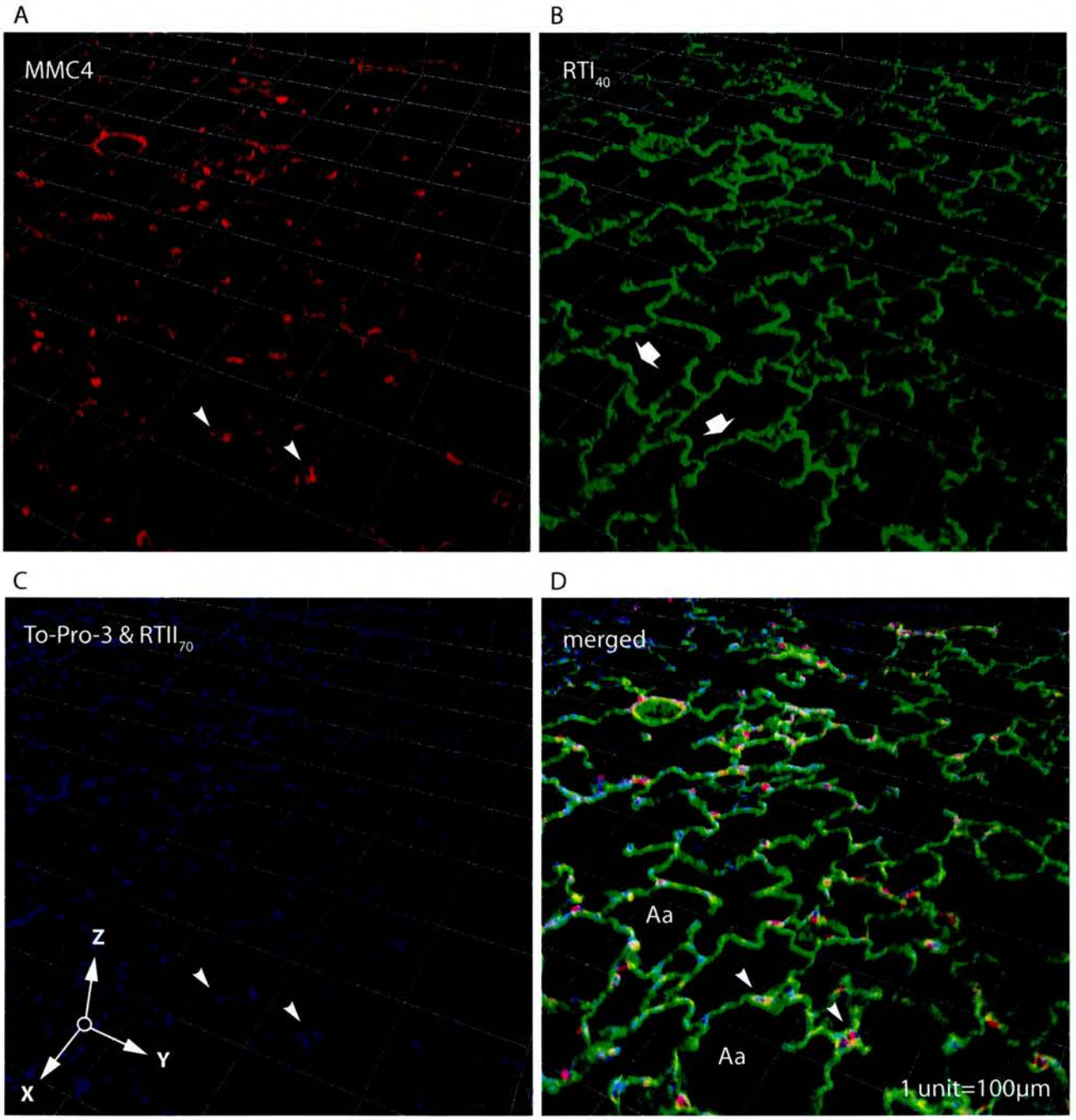

A section of adult rat lung stained with MMC4 (red 546), RTI_{40} (green 488), $RTII_{70}$ and TO-PRO-3 (blue 647). The tissue has been scanned as a stack of optical sections and rendered to give a 3D image which is rotated slightly to show the depth of the tissue section. MMC4/$RTII_{70}$ positive ATII cells can be seen in the corners of the alveoli (arrowheads) which are lined by RTI_{40} positive ATI cells (broad arrows).

figure 38

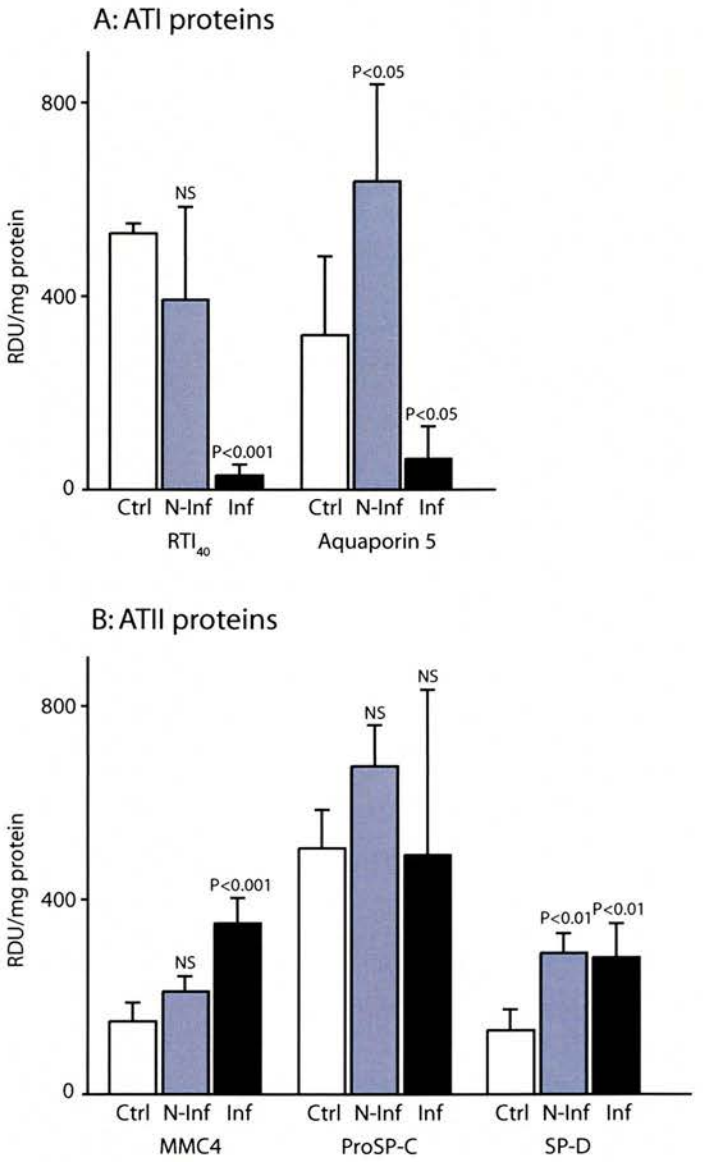

Biochemical analysis of ATI and ATII cell-selective proteins in lung homogenates from control and *S. aureus*-injured lungs (n=3). Western blots were performed and RTI_{40} (band at 40 kDa), Aquaporin 5 (band at 28 kDa), pro-SP-C (band at 21 kDa), and SP-D (band at 42 kDa) were scanned and relative densitometry units are shown per mg of protein. The data for the MMC4 protein (which does not Western blot) were derived from an ELISA-based dot blot assay.

Abbreviations - Controls (Ctrl) and S. aureus instilled lungs: non-inflamed (N-Inf) and inflamed (Inf) regions. Values significantly different from control values are shown (data analyzed using ANOVA). Error bars show SEM.

Appendix A: List of solutions

Stock solutions for ATII cell isolation

Name	FW	Concentration	Weight	Volume
NaCl	58.44	9% (10x stock)	45 g	500 mls
KCl	74.55	0.15M	5.6 g	500 mls
$CaCl_2.2H_20$	147	0.11 M	1.62 g	100 mls
$MgSO_4.7H_20$	246.5	0.15M	2.45 g	100 mls
Sodium phosphate		0.1M	0.275g monobasic to 1.13g dibasic, pH 7.4	200 mls
Hepes	260.3	0.2M	4.766 g, pH 7.4	100 mls
TRIS base	121.1	50 mM	6.05 g pH 9.4 with HCl	1000 mls

'With' Ca/Mg buffer

Name	Qty of Stock Soln.	Notes
NaCl	0.9%	20mls of 10X stock to 180 mls DDW
KCl	8mls	
$CaCl_2$	2mls	
$MgSO_4$	2mls	
PO_4	6mls	
Hepes	12mls	
Glucose	232 mg	Add on day of use
Final Vol	230mls	

'Without' Ca/Mg buffer

Name	Qty of Stock Soln.	Notes
NaCl	0.9%	20mls of 10X stock to 180 mls DDW
KCl	8mls	
PO_4	6mls	
Hepes	12mls	
Glucose	232 mg	Add on day of use
EGTA	0.0172 g	Add on day of use
Final Vol	**226mls**	

Coating IgG plates

Bacteriologic plastic petri dishes (100x15mm) were coated with IgG solution: 5mg IgG (rat serum, reagent grade, Sigma-Aldridge Ltd, Poole, Dorset, UK) into 10mls of 50mM tris buffer (pH 9). IgG is allowed to come up to room temperature before weighing.

3. Filter sterilise (pass solution through 0.2 m Millipore filter).
4. Place 5mls of IgG solution into each petri dish.
5. Leave in tissue culture hood at room temperature for 1-3 hours (can turn dishes occasionally to ensure even coating).

Standard cell culture medium.

Dulbecco's Modified Eagles Medium (Sigma-Aldridge Ltd, Poole, Dorset, UK) with 10mls, 10% Foetal calf serum 500μls, 1% L-Glutamine, 100μl, 1% Penicillin G (10,000 units per ml)/Streptomycin sulphate (10,000 μg per ml) 100μl (Gibco).

Solutions for immunohistochemistry:

Blocking Buffer (BB): 2.2g fish skin gelatin per 500mls of 20% Goat serum solution (in PBS).

BB + triton (BBT): 1ml BB with 10μl of 10% triton (in PBS) solution.

4% paraformaldehyde: 4g Paraformaldehyde in 100 mls of CMF PBS, heat on hot plate in fume cupboard at 70°C until dissolves (30 mins). Store at 4°C (or aliquot and freeze if storing for significant period i.e. months). Filter.

30% Sucrose solution: 15g sucrose in 50 mls PBS. Filter.

Appendix B: Published work arising from thesis

Coexpression of RTI_{40} with alveolar epithelial type II cell proteins in lungs following injury: identification of alveolar intermediate cell types

Am J Physiol Lung Cell Mol Physiol 289: L382–L390, 2005.
First published April 22, 2005; doi:10.1152/ajplung.00476.2004.

Coexpression of RTI_{40} with alveolar epithelial type II cell proteins in lungs following injury: identification of alveolar intermediate cell types

Gareth R. Clegg,[1]* Christine Tyrrell,[1]* Stuart R. McKechnie,[1] Michael F. Beers,[2] David Harrison,[1] and Mary C. McElroy[1]

[1]*Edinburgh Medical Research Council Centre for Inflammation Research, University of Edinburgh, Scotland, United Kingdom; and* [2]*University of Pennsylvania Medical Center, Pulmonary, Allergy, and Critical Care Division, Philadelphia, Pennsylvania*

Submitted 30 December 2004; accepted in final form 17 April 2005

Clegg, Gareth R., Christine Tyrrell, Stuart R. McKechnie, Michael F. Beers, David Harrison, and Mary C. McElroy. Coexpression of RTI_{40} with alveolar epithelial type II cell proteins in lungs following injury: identification of alveolar intermediate cell types. Am J Physiol Lung Cell Mol Physiol 289: L382–L390, 2005. First published April 22, 2005; doi:10.1152/ajplung.00476.2004.—Injured alveolar epithelial type (AT) I cells are replaced following the proliferation and transformation of ATII cells to new ATI cells. RTI_{40} is an ATI cell-specific protein required for normal lung development. We hypothesized that intermediate cell types in the ATII-to-ATI cell transformation would coexpress RTI_{40} and ATII cell-selective proteins. To test this hypothesis, we used a rat model of Staphylococcus aureus-induced acute lung injury and a panel of ATI and ATII cell-specific and -selective antibodies. S. aureus induced an acute inflammatory reaction that was resolving by day 3 postinoculation. At day 3 postinoculation, the alveolar wall was thickened secondary to ATII cell hyperplasia. With the use of confocal microscopy, there was a fivefold increase in the fractional surface area of alveolar walls stained with ATII cell membrane proteins ($RTII_{70}$ and MMC4) and a decrease in the fractional surface area associated with RTI_{40}-expressing cells. S. aureus-treated lungs also contained unique cell types that coexpressed the RTI_{40} and ATII markers RTI_{40}/MMC4/$RTII_{70}$- and RTI_{40}/MMC4-positive cells. These cells were not observed in control lungs. RTI_{40}/MMC4-positive cells were also found in cultured ATII cells before they transformed to an ATI-like phenotype. Our data suggest that RTI_{40}/MMC4/$RTII_{70}$- and RTI_{40}/MMC4-positive cells are intermediates in the ATII-to-ATI cell transformation. These data also suggest that the coexpression of RTI_{40} with ATII cell proteins may be used to identify and investigate ATII cell transdifferentiation to ATI cells following injury.

Staphylococcus aureus; aquaporin-5; MMC4 antigen

THE ALVEOLAR EPITHELIUM **in normal lungs is composed of two ultrastructurally distinct cell types, alveolar epithelial type** I **and** II **cells** (ATI **and** ATII **cells). ATI cells are large, thin cells that together cover** 97% **of the internal surface area of the lung** (34). **ATI cells are important for gas exchange, alveolar fluid regulation, and stretch-induced modulation of surfactant secretion** (2, 20, 30). **Cuboidal** ATII **cells are located between** ATI **cells** (34). ATII **cells contain characteristic lamellar bodies in their cytoplasm and apical microvilli** (35). ATII **cells have many known functions, including synthesis and secretion of lung surfactant, fluid transport, and host defense** (13).

ATII **cells are also required for alveolar epithelial repair** (1, 10, 11, 33). **After injury,** ATII **cells proliferate, and a subset of daughter cells transform to new** ATI **cells** (1, 10, 11, 33). **Ultrastructural studies demonstrated that the formation of** ATI **cells is preceded by the presence of intermediate cell types characterized as** ATII- **or** ATI-**like** (10, 19). **However, we know little about the mechanism of** ATI **formation following injury because of the difficulties in both identifying and quantifying intermediate cell types by electron microscopy.**

ATI **and** ATII **cells can be distinguished by the expression of selective proteins** (6, 16, 24, 36). **These proteins can be used to inform the differences in** ATII **and** ATI **cell biology, and as tools to investigate alveolar epithelial injury and repair in response to toxic agents** (23). **Intermediate cells in the** ATII-to-ATI **cell transition have been identified based on the coexpression of an** ATI **cell-associated lectin and the** ATII **cell-selective protein surfactant protein** (SP) **D during the resolution of keratinocyte growth factor** (KGF)-**induced** ATII **cell hyperplasia** (14).

RTI_{40} **or** T1α **protein is a membrane protein expressed selectively on the apical surface of** ATI **cells in the lung** (8, 31). **The function of** RTI_{40} **is not known, although it is required for** ATI **cell morphogenesis during lung development** (29). **We hypothesized that alveolar epithelial intermediate cell types coexpress** RTI_{40} **and** ATII **cell-specific or -selective proteins. We tested this hypothesis in a rat model of Staphylococcus aureus-induced lung injury** (22), **using the monoclonal antibody raised by Dobbs and colleagues** (8) **to detect** RTI_{40}. **To identify** ATII **cells, we used antibodies against apical membrane proteins:** $RTII_{70}$ (**rat type** II **cell, mol wt** 70 kDa) (7) **and the MMC4 antigen (clone name M McElroy** 4) (5, 15).

Here we demonstrate the presence of epithelial cells that coexpress both ATI **and** ATII **cell proteins (that is,** RTI_{40}, $RTII_{70}$, **and MMC4) in lungs following S. aureus-induced injury. In addition, we detect** RTI_{40}/MMC4-**positive cells in cultured** ATII **cells as they become** ATI-**like. We propose that the coexpression of** RTI_{40} **with** ATII **cell membrane proteins is a morphology independent method to identify and study** ATII **transformation to new** ATI **cells in vivo.**

MATERIALS AND METHODS

S. aureus. S. aureus, strain 8325-4, *was prepared from glycerol stocks as described previously* (22).

S. aureus-induced lung injury. Rats (specific pathogen-free Sprague-Dawley males, 300–350 *g; Harlan, UK) were anesthetized with an intraperitoneal injection of fentanyl chloride* (1 *mg/kg) and fluanisone* (33 *mg/kg) mixed with midazolam hydrochloride* (17 *mg/kg). Once the rats were anesthetized, S. aureus* (10^8 *colony forming units) was instilled into the distal airways as previously described* (22). *Control rats were instilled with PBS. The lungs were examined at days* 3, 5, 7, *and* 21 *post-S. aureus or post-PBS instillation. All animal experiments had the prior approval of the University*

* G. R. Clegg and C. Tyrrell contributed equally to this work.

Address for reprint requests and other correspondence: M. C. McElroy, Edinburgh MRC Centre for Inflammation Research, Univ. of Edinburgh, Teviot Place, Edinburgh EH8 9AG, Scotland, United Kingdom (e-mail: mary.mcelroy@ukonline.co.uk).

of Edinburgh Ethical Review Committee and the Home Office and were carried out according to the Animals (Scientific Procedures) Act, 1986.

Collection of bronchoalveolar lavage fluid. At day 3 postinstillation, PBS-instilled lungs ($n = 4$) and *S. aureus*-instilled lungs ($n = 4$) were lavaged twice with PBS as described previously. Bronchoalveolar lavage (BAL) fluid was centrifuged (1,000 rpm × 10 min), and the supernatant was retained for determination of total protein and RTI_{40} concentrations. The cell pellets were used to determine the total and differential cell counts as described previously (22). The volume of BAL fluid recovered from *S. aureus*-treated lungs was not different from PBS-treated lungs (data not shown). Data are presented as the total number of cells, protein, and RTI_{40} recovered in BAL fluid.

Lung homogenization. At day 3 postinstillation, after lavage, *S. aureus*-instilled lungs were removed, and the inflamed and noninflamed regions were homogenized separately as previously described ($n = 4$) (22). The PBS-instilled lungs (controls) were normal in appearance and were therefore homogenized whole ($n = 4$). The protein concentration of homogenized lungs was determined using a Bio-Rad protein assay.

ELISA-based dot blot analysis. The amount of the MMC4 and RTI_{40} proteins in BAL fluid and lung homogenates was quantified using ELISA based dot blot assay as previously described (5, 26).

Western blot analysis. Lung proteins were resolved on 12% NuPAGE Bis·Tris {[bis (2 hydroxyethyl) amino] tris (hydroxymethyl) methane} Gels Electrophoresis System (Invitrogen, Paisley, UK) and electrophoretically transferred to polyvinylidene difluoride membrane (Immobilon-P) using the NuPAGE transfer buffer. Membranes were blocked in 2.5% casein in Tris-buffered saline (10 mM Tris·HCl and 0.15 M NaCl, pH 8.2) and developed as for the ELISA-based dot blots. Anti-RTI_{40} was detected using an anti-mouse IgG horseradish peroxidase (1 in 2,000 in blocking buffer, Rockland Immunochemicals). Aquaporin-5 (Chemicon International, 1 in 100 in DMEM + 10% FCS) was detected with anti-rabbit IgG horseradish peroxidase (either 1 in 1,000 or 2,000 dilution in blocking buffer, Rockland Immunochemicals). The optical density of Western blot bands was determined using a gel documentation and analysis system (UVP GDS7600).

Electron microscopic analysis. At day 3 postinstillation, PBS- ($n = 2$) and *S. aureus*-treated lungs ($n = 2$) were fixed and processed for electron microscopy as described previously (22).

Lung fixation for paraffin sections. At day 3 ($n = 4$), day 5 ($n = 3$), day 7 ($n = 2$), and day 21 ($n = 3$) postinstillation, PBS- and *S. aureus*-treated lungs were fixed in formalin. Sections were stained with hematoxylin and eosin.

Lung fixation for confocal microscopy. At day 3 postinstillation, PBS- ($n = 3$) and *S. aureus*- ($n = 3$) treated lungs were fixed with 4% paraformaldehyde for 2 h. Small cubes from the macroscopically inflamed lobes were selected and cryoprotected overnight in 30% (wt/vol) sucrose. Frozen sections were cut the next day as previously described (5, 22).

Immunostaining. Frozen lung sections and cultured alveolar epithelial cells were incubated with various cocktails of primary antibodies followed by isotype- or species-specific secondary antibodies (Molecular Probes, Leiden, Netherlands) as described previously (5, 22) (Table 1). The nucleus was stained with the DNA probe To-Pro-3 (Molecular Probes).

Confocal imaging and analysis. Fluorescent images were acquired using a Zeiss Axiovert LSM 510 confocal microscope. AlexaFluor 488 (green) was imaged with an excitation wavelength of 488 nm. AlexaFluor 546 (red) was imaged at 543 nm. Alexa 647 (blue) was imaged at 633 nm. The sections were sequentially scanned at different excitation wavelengths to ensure discrimination between the overlapping fluorescent spectra of Alexa dyes 488 and 546.

For quantification, a computer-controlled motorized stage was used to obtain tiled images consisting of 16 (4 × 4) high-powered (×63 objective) contiguous fields combined into a single red, green, and blue TIFF file. Openlab 3.5.1 analysis software (Improvision) was used to create a binary mask consisting of the positively stained areas in each separate color channel; binary masks were combined to identify areas of colocalization. To determine the length of a positively stained wall for a given color or combination of colors, binary masks were overlaid on the corresponding transmitted light image, and the length of the positively stained alveolar wall was traced and measured using a graphics tablet (WACOM Technology). Data are reported as the percentage of alveolar wall stained with a given antibody.

For three-dimensional viewing of alveolar wall membranes, confocal scanning was carried out using Nyquist settings. The raw data were deconvoluted using Huygens 2 (SVI) software and reconstructed and analyzed for colocalization using Imaris 4.0 software (Bitplane, Zurich, Switzerland) (9).

ATII cell isolations. Type II cells were isolated from the lungs of male Sprague-Dawley specific pathogen-free rats (Harlan) using previously described methods (5, 8) ($n = 3$ isolations). ATII cells were fixed in 4% paraformaldehyde at days 0, 1, and 5. The ATII cells were 75% pure immediately following isolation; contaminating cells included macrophages, lymphocytes, and ATI cells (RTI_{40}-positive cells accounted for ~1% of the total cells).

Statistics. Data are expressed as means (SD). Comparison between samples was analyzed using Student's *t*-test. $P < 0.05$ was considered significant. Tests were performed with GraphPad Instat version 3.0a.

Table 1. ATI and ATII cell-specific or selective proteins

Name	Cell Specificity	Isotype	Alexa Fluor Anti-Mouse Secondary Antibodies
MMC4 MAb	ATII and Clara	IgG_{2a}	546 (red)
Anti-$RTII_{70}$	ATII	IgG_3	647 (blue)
Anti-RTI_{40}	ATI	IgG_1	488 (green)
Anti-aquaporin-5	ATI and Clara cells	Rabbit polyclonal	Western blot only

ATI and ATII, alveolar epithelial types I and II, respectively.

RESULTS

General histology of *S. aureus*-instilled lungs: day 3 to day 21 postinstillation. At day 3 postinstillation, the alveolar walls from inflamed regions of *S. aureus* instilled lungs were thickened compared with the alveolar walls in the noninflamed regions and control lungs (Fig. 1). The number of inflammatory cells present in the air spaces was also increased in *S. aureus* instilled lungs (Fig. 1). By day 7 postinstillation, *S. aureus*-treated lungs were almost normal; the alveolar walls were thinner and there were fewer inflammatory cells in the air spaces (Fig. 1). By day 21, *S. aureus*-inoculated lungs were indistinguishable from control lungs (data not shown).

Ultrastructure of the alveolar wall at day 3 post-*S. aureus* instillation. The thickened alveolar walls in *S. aureus* instilled lungs were due to increased numbers of ATII cells (i.e., cells containing lamellar bodies and apical microvilli) or cuboidal epithelial cells with, and without, some ATII cell ultrastructural features (that is, ATII-like cells). ATII-like cells included cells with apical microvilli and lamellar bodies but reduced perinuclear cytoplasm, cells with apical microvilli and no lamellar bodies, and cells with no apical microvilli or lamellar bodies (Fig. 2). In addition, ATI cells were also observed overlaying ATII cells (Fig. 2). The alveolar epithelium in the noninstilled region from *S. aureus*-instilled lungs was the same as shown previously for control lungs (data not shown).

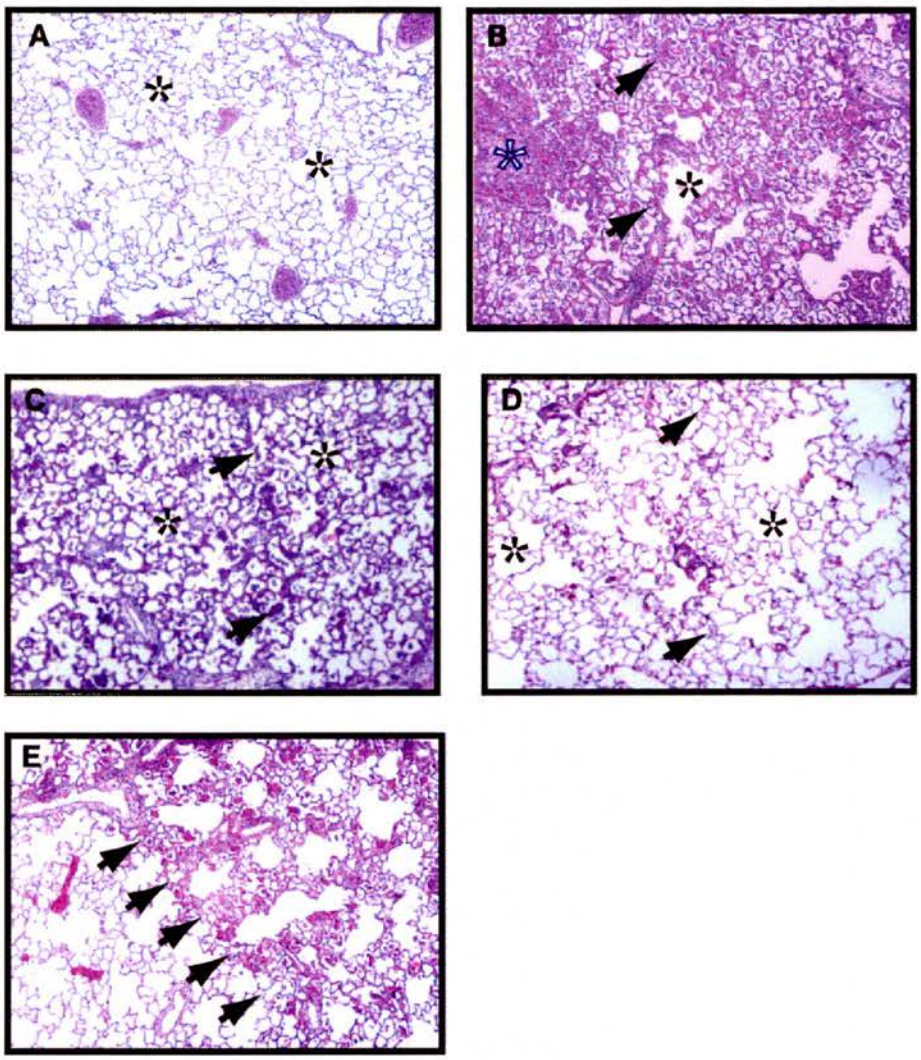

Fig. 1. Hematoxylin and eosin-stained lung sections from control and Staphylococcus aureus-injured lungs are shown. A: control lung shows a characteristic mesh of air spaces (*) bounded by thin alveolar walls. *B*: at day 3 post-S. aureus instillation, there is an intense inflammatory infiltrate (arrows). Remaining air spaces (black asterisk) have thickened walls. In consolidated areas, the alveolar air space is obliterated (white asterisk). C: at day 5 post-S. aureus instillation, there are less inflammatory cells in the air spaces (arrows), although the alveolar walls are still thicker than control lungs. D: by day 7 post-S. aureus instillation, only occasional inflammatory cells are observed in the air spaces (arrows), and the alveolar wall appears normal. E: boundary between an area of normal looking noninflamed lung and an area of inflamed tissue at day 3 post-S. aureus instillation (arrows).

Alveolar barrier injury and inflammation on day 3 post-S. aureus instillation. At day 3 post-S. aureus instillation, the total amount of protein recovered in BAL fluid was elevated 1.6-fold above control values (i.e., 3.03 ± 0.89 mg vs. 1.87 ± 0.43 mg, $P < 0.05$, $n = 3$). In contrast, our previous study demonstrated that the total amount of protein recovered in BAL fluid was elevated 6.8-fold at day 1 post-S. aureus instillation compared with control values (22).

The total number of BAL leukocytes was elevated 2.5-fold above control values (i.e., $8.33 \times 10^5 \pm 1.95 \times 10^5$ vs. $3.53 \times 10^5 \pm 0.37 \times 10^5$, $P < 0.05$, $n = 3$) at day 3 post-S. aureus instillation. In contrast, the total number of leukocytes recovered in BAL fluid was elevated 57-fold above control values at day 1 post-S. aureus instillation (22).

The amount of RTI_{40} recovered in BAL fluid can be used to assess the extent of ATI cell necrosis (25, 26). The amount of RTI_{40} recovered in BAL fluid at day 3 postinstillation was not different from control values (data not shown).

These protein and inflammatory cell data confirm the acute inflammatory response to S. aureus is resolving by day 3 postinstillation, and there is no evidence of ATI cell necrosis.

Concentration of RTI_{40}, aquaporin-5, and the MMC4 antigen in lung homogenates at day 3 post-S. aureus instillation. The concentration of RTI_{40} was decreased by >18-fold in lung homogenates from the inflamed regions of S. aureus-inoculated lungs compared with control lungs (Fig. 3). Similarly, the concentration of aquaporin-5, expressed by ATI cells and nonciliated bronchiolar epithelial cells (27), was decreased by fivefold in inflamed regions from S. aureus-inoculated lungs compared with control lungs (Fig. 3). However, in the noninflamed regions, the concentration of RTI_{40} was not different from control values, whereas the concentration of aquaporin-5 was increased by nearly twofold (Fig. 3).

The concentration of the MMC4 antigen was increased in lung homogenates from the inflamed region of S. aureus-treated lungs compared with control values, whereas in the noninflamed region of S. aureus-instilled lungs, the concentration of MMC4 antigen was not different from control values (Fig. 3).

Phenotype of the alveolar epithelium in control lungs. The antibodies used here have been shown previously to bind selectively to ATI or ATII cells (Table 1). Here we demon-

strate that these antibodies can be used in combination to investigate the phenotype of ATI and ATII cells simultaneously. RTI_{40} is expressed on the apical surface of ATI cells, whereas $RTII_{70}$ and MMC4 are expressed on the apical surface

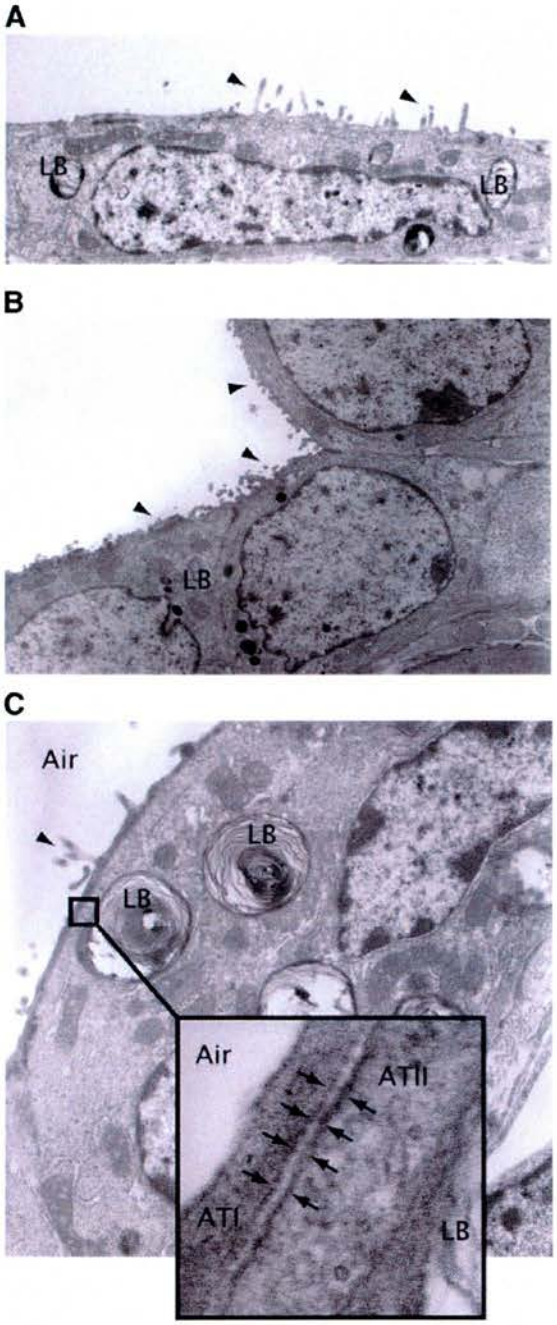

Fig. 2. Electron micrographs of alveolar epithelial cells in S. aureus-injured lungs at day 3 postinstillation are shown. A: flattened epithelial cell containing microvilli (arrowheads) and lamellar bodies (*LB*) but with reduced perinuclear cytoplasm. Original magnification, ×6,700. *B*: group of cuboidal epithelial cells with reduced cytoplasm and numbers of *LB* but with microvilli (arrowheads). Original magnification, ×5,000. C: alveolar epithelial type (AT) I cell overlaying an ATII cell. Inset demonstrates the presence of a membrane between the 2 cell types. Original magnification, ×1,000; for inset, ×125,000.

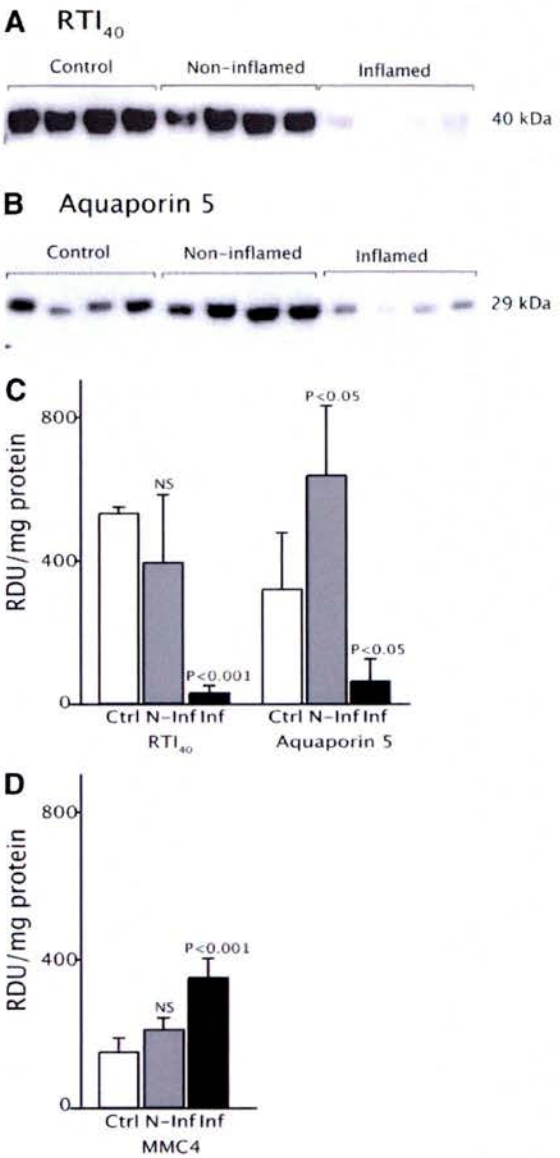

Fig. 3. Concentration of RTL_{40}, aquaporin-5, and the MMC4 antigen in lung homogenates from control and S. aureus-injured lungs at day 3 postinstillation. Western blots were performed as described in MATERIALS AND METHODS. Protein (10 μg) was loaded per lane. Each lane represents a different lung sample. A: Western blot demonstrates RTL_{40} is downregulated in lung homogenates from inflamed lungs (Inf) compared with controls (Ctrl) and the noninflamed regions (N-Inf). *B*: Western blot demonstrates aquaporin-5 is downregulated in lung homogenates from inflamed lungs but upregulated in noninflamed regions compared with control values. C: quantitative changes in the concentration of RTL_{40} and aquaporin-5. D: concentration of the MMC4 protein was increased in inflamed regions compared with values from controls and from noninflamed regions (data obtained using an ELISA-based dot blot assay). Data in C and D are shown as means (SD). Values significantly different from control values are shown (data analyzed using ANOVA). NS, not significant; RDU, relative densitometry units.

of ATII cells (Fig. 4) (5, 7, 8). The relative proportion of alveolar surface area occupied by ATI to ATII cells, assessed by measuring the fractional surface area of the alveolar wall associated with RTI_{40} and $RTII_{70}$/MMC4 staining, was 97.0% vs. 2.5% (a ratio of 39:1) (Fig. 4). This ratio is identical to the

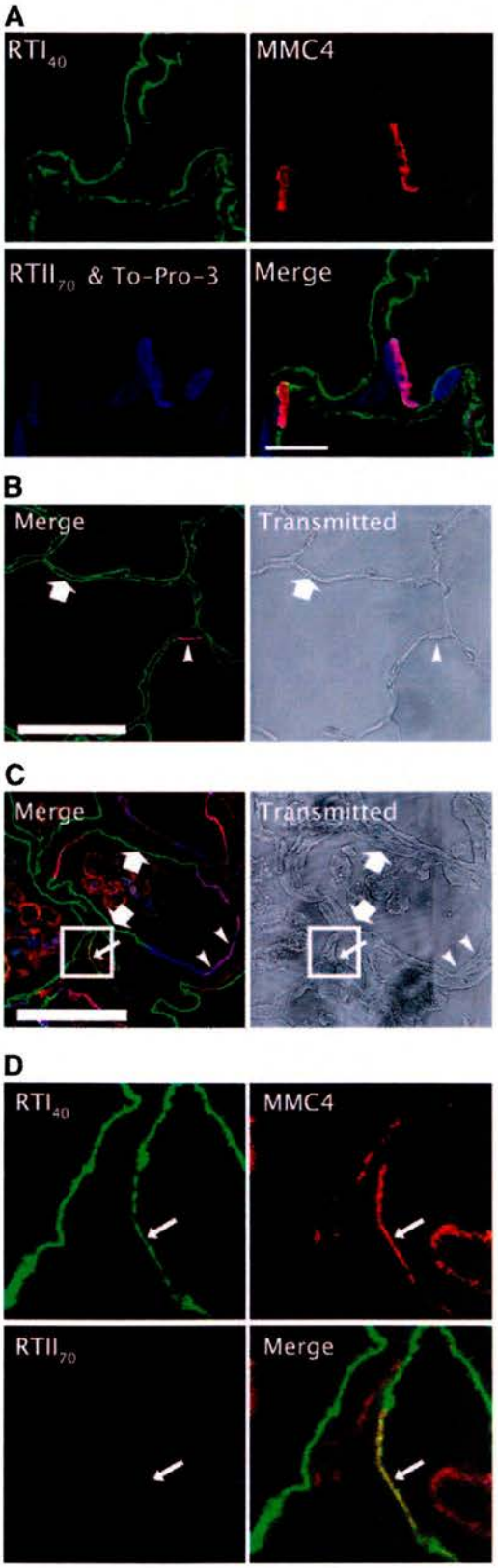

ratio of 39:1 obtained from measurements made from electron micrographs of rat lungs and suggests that $RTII_{70}$/MMC4 coexpression identifies most ATII cells (18).

Phenotype of the alveolar epithelium at day 3 post-S. aureus instillation. As in control lungs, the alveolar walls in the inflamed regions were lined by both RTI_{40}-positive cells (ATI cells) and MMC4/$RTII_{70}$-positive cells (ATII cells) (Fig. 4). However, the fractional surface area covered by MMC4/$RTII_{70}$-positive cells (ATII cells) was increased by more than fivefold in S. aureus-injured lungs compared with control lungs (Fig. 4). The MMC4 monoclonal antibody also stained ED1-positive cells (a macrophage marker) in the air spaces (data not shown); this is consistent with our observation that the MMC4 monoclonal antibody binds to aminopeptidase N (15). The fractional surface area covered by RTI_{40} (ATI cells) in S. aureus-injured lungs was significantly decreased compared with control lungs (Fig. 4). The fractional surface area ratio of ATI to ATII cells decreased from 39:1 in control lungs to ~7:1 in S. aureus-instilled lungs (Fig. 5).

In regions with thickened alveolar walls and hyperplastic ATII cells, we observed RTI_{40}/$RTII_{70}$/MMC4-postive and RTI_{40}/MMC4-positive alveolar membranes (Figs. 4 and 6). Three-dimensional analysis of RTI_{40}/MMC4-coexpressing membranes, with deconvolution, confirmed coexpression of these proteins on the same membrane (Fig. 7). Quantitative analysis demonstrated that RTI_{40}/MMC4-positive membranes in S. aureus-injured lungs accounted for ~3% of the fractional alveolar surface area in the inflamed region (Fig. 5). RTI_{40}/MMC4-positive cells, which also expressed $RTII_{70}$, accounted for one-third of this percentage. The average length of RTI_{40}/MMC4-positive membranes in S. aureus-treated lungs was 13.6 ± 11.4 μm (n = 3) compared with an average length of 7.2 ± 0.7 μm for ATII cells in control lungs.

The small area of RTI_{40}/MMC4-coexpressing epithelium in control lungs (0.1%) was limited to areas where ATI cells (RTI_{40}-positive) and the apical membrane of ATII cells (MMC4/$RTII_{70}$-positive) were adjacent. These areas are likely to represent the interface of separate red- and green-staining membranes within the same voxel rather than coexpression on the same membrane (Fig. 7).

Phenotype of cultured ATII cells. Primary ATII cells rapidly lose ATII characteristics and gain some ATI-like characteristics in culture. Specifically, cuboidal ATII cells spread and

Fig. 4. Expression of ATI and ATII cell-selective markers in control and S. aureus-injured lungs is shown. Lung sections (5–7 μm thick) were incubated with antibodies as described in MATERIALS AND METHODS and imaged using confocal microscopy. A: control lung, individual channels, and merged image demonstrating MMC4 (red) and $RTII_{70}$ (blue) are coexpressed on an alveolar epithelial cell located between RTI_{40}-positive cells (green). *Bar* = 10 μm. *B*: lower magnification of control lung demonstrating MMC4/$RTII_{70}$ colocalization (pink cell, arrowhead). RTI_{40} staining is shown in green (arrow). Corresponding transmitted image is also shown. *Bar* = 25 μm. C: S. aureus-injured lung on day 3 postinstillation. Image demonstrates that the surface area of alveolar walls coexpressing the ATII cell markers MMC4/$RTII_{70}$ is increased compared with control lungs (purple cells, arrowheads). Whereas the alveolar surface is covered by the ATI cell marker, RTI_{40} is decreased compared with control lungs (green, thick arrows). Some alveolar membranes are stained with a new combination of MMC4 (red) and RTI_{40} (green) to generate yellow membranes (thin arrow). Image also demonstrates that monocytes/macrophages in the air spaces express the MMC4 antigen. *Bar* = 25 μm. D: higher magnification and individual channels of RTI_{40}/MMC4-positive membranes seen in C.

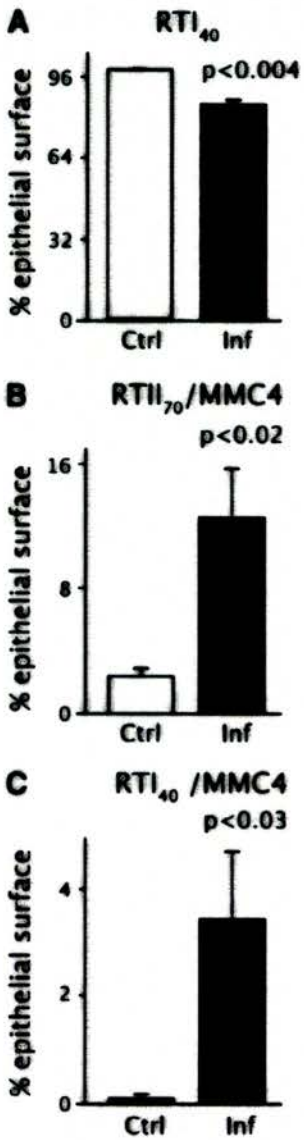

Fig. 5. Shown is the percentage of the alveolar wall covered by ATI and ATII cell markers in S. aureus-injured and control lungs. Images are captured and analyzed as detailed in MATERIALS AND METHODS. The total epithelial surface measured in control and S. aureus-treated lungs was 16,063 ± 3,058 μm and 15,783 ± 1,203 μm, respectively. A: ATI cells (RTL_{40}-positive membranes). *B*: ATII cells ($RTII_{70}$/MMC4-coexpressing membranes). C: alveolar intermediate cells (RTL_{40}/MMC4-coexpressing membranes).

flatten and lose lamellar bodies (4, 8). While accompanying these morphological changes, ATII cells stop expressing ATII proteins (for example, SP and $RTII_{70}$) and express some ATI cell-associated proteins such as RTI_{40} and aquaporin-5 (4, 6, 8, 16). Unlike most previous studies, we followed this transition by examining the phenotype of alveolar epithelial cells in culture. We demonstrated that freshly isolated ATII cells coexpressed $RTII_{70}$ and MMC4 but not RTI_{40} (Fig. 8). By day 5 in culture, cells expressed RTI_{40} but not $RTII_{70}$ or MMC4 (Fig. 8). However, on day 1, although most cells were negative or slightly positive for RTI_{40}, some cells (5.9 ± 1.4%, n = 3) coexpressed RTI_{40} and MMC4 (Fig. 8). We did not detect $RTII_{70}$ at day 1 of culture.

DISCUSSION

In a previous study we demonstrated that S. aureus induced an inflammatory reaction at day 1 postinstillation (22). Here we demonstrate at day 3 post-S. aureus instillation that general markers of acute inflammation (i.e., total number of BAL fluid leukocytes) and alveolar wall damage (as assessed by total amount of protein in BAL fluid) are returning to control values. Using morphological methods, we also demonstrate that S. aureus instillation induced a localized inflammatory reaction, probably at the initial site of bacterial deposition. By day 3 postinstillation, the lungs are easily separated into noninflamed and inflamed regions. The inflamed regions have a markedly thickened alveolar wall secondary to ATII cell hyperplasia. The noninflamed regions appear normal. After S. aureus-induced acute lung injury, our morphological data indicate that the lungs are normal by day 21.

To characterize the regional nature of S. aureus-induced ATII cell hyperplasia, we analyzed the concentration of ATI and ATII cell-specific and -selective proteins in inflamed and noninflamed regions at day 3 postinstillation. The concentration of both ATI cell proteins (e.g., RTI_{40} and aquaporin-5) were specifically decreased in inflamed regions from S. aureus-injured lungs. This result is consistent with a decrease in the

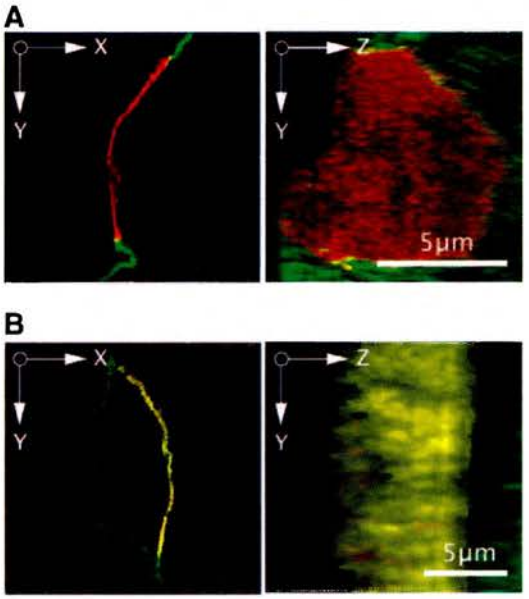

Fig. 6. Comparison of RTL_{40}/MMC4-positive membranes in control and S. aureus-injured lungs following deconvolution is shown. Deconvoluted images were restored in 3 dimensions and then subjected to an object-independent extraction of red (MMC4 expression) and green (RTL_{40} expression) colors using Colocalization 2.0 (*B*itplane) software. Colocalized voxels are shown in yellow. A: RTL_{40}/MMC4 coexpression in the control lung. Colocalization of red and green voxels (yellow) were limited to the junction between RTL_{40}- and MMC4-positive cells in both the x, y, and z, y dimensions. An MMC4-positive cell surrounded by an RTL_{40}-positive cell with colocalization (in yellow) was limited to areas at the junction between RTL_{40}/MMC4-positive cells. *B*: RTL_{40}/MMC4 coexpression in S. aureus-injured lung. In contrast with control lung, colocalization of red and green voxels (yellow) extend across the surface of the alveolar wall in both the x, y, and z, y, dimensions.

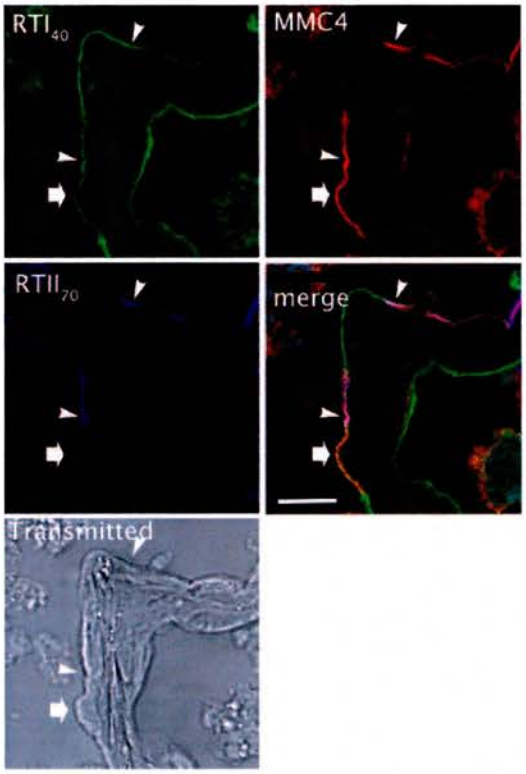

Fig. 7. Coexpression of **RTL40**, **MMC4**, and **RTII70** on alveolar membranes in S. aureus-injured lungs. An area of the alveolar wall from S. aureus-instilled lung shows **MMC4/RTL40** coexpression (arrow) adjacent to an area of **MMC4/RTL40/RTII70** coexpression (arrowheads). Separate and merged confocal images are shown as well as the corresponding transmitted image. *Bar* = 10 μm.

number of ATI cells, and/or a decrease in the fractional surface area of ATI cells, secondary to ATII cell hyperplasia. In the noninflamed regions, the concentration of aquaporin-5 was upregulated relative to control values. In contrast, aquaporin-5 is downregulated in regions without overt inflammation (noninflamed) in an experimental model of viral pneumonia (32).

Our attempts to demonstrate increased numbers of ATII cells by measuring the concentration of ATII cell-specific and -selective proteins were less clear-cut than for the ATI cell proteins. By Western blot analysis, the concentration of pro-SP-C, expressed by ATII cells (3, 21), was not different from control values (data not shown). Potential reasons could include a nonhomogeneous regulation of SP-C expression that could occur with foci of both upregulation and downregulation in different areas of inflammation and of proliferative repair (hyperplasia) known to occur in these lungs. Interestingly, the concentration of SP-D, expressed by ATII cells and Clara cells (26), was elevated in both inflamed and noninflamed regions (data not shown) and was most likely influenced by the complex regulation of this protein by a variety of cytokines and mediators. The concentration of the MMC4 protein, however, was selectively elevated over the concentration of MMC4 protein in noninflamed regions; this may in part be representative of ATII cell hyperplasia. In general, only the concentration of the ATI cell proteins, and the MMC4 antigen, revealed the regional nature of S. aureus-induced injury and supported the observation that ATII cell hyperplasia is accompanied by decreased ATI cell numbers, or fractional surface area, following S. aureus-induced acute lung injury.

Using a panel of ATI and ATII cell-specific and -selective antibodies, we investigated the phenotype of the alveolar epithelium following S. aureus-induced acute lung injury at day 3 postinstillation. As in controls, the alveolar walls in inflamed regions were lined with $RTII_{70}$/MMC4-positive cells (ATII cells) and RTI_{40}-positive cells (ATI cells). However, the fractional surface area covered by $RTII_{70}$/MMC4-positive cells was significantly increased compared with control lungs, indicative of ATII cell hyperplasia. $RTII_{70}$/MMC4-postive cells in S. aureus-injured lungs were not uniformly positive for

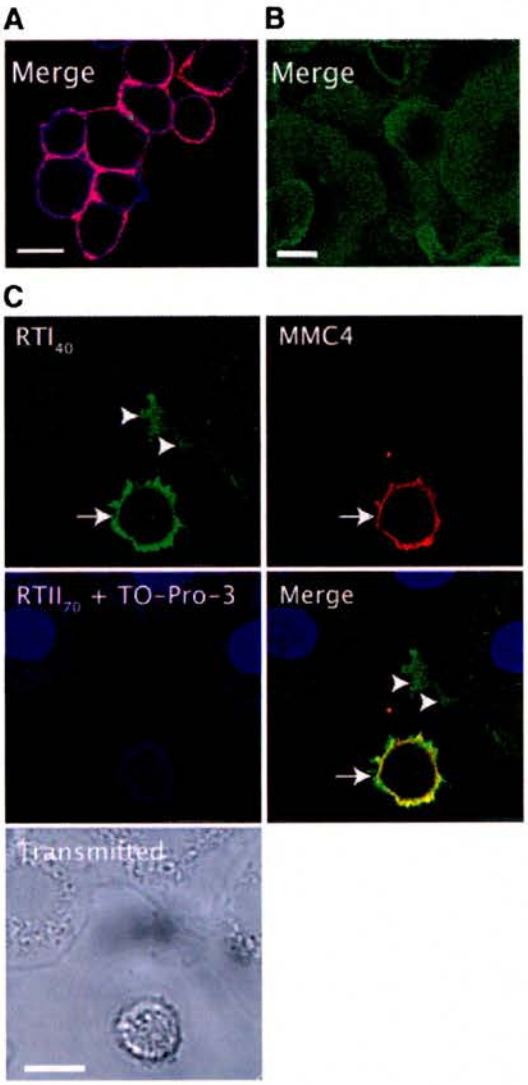

Fig. 8. Expression of **ATI** and **ATII** cell-selective proteins in cultured alveolar epithelial cells is shown. A: freshly isolated **ATII** cells coexpress **RTII70** (blue) and the **MMC4** antigen (red). A merged image is shown. *Bar* = 10 μm. *B*: by 7 days in culture, alveolar epithelial cells are spread out and express **RTL40** but not **RTII70** or the **MMC4** antigen. A merged image is shown. *Bar* = 10 μm. C: on day 1 of culture, some cells coexpress **RTL40** and the **MMC4** antigen (arrow). Some flattened and spreading cells are slightly positive for **RTL40** (arrowheads). Separate channels, merged image, and corresponding transmitted images are shown. *Bar* = 10 μm.

pro-SP-C (data not shown). These data suggest that $RTII_{70}$/MMC4-postive cells may recognize both the ATII- and ATII-like cells, with few or no lamellar bodies, seen by ultrastructural analysis of the lungs.

In regions associated with increased numbers of $RTII_{70}$/MMC4-positive cells, we observed membranes that coexpressed ATI and ATII cell proteins, RTI_{40}, MMC4, and $RTII_{70}$. RTI_{40}/MMC4 cells were the most abundantly mixed phenotype. We did not observe RTI_{40}/MMC4-positive alveolar wall cells in the noninstilled regions from S. aureus-instilled lungs or control lungs. Our ultrastructural studies demonstrated that some ATI cells overlay ATII cells following injury. Alveolar epithelial multilayering has been previously described following a range of different toxic stimuli [for example, nitrogen dioxide (11), Freund's adjuvant (12), and nitric acid (17)]. To rule out the possibility that areas of RTI_{40}/MMC4 coexpression were secondary to ATI cells overlaying ATII cells, confocal images were subject to deconvolution and increasing image resolution, particularly in the z-plane. Deconvoluted images confirmed the coexpression of RTI_{40} and MMC4 on the same membrane.

Intermediates in the ATII to ATI cell transformation have multiple ultrastructural phenotypes ranging from ATII cells spreading out over the basement membrane to ATI cells with occasional microvilli and dense inclusions (10, 19). It is therefore possible that we have phenotyped two intermediate cell types based on the coexpression of RTI_{40} with various ATII cell markers. Early intermediate cell types may coexpress RTI_{40}/MMC4/$RTII_{70}$, whereas later intermediates may coexpress RTI_{40}/MMC4. Additionally, RTI_{40}/MMC4-positive cells were found on average to have a luminal surface length twice that of ATII cells (i.e., 13.6 μm vs. 7.40 μm), suggesting that these cells are in the process of becoming attenuated and flattened ATI cells.

Cultured ATII cells rapidly loose ATII cell phenotypic characteristics and gain ATI cell-like characteristics. We demonstrated that RTI_{40}/MMC4-positive cells could be detected in cultured ATII cells before they become ATI cell-like. These in vitro data additionally suggest that RTI_{40}/MMC4-positive cells are kinetically competent to be intermediate cell types.

Others have also described putative intermediate cell types based on the coexpression of ATI and ATII cell markers (14). Fehrenbach and colleagues (14) demonstrated that the ATI cell lectin Lycopersicon esculentum agglutinin and SP-D were coexpressed on alveolar epithelial cells following KGF-induced ATII cell hyperplasia. However, given that alveolar epithelial cells tend to overlay ATII cells in many lung injury models, coexpression of a membrane (e.g., lectin) and cytoplasmic marker (e.g., SP-D) would not distinguish between multilayering and potential intermediate cell types. Coexpression of ATI- and ATII-selective membrane proteins is therefore more likely to identify intermediate cell types in the lung following injury.

In summary, we have characterized the phenotype of the alveolar epithelium in a rat model of focal acute lung injury caused by distal airway instillation of S. aureus. Our data demonstrate that in inflamed lung, there are increased numbers of ATII cells (defined by $RTII_{70}$/MMC4 coexpression) and reduced ATI cell numbers or surface area (defined by RTI_{40} expression). Within these regions, we observed alveolar epithelial cells that coexpressed RTI_{40}, $RTII_{70}$, and MMC4. These coexpressing cells were not seen in control lungs or in the noninflamed regions from S. aureus-instilled lungs. However, RTI_{40}/MMC4-positive cells were observed in vitro as ATII cells transformed to ATI-like cells. These data suggest that the coexpression of RTI_{40} with ATII cell proteins, such as $RTII_{70}$ and MMC4, may be used to detect ATII cells in the process of transforming to new ATI cells and therefore provides a means of investigating the mechanism of ATI cell formation following injury.

ACKNOWLEDGMENTS

We thank Leland Dobbs for critically reading this manuscript and for providing antibodies against RTI_{40} and $RTII_{70}$ and Linda Wilson for help with confocal microscopy.

GRANTS

This work was funded by Salvesen Emphysema Research Trust, Scottish Hospital Endowments Research Trust, and Wellcome Trust.

REFERENCES

1. Adamson IY and Bowden DH. The type 2 cell as progenitor of alveolar epithelial regeneration. A cytodynamic study in mice after exposure to oxygen. Lab Invest 30: 35–42, 1974.
2. Ashino Y, Ying X, Dobbs LG, and Bhattacharya J. $[Ca^{2+}]_i$ oscillations regulate type II cell exocytosis in the pulmonary alveolus. Am J Physiol Lung Cell Mol Physiol 279: L5–L13, 2000.
3. Beers MF, Wali A, Eckenhoff MF, Feinstein SI, Fisher JH, and Fisher AB. An antibody with specificity for surfactant protein C precursors: identification of pro-SP-C in rat lung. Am J Respir Cell Mol Biol 7: 368–378, 1992.
4. Borok Z, Danto SI, Lubman RL, Cao Y, Williams MC, and Crandall ED. Modulation of t1α expression with alveolar epithelial cell phenotype in vitro. Am J Physiol Lung Cell Mol Physiol 275: L155–L164, 1998.
5. Boylan GM, Pryde JG, Dobbs LG, and McElroy MC. Identification of a novel antigen on the apical surface of rat alveolar epithelial type II and Clara cells. Am J Physiol Lung Cell Mol Physiol 280: L1318–L1326, 2001.
6. Dahlin K, Mager EM, Allen L, Tigue Z, Goodglick L, Wadehra M, and Dobbs L. Identification of genes differentially expressed in rat alveolar type I cells. Am J Respir Cell Mol Biol 31: 309–316, 2004.
7. Dobbs LG, Pian MS, Maglio M, Dumars S, and Allen L. Maintenance of the differentiated type II cell phenotype by culture with an apical air surface. Am J Physiol Lung Cell Mol Physiol 273: L347–L354, 1997.
8. Dobbs LG, Williams MC, and Gonzalez R. Monoclonal antibodies specific to apical surfaces of rat alveolar type I cells bind to surfaces of cultured, but not freshly isolated, type II cells. Biochim Biophys Acta 970: 146–156, 1988.
9. Duncan RR, Greaves J, Wiegand UK, Matskevich I, Bodammer G, Apps DK, Shipston MJ, and Chow RH. Functional and spatial segregation of secretory vesicle pools according to vesicle age. Nature 422: 176–180, 2003.
10. Evans MJ, Cabral LJ, Stephens RJ, and Freeman G. Transformation of alveolar type 2 cells to type 1 cells following exposure to NO_2. Exp Mol Pathol 22: 142–150, 1975.
11. Evans MJ, Stephens RJ, Cabral LJ, and Freeman G. Cell renewal in the lungs of rats exposed to low levels of NO_2. Arch Environ Health 24: 180–188, 1972.
12. Faulkner CS II and Esterly JR. Ultrastructural changes in the alveolar epithelium in response to Freund's adjuvant. Am J Pathol 64: 559–566, 1971.
13. Fehrenbach H. Alveolar epithelial type II cell: defender of the alveolus revisited. Respir Res 2: 33–46, 2001.
14. Fehrenbach H, Kasper M, Tschernig T, Pan T, Schuh D, Shannon JM, Muller M, and Mason RJ. Keratinocyte growth factor-induced hyperplasia of rat alveolar type II cells in vivo is resolved by differentiation into type I cells and by apoptosis. Eur Respir J 14: 534–544, 1999.
15. Franklin L, Cronshaw AD, Harrison DJ, and McElroy MC. The type II and Clara cell specific monoclonal antibody (MMC4) recognizes aminopeptidase N. Eur Respir J 24: 719s, 2004.
16. Gonzalez R, Yang YH, Griffin C, Allen L, Tigue Z, and Dobbs L. Freshly isolated rat alveolar type I cells, type II cells, and cultured type II

cells have distinct molecular phenotypes. Am J Physiol Lung Cell Mol Physiol 288: L179–L189, 2005.
17. Greenberg SD, Gyorkey F, Jenkins DE, and Gyorkey P. Alveolar epithelial cells following exposure to nitric acid. Electron microscopic study in rats. Arch Environ Health 22: 655–662, 1971.
18. Haies DM, Gil J, and Weibel ER. Morphometric study of rat lung cells. I. Numerical and dimensional characteristics of parenchymal cell population. Am Rev Respir Dis 123: 533–541, 1981.
19. Hirai K, Yamauchi M, Witschi H, and Cote MG. Disintegration of lung peroxisomes during differentiation of type II cells to type I cells in butylated hydroxytoluene-administered mice. Exp Mol Pathol 39: 129–138, 1983.
20. Johnson MD, Widdicombe JH, Allen L, Barbry P, and Dobbs LG. Alveolar epithelial type I cells contain transport proteins and transport sodium, supporting an active role for type I cells in regulation of lung liquid homeostasis. Proc Natl Acad Sci USA 99: 1966–1971, 2002.
21. Kalina M, Mason RJ, and Shannon JM. Surfactant protein C is expressed in alveolar type II cells but not in Clara cells of rat lung. Am J Respir Cell Mol Biol 6: 594–600, 1992.
22. McElroy MC, Cain DJ, Tyrrell C, Foster TJ, and Haslett C. Increased virulence of a fibronectin-binding protein mutant of Staphylococcus aureus in a rat model of pneumonia. Infect Immun 70: 3865–3873, 2002.
23. McElroy MC and Kasper M. The use of alveolar epithelial type I cell-selective markers to investigate lung injury and repair. Eur Respir J 24: 664–673, 2004.
24. McElroy MC and Kasper M. The use of alveolar epithelial type I cell selective markers to investigate lung injury and repair. Eur Respir J 24: 664–673, 2004.
25. McElroy MC, Pittet JF, Allen L, Wiener-Kronish JP, and Dobbs LG. Biochemical detection of type I cell damage after nitrogen dioxide-induced lung injury in rats. Am J Physiol Lung Cell Mol Physiol 273. L1228–L1234, 1997.
26. McElroy MC, Pittet JF, Hashimoto S, Allen L, Wiener-Kronish JP, and Dobbs LG. A type I cell-specific protein is a biochemical marker of epithelial injury in a rat model of pneumonia. Am J Physiol Lung Cell Mol Physiol 268: L181–L186, 1995.
27. Nielsen S, King LS, Christensen BM, and Agre P. Aquaporins in complex tissues. II. Subcellular distribution in respiratory and glandular tissues of rat. Am J Physiol Cell Physiol 273: C1549–C1561, 1997.
28. Phelps DS and Floros J. Localization of pulmonary surfactant proteins using immunohistochemistry and tissue in situ hybridization. Exp Lung Res 17: 985–995, 1991.
29. Ramirez MI, Millien G, Hinds A, Cao Y, Seldin DC, and Williams MC. T1α, a lung type I cell differentiation gene, is required for normal lung cell proliferation and alveolus formation at birth. Dev Biol 256: 61–72, 2003.
30. Ridge K, Olivera W, Rutschman DH, Mercer RW, Uhal B, Horowitz S, Hughes F, Factor P, Barnard ML, and Sznajder JI. α_2 Na,K-ATPase contributes to lung liquid clearance. Ann NY Acad Sci 834: 651–652, 1997.
31. Rishi AK, Joyce-Brady M, Fisher J, Dobbs LG, Floros J, VanderSpek J, Brody JS, and Williams MC. Cloning, characterization, and development expression of a rat lung alveolar type I cell gene in embryonic endodermal and neural derivatives. Dev Biol 167: 294–306, 1995.
32. Towne JE, Harrod KS, Krane CM, and Menon AG. Decreased expression of aquaporin (AQP)1 and AQP5 in mouse lung after acute viral infection. Am J Respir Cell Mol Biol 22: 34–44, 2000.
33. Uhal BD. Cell cycle kinetics in the alveolar epithelium. Am J Physiol Lung Cell Mol Physiol 272: L1031–L1045, 1997.
34. Weibel ER. The Pathway for Oxygen. London: Havard University Press, 1984, p. 231–271.
35. Weibel ER and Gomez DM. Architecture of the human lung. Use of quantitative methods establishes fundamental relations between size and number of lung structures. Science 137: 577–585, 1962.
36. Williams MC. Alveolar type I cells: molecular phenotype and development. Annu Rev Physiol 65: 669–695, 2003.

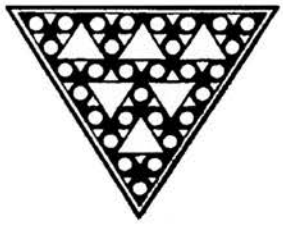

Bibliography

(2000). "American Thoracic Society. Idiopathic pulmonary fibrosis: diagnosis and treatment. International consensus statement. American Thoracic Society (ATS), and the European Respiratory Society (ERS)." Am J Respir Crit Care Med **161**(2 Pt 1): 646-64.

(2000). "Ventilation with lower tidal volumes as compared with traditional tidal volumes for acute lung injury and the acute respiratory distress syndrome. The Acute Respiratory Distress Syndrome Network." N Engl J Med **342**(18): 1301-8.

Abel, S. J., S. J. Finney, et al. (1998). "Reduced mortality in association with the acute respiratory distress syndrome (ARDS)." Thorax **53**(4): 292-4.

Adamson, I. Y. and D. H. Bowden (1974). "The type 2 cell as progenitor of alveolar epithelial regeneration. A cytodynamic study in mice after exposure to oxygen." Lab Invest **30**(1): 35-42.

Adamson, I. Y. and D. H. Bowden (1975). "Derivation of type 1 epithelium from type 2 cells in the developing rat lung." Lab Invest **32**(6): 736-45.

Adamson, I. Y., C. Hedgecock, et al. (1990). "Epithelial cell-fibroblast interactions in lung injury and repair." Am J Pathol **137**(2): 385-92.

Adamson, I. Y., L. Young, et al. (1988). "Relationship of alveolar epithelial injury and repair to the induction of pulmonary fibrosis." Am J Pathol **130**(2): 377-83.

Adhikari, N., K. Burns, et al. (2004). "Pharmacologic therapies for adults with acute lung injury and acute respiratory distress syndrome." Cochrane Database Syst Rev(4): CD004477.

Albertine, K. H. (1998). Histopathology of pulmonary edema and the acute respiratory distress syndrome. Pulmonary edema. M. A. Matthay, Ingbar, D.H. New York, Marcel Dekker**:** 37-83.

Alonso, L. and E. Fuchs (2003). "Stem cells of the skin epithelium." Proc Natl Acad Sci U S A **100 Suppl 1**: 11830-5.

Ashbaugh, D. G., D. B. Bigelow, et al. (1967). "Acute respiratory distress in adults." Lancet **2**(7511): 319-23.

Bachofen, M. and E. R. Weibel (1974). "Basic pattern of tissue repair in human lungs following unspecific injury." Chest **65**: Suppl:14S-19S.

Bakker-Woudenberg, I. A. (2003). "Experimental models of pulmonary infection." J Microbiol Methods **54**(3): 295-313.

Bakker-Woudenberg, I. A., J. Y. de Jong-Hoenderop, et al. (1979). "Efficacy of antimicrobial therapy in experimental rat pneumonia: effects of impaired phagocytosis." Infect Immun **25**(1): 366-75.

Baudouin, S. V. (2004). "Exogenous surfactant replacement in ARDS--one day, someday, or never?" N Engl J Med **351**(9): 853-5.

Beers, M. F., C. Y. Kim, et al. (1994). "Localization, synthesis, and processing of surfactant protein SP-C in rat lung analyzed by epitope-specific antipeptide

antibodies." J Biol Chem **269**(32): 20318-28.

Beers, M. F., C. Y. Kim, et al. (1994). "Synthesis of type II cell lamellar body lysozyme-15 kD protein (lbl-15) by perfused rat lung." Am J Respir Cell Mol Biol **11**(2): 240-8.

Beers, M. F., A. Wali, et al. (1992). "An antibody with specificity for surfactant protein C precursors: identification of pro-SP-C in rat lung." Am J Respir Cell Mol Biol **7**(4): 368-78.

Beitel, G. J. and M. A. Krasnow (2000). "Genetic control of epithelial tube size in the Drosophila tracheal system." Development **127**(15): 3271-82.

Bell, R. C., J. J. Coalson, et al. (1983). "Multiple organ system failure and infection in adult respiratory distress syndrome." Ann Intern Med **99**(3): 293-8.

Bernard, G. R., A. Artigas, et al. (1994). "The American-European Consensus Conference on ARDS. Definitions, mechanisms, relevant outcomes, and clinical trial coordination." Am J Respir Crit Care Med **149**(3 Pt 1): 818-24.

Berthiaume, Y., O. Lesur, et al. (1999). "Treatment of adult respiratory distress syndrome: plea for rescue therapy of the alveolar epithelium." Thorax **54**(2): 150-60.

Berthiaume, Y., M. Sapijaszko, et al. (1991). "Protein kinase C activation does not stimulate lung liquid clearance in anesthetized sheep." Am Rev Respir Dis **144**(5): 1085-90.

Bonten, M. J., M. H. Kollef, et al. (2004). "Risk factors for ventilator-associated pneumonia: from epidemiology to patient management." Clin Infect Dis **38**(8): 1141-9.

Boone, C. W., G. S. Harell, et al. (1968). "The resolution of mixtures of viable mammalian cells into homogeneous fractions by zonal centrifugation." J Cell Biol **36**(2): 369-78.

Boylan, G. M., J. G. Pryde, et al. (2001). "Identification of a novel antigen on the apical surface of rat alveolar epithelial type II and Clara cells." Am J Physiol Lung Cell Mol Physiol **280**(6): L1318-26.

Bradford, M. M. (1976). "A rapid and sensitive method for the quantitation of microgram quantities of protein utilizing the principle of protein-dye binding." Anal Biochem **72**: 248-54.

Breuss, J. M., J. Gallo, et al. (1995). "Expression of the beta 6 integrin subunit in development, neoplasia and tissue repair suggests a role in epithelial remodeling." J Cell Sci **108 (Pt 6)**: 2241-51.

Buckley, S., B. Driscoll, et al. (2001). "Migration and gelatinases in cultured fetal, adult, and hyperoxic alveolar epithelial cells." Am J Physiol Lung Cell Mol Physiol **281**(2): L427-34.

Cao, Y., J. Q. Tao, et al. (2004). "IL-4 induces production of the lung collectin surfactant protein-D." J Allergy Clin Immunol **113**(3): 439-44.

Clegg, G. R., C. Tyrrell, et al. (2005). "Coexpression of RTI40 with alveolar epithelial

type II cell proteins in lungs following injury: identification of alveolar intermediate cell types." Am J Physiol Lung Cell Mol Physiol **289**(3): L382-90.

Cruz-Orive, L. M. and E. R. Weibel (1990). "Recent stereological methods for cell biology: a brief survey." Am J Physiol **258**(4 Pt 1): L148-56.

Daly, H. E., C. M. Baecher-Allan, et al. (1998). "Cell-specific gene expression reveals changes in epithelial cell populations after bleomycin treatment." Lab Invest **78**(4): 393-400.

Dobbs, L. G. (1990). "Isolation and culture of alveolar type II cells." American Journal of Physiology **258**(4 Pt 1): L134-47.

Dobbs, L. G., E. F. Geppert, et al. (1980). "Metabolic properties and ultrastructure of alveolar type II cells isolated with elastase." Biochim Biophys Acta **618**(3): 510-23.

Dobbs, L. G., M. S. Pian, et al. (1997). "Maintenance of the differentiated type II cell phenotype by culture with an apical air surface." Am J Physiol **273**(2 Pt 1): L347-54.

Dobbs, L. G., M. C. Williams, et al. (1988). "Monoclonal antibodies specific to apical surfaces of rat alveolar type I cells bind to surfaces of cultured, but not freshly isolated, type II cells." Biochim Biophys Acta **970**(2): 146-56.

Doyle, R. L., N. Szaflarski, et al. (1995). "Identification of patients with acute lung injury. Predictors of mortality." Am J Respir Crit Care Med **152**(6 Pt 1): 1818-24.

Dreyfuss, D. and G. Saumon (1998). "Ventilator-induced lung injury: lessons from experimental studies." Am J Respir Crit Care Med **157**(1): 294-323.

Evans, M. J., L. J. Cabral, et al. (1975). "Transformation of alveolar type 2 cells to type 1 cells following exposure to NO2." Exp Mol Pathol **22**(1): 142-50.

Evans, M. J., R. J. Stephens, et al. (1972). "Cell renewal in the lungs of rats exposed to low levels of NO2." Arch Environ Health **24**(3): 180-8.

Evans, M. J., L. S. Van Winkle, et al. (1999). "The attenuated fibroblast sheath of the respiratory tract epithelial-mesenchymal trophic unit." Am J Respir Cell Mol Biol **21**(6): 655-7.

Fan, J., J. C. Marshall, et al. (1998). "Hemorrhagic shock primes for increased expression of cytokine-induced neutrophil chemoattractant in the lung: role in pulmonary inflammation following lipopolysaccharide." J Immunol **161**(1): 440-7.

Fang, K. C. (2000). "Mesenchymal regulation of alveolar repair in pulmonary fibrosis." Am J Respir Cell Mol Biol **23**(2): 142-5.

Faulkner, C. S., 2nd and J. R. Esterly (1971). "Ultrastructural changes in the alveolar epithelium in response to Freund's adjuvant." Am J Pathol **64**(3): 559-66.

Fehrenbach, H. (2001). "Alveolar epithelial type II cell: defender of the alveolus revisited." Respir Res **2**(1): 33-46.

Fehrenbach, H., M. Kasper, et al. (1999). "Keratinocyte growth factor-induced

hyperplasia of rat alveolar type II cells in vivo is resolved by differentiation into type I cells and by apoptosis." Eur Respir J **14**(3): 534-44.

Flecknoe, S., R. Harding, et al. (2000). "Increased lung expansion alters the proportions of type I and type II alveolar epithelial cells in fetal sheep." Am J Physiol Lung Cell Mol Physiol **278**(6): L1180-5.

Flecknoe, S. J., R. E. Boland, et al. (2004). "Regulation of alveolar epithelial cell phenotypes in fetal sheep: role of cortisol and lung expansion." Am J Physiol Lung Cell Mol Physiol.

Flecknoe, S. J., M. J. Wallace, et al. (2003). "Changes in alveolar epithelial cell proportions during fetal and postnatal development in sheep." Am J Physiol Lung Cell Mol Physiol **285**(3): L664-70.

Flecknoe, S. J., M. J. Wallace, et al. (2002). "Determination of alveolar epithelial cell phenotypes in fetal sheep: evidence for the involvement of basal lung expansion." J Physiol **542**(Pt 1): 245-53.

Fleury, V. and T. Watanabe (2004). "About the equilibrium shape of fibred structures, and biological shapes." C R Biol **327**(7): 663-77.

Fowler, A. A., R. F. Hamman, et al. (1983). "Adult respiratory distress syndrome: risk with common predispositions." Ann Intern Med **98**(5 Pt 1): 593-7.

Franklin, L., Cronshaw, A. D., Harrison, D. J., McElroy, M. C. (2004). "The type II and clara cell specific monoclonal antibody (MMC4) recognises aminopeptidase N." ERJ in press.

Funkhouser, J. D., L. B. Cheshire, et al. (1987). "Monoclonal antibody identification of a type II alveolar epithelial cell antigen and expression of the antigen during lung development." Dev Biol **119**(1): 190-8.

Funkhouser, J. D. and R. D. Peterson (1989). "Immunotargeting: a contemporary approach to the study of lung development." Am J Physiol **257**(6 Pt 1): L311-7.

Funkhouser, J. D., S. D. Tangada, et al. (1991). "p146 type II alveolar epithelial cell antigen is identical to aminopeptidase N." Am J Physiol **260**(4 Pt 1): L274-9.

Gajic, O., J. Lee, et al. (2003). "Ventilator-induced cell wounding and repair in the intact lung." Am J Respir Crit Care Med **167**(8): 1057-63.

Gattinoni, L., P. Pelosi, et al. (1998). "Acute respiratory distress syndrome caused by pulmonary and extrapulmonary disease. Different syndromes?" Am J Respir Crit Care Med **158**(1): 3-11.

Gauldie, J., M. Kolb, et al. (2002). "A new direction in the pathogenesis of idiopathic pulmonary fibrosis?" Respir Res **3**(1): 1.

Geiser, T. (2003). "Idiopathic pulmonary fibrosis--a disorder of alveolar wound repair?" Swiss Med Wkly **133**(29-30): 405-11.

Giangreco, A., S. D. Reynolds, et al. (2002). "Terminal bronchioles harbor a unique airway stem cell population that localizes to the bronchoalveolar duct junction." Am J Pathol **161**(1): 173-82.

Goss, C. H., R. G. Brower, et al. (2003). "Incidence of acute lung injury in the United

States." Crit Care Med **31**(6): 1607-11.

Greenberg, S. D., F. Gyorkey, et al. (1971). "Alveolar epithelial cells following exposure to nitric acid. Electron microscopic study in rats." Arch Environ Health **22**(6): 655-62.

Grove, J. E., C. Lutzko, et al. (2002). "Marrow-derived cells as vehicles for delivery of gene therapy to pulmonary epithelium." Am J Respir Cell Mol Biol **27**(6): 645-51.

Guo, J., E. S. Yi, et al. (1998). "Intravenous keratinocyte growth factor protects against experimental pulmonary injury." Am J Physiol **275**(4 Pt 1): L800-5.

Gutierrez, J. A., R. F. Gonzalez, et al. (1998). "Mechanical distension modulates pulmonary alveolar epithelial phenotypic expression in vitro." Am J Physiol **274**(2 Pt 1): L196-202.

Haczku, A., E. N. Atochina, et al. (2001). "Aspergillus fumigatus-induced allergic airway inflammation alters surfactant homeostasis and lung function in BALB/c mice." Am J Respir Cell Mol Biol **25**(1): 45-50.

Haies, D. M., J. Gil, et al. (1981). "Morphometric study of rat lung cells. I. Numerical and dimensional characteristics of parenchymal cell population." Am Rev Respir Dis **123**(5): 533-41.

Haitsma, J. J., P. J. Papadakos, et al. (2004). "Surfactant therapy for acute lung injury/acute respiratory distress syndrome." Curr Opin Crit Care **10**(1): 18-22.

Hashimoto, N., H. Jin, et al. (2004). "Bone marrow-derived progenitor cells in pulmonary fibrosis." J Clin Invest **113**(2): 243-52.

Heffner, J. E., L. K. Brown, et al. (1995). "Prospective validation of an acute respiratory distress syndrome predictive score." Am J Respir Crit Care Med **152**(5 Pt 1): 1518-26.

Hirai, K., M. Yamauchi, et al. (1983). "Disintegration of lung peroxisomes during differentiation of type II cells to type I cells in butylated hydroxytoluene-administered mice." Exp Mol Pathol **39**(2): 129-38.

Holmskov, U., P. Lawson, et al. (1997). "Isolation and characterization of a new member of the scavenger receptor superfamily, glycoprotein-340 (gp-340), as a lung surfactant protein-D binding molecule." J Biol Chem **272**(21): 13743-9.

Hong, K. U., S. D. Reynolds, et al. (2004). "Basal cells are a multipotent progenitor capable of renewing the bronchial epithelium." Am J Pathol **164**(2): 577-88.

Huang, X., J. Wu, et al. (1998). "Expression of the human integrin beta6 subunit in alveolar type II cells and bronchiolar epithelial cells reverses lung inflammation in beta6 knockout mice." Am J Respir Cell Mol Biol **19**(4): 636-42.

Johnson, M. D., J. H. Widdicombe, et al. (2002). "Alveolar epithelial type I cells contain transport proteins and transport sodium, supporting an active role for type I cells in regulation of lung liquid homeostasis." Proc Natl Acad Sci U S A **99**(4): 1966-71.

Kikkawa, Y. and F. Smith (1983). "Cellular and biochemical aspects of pulmonary

surfactant in health and disease." Lab Invest **49**(2): 122-39.

Kleeberger, W., A. Versmold, et al. (2003). "Increased chimerism of bronchial and alveolar epithelium in human lung allografts undergoing chronic injury." Am J Pathol **162**(5): 1487-94.

Kollef, M. H. (1999). "The prevention of ventilator-associated pneumonia." N Engl J Med **340**(8): 627-34.

Kondo, M., A. J. Wagers, et al. (2003). "Biology of hematopoietic stem cells and progenitors: implications for clinical application." Annu Rev Immunol **21**: 759-806.

Kotton, D. N., B. Y. Ma, et al. (2001). "Bone marrow-derived cells as progenitors of lung alveolar epithelium." Development **128**(24): 5181-8.

Kuhn, C., 3rd, J. Boldt, et al. (1989). "An immunohistochemical study of architectural remodeling and connective tissue synthesis in pulmonary fibrosis." Am Rev Respir Dis **140**(6): 1693-703.

Lecuona, E., F. Saldias, et al. (1999). "Ventilator-associated lung injury decreases lung ability to clear edema and downregulates alveolar epithelial cell Na,K-adenosine triphosphatase function." Chest **116**(1 Suppl): 29S-30S.

Marshall, R. P., G. Bellingan, et al. (2000). "Fibroproliferation occurs early in the acute respiratory distress syndrome and impacts on outcome." Am J Respir Crit Care Med **162**(5): 1783-8.

Marshman, E., C. Booth, et al. (2002). "The intestinal epithelial stem cell." Bioessays **24**(1): 91-8.

Mason, C. M., B. P. Guery, et al. (1996). "Keratinocyte growth factor attenuates lung leak induced by alpha-naphthylthiourea in rats." Crit Care Med **24**(6): 925-31.

Mason, R. J., K. Greene, et al. (1998). "Surfactant protein A and surfactant protein D in health and disease." Am J Physiol **275**(1 Pt 1): L1-13.

Mason, R. J. and M. C. Williams (1977). "Type II alveolar cell. Defender of the alveolus." Am Rev Respir Dis **115**(6 Pt 2): 81-91.

Matthay, M. A., S. Bhattacharya, et al. (2002). "Ventilator-induced lung injury: in vivo and in vitro mechanisms." Am J Physiol Lung Cell Mol Physiol **283**(4): L678-82.

Matthay, M. A., H. G. Folkesson, et al. (2002). "Lung epithelial fluid transport and the resolution of pulmonary edema." Physiol Rev **82**(3): 569-600.

Matthay, M. A. and J. P. Wiener-Kronish (1990). "Intact epithelial barrier function is critical for the resolution of alveolar edema in humans." Am Rev Respir Dis **142**(6 Pt 1): 1250-7.

McElroy, M. C., D. J. Cain, et al. (2002). "Increased virulence of a fibronectin-binding protein mutant of Staphylococcus aureus in a rat model of pneumonia." Infect Immun **70**(7): 3865-73.

McElroy, M. C., H. R. Harty, et al. (1999). "Alpha-toxin damages the air-blood barrier of the lung in a rat model of Staphylococcus aureus-induced pneumonia." Infect

Immun **67**(10): 5541-4.

McElroy, M. C. and M. Kasper (2004). "The use of alveolar epithelial type I cell-selective markers to investigate lung injury and repair." Eur Respir J **24**(4): 664-73.

McElroy, M. C., Kasper, M (2004). "The Use of Alveolar Epithelial Type I Cell Selective Markers to Investigate Lung Injury and Repair." Eur Respir J **in press**.

McElroy, M. C., J. F. Pittet, et al. (1995). "A type I cell-specific protein is a biochemical marker of epithelial injury in a rat model of pneumonia." Am J Physiol **268**(2 Pt 1): L181-6.

Metzger, R. J. and M. A. Krasnow (1999). "Genetic control of branching morphogenesis." Science **284**(5420): 1635-9.

Milberg, J. A., D. R. Davis, et al. (1995). "Improved survival of patients with acute respiratory distress syndrome (ARDS): 1983-1993." Jama **273**(4): 306-9.

Min, H., D. M. Danilenko, et al. (1998). "Fgf-10 is required for both limb and lung development and exhibits striking functional similarity to Drosophila branchless." Genes Dev **12**(20): 3156-61.

Miyamura, K., L. E. Leigh, et al. (1994). "Surfactant protein D binding to alveolar macrophages." Biochem J **300 (Pt 1)**: 237-42.

Modelska, K., M. A. Matthay, et al. (1997). "Upregulation of alveolar liquid clearance after fluid resuscitation for hemorrhagic shock in rats." Am J Physiol **273**(2 Pt 1): L305-14.

Montgomery, A. B., M. A. Stager, et al. (1985). "Causes of mortality in patients with the adult respiratory distress syndrome." Am Rev Respir Dis **132**(3): 485-9.

Morrison, S. J., N. M. Shah, et al. (1997). "Regulatory mechanisms in stem cell biology." Cell **88**(3): 287-98.

Murphy, S. A., D. Dinsdale, et al. (1999). "A comparative study of the isolation of type II epithelial cells from rat, hamster, pig and human lung tissue." Methods Cell Sci **21**(1): 31-8.

Mutsaers, S. E., J. E. Bishop, et al. (1997). "Mechanisms of tissue repair: from wound healing to fibrosis." Int J Biochem Cell Biol **29**(1): 5-17.

National Institutes of Health, N. (1977). "Conference report: Mechanisms of acute respiratory failure." Am Rev Respir Dis **115**(6): 1071-8.

Neuringer, I. P. and S. H. Randell (2004). "Stem cells and repair of lung injuries." Respir Res **5**(1): 6.

Nielsen, S., L. S. King, et al. (1997). "Aquaporins in complex tissues. II. Subcellular distribution in respiratory and glandular tissues of rat." Am J Physiol **273**(5 Pt 1): C1549-61.

Ohmichi, H., K. Matsumoto, et al. (1996). "In vivo mitogenic action of HGF on lung epithelial cells: pulmotrophic role in lung regeneration." Am J Physiol **270**(6 Pt 1): L1031-9.

Ortiz, L. A., F. Gambelli, et al. (2003). "Mesenchymal stem cell engraftment in lung is

enhanced in response to bleomycin exposure and ameliorates its fibrotic effects." Proc Natl Acad Sci U S A **100**(14): 8407-11.

Pelosi, P., D. D'Onofrio, et al. (2003). "Pulmonary and extrapulmonary acute respiratory distress syndrome are different." Eur Respir J Suppl **42**: 48s-56s.

Pinkerton, K. E., P. Gehr, et al. (1992). Architecture and cellular composition of the air blood barrier. Comparative Biology of the Normal Lung. R. A. Parent. Boca Raton, CRC Press**:** 121-128.

Ramirez, M. I., G. Millien, et al. (2003). "T1alpha, a lung type I cell differentiation gene, is required for normal lung cell proliferation and alveolus formation at birth." Dev Biol **256**(1): 61-72.

Ranieri, V. M., F. Giunta, et al. (2000). "Mechanical ventilation as a mediator of multisystem organ failure in acute respiratory distress syndrome." Jama **284**(1): 43-4.

Rhodes, G. C., A. W. Lykke, et al. (1989). "Abnormal alveolar epithelial repair associated with failure of resolution in experimental streptococcal pneumonia." J Pathol **159**(3): 245-53.

Richards, R. J., N. Davies, et al. (1987). "Isolation, biochemical characterization, and culture of lung type II cells of the rat." Lung **165**(3): 143-58.

Rubenfeld, G. D. a. N., M .J. (2003). Epidemiology of Acute Lung Injury - A Public Health Perspective. Acute Respiratory Distress Syndrome. M. A. Matthay. New York, Marcel Dekker. **179:** 37-54.

Schacht, V., M. I. Ramirez, et al. (2003). "T1alpha/podoplanin deficiency disrupts normal lymphatic vasculature formation and causes lymphedema." Embo J **22**(14): 3546-56.

Scholl, F. G., C. Gamallo, et al. (1999). "Identification of PA2.26 antigen as a novel cell-surface mucin-type glycoprotein that induces plasma membrane extensions and increased motility in keratinocytes." J Cell Sci **112 (Pt 24)**: 4601-13.

Sekine, K., H. Ohuchi, et al. (1999). "Fgf10 is essential for limb and lung formation." Nat Genet **21**(1): 138-41.

Selman, M., T. E. King, et al. (2001). "Idiopathic pulmonary fibrosis: prevailing and evolving hypotheses about its pathogenesis and implications for therapy." Ann Intern Med **134**(2): 136-51.

Selman, M. and A. Pardo (2002). "Idiopathic pulmonary fibrosis: an epithelial/fibroblastic cross-talk disorder." Respir Res **3**(1): 3.

Shannon, J. M., S. D. Jennings, et al. (1992). "Modulation of alveolar type II cell differentiated function in vitro." Am J Physiol **262**(4 Pt 1): L427-36.

Sheppard, D. (2001). "Pulmonary fibrosis: a cellular overreaction or a failure of communication?" J Clin Invest **107**(12): 1501-2.

Sirianni, F. E., F. S. Chu, et al. (2003). "Human alveolar wall fibroblasts directly link epithelial type 2 cells to capillary endothelium." Am J Respir Crit Care Med **168**(12): 1532-7.

Slutsky, A. S. and L. N. Tremblay (1998). "Multiple system organ failure. Is mechanical ventilation a contributing factor?" Am J Respir Crit Care Med **157**(6 Pt 1): 1721-5.

Spees, J. L., S. D. Olson, et al. (2003). "Differentiation, cell fusion, and nuclear fusion during ex vivo repair of epithelium by human adult stem cells from bone marrow stroma." Proc Natl Acad Sci U S A **100**(5): 2397-402.

Suchyta, M. R., T. P. Clemmer, et al. (1992). "The adult respiratory distress syndrome. A report of survival and modifying factors." Chest **101**(4): 1074-9.

Takahashi, Y., S. Aida, et al. (1994). "Cytochrome P450 2B1 immunoreactivity in bronchiolar and alveolar epithelial cells after exposure of rats to ozone." Toxicol Appl Pharmacol **128**(2): 207-15.

Takeoka, M., W. F. Ward, et al. (1997). "KGF facilitates repair of radiation-induced DNA damage in alveolar epithelial cells." Am J Physiol **272**(6 Pt 1): L1174-80.

Theise, N. D., O. Henegariu, et al. (2002). "Radiation pneumonitis in mice: a severe injury model for pneumocyte engraftment from bone marrow." Exp Hematol **30**(11): 1333-8.

Thomsen, G. E. and A. H. Morris (1995). "Incidence of the adult respiratory distress syndrome in the state of Utah." Am J Respir Crit Care Med **152**(3): 965-71.

Tomashefski, J. F. J. (2003). Pulmonary Pathology of the Acute Respiratory Distress Syndrome - Diffuse Alveolar Damage. Acute Respiratory Distress Syndrome. M. A. Matthay. New York, Marcel Dekker. **179:** 75-114.

Uhal, B. D. (1997). "Cell cycle kinetics in the alveolar epithelium." Am J Physiol **272**(6 Pt 1): L1031-45.

Viget, N. B., B. P. Guery, et al. (2000). "Keratinocyte growth factor protects against Pseudomonas aeruginosa-induced lung injury." Am J Physiol Lung Cell Mol Physiol **279**(6): L1199-209.

Villar, J. and A. S. Slutsky (1989). "The incidence of the adult respiratory distress syndrome." Am Rev Respir Dis **140**(3): 814-6.

Vlahakis, N. E. and R. D. Hubmayr (2000). "Invited review: plasma membrane stress failure in alveolar epithelial cells." J Appl Physiol **89**(6): 2490-6;discussion 2497.

Vlahakis, N. E. and R. D. Hubmayr (2005). "Cellular stress failure in ventilator-injured lungs." Am J Respir Crit Care Med **171**(12): 1328-42.

Vuichard, D., M. T. Ganter, et al. (2005). "Hypoxia aggravates lipopolysaccharide-induced lung injury." Clin Exp Immunol **141**(2): 248-60.

Wang, R., O. Ibarra-Sunga, et al. (2000). "Abrogation of bleomycin-induced epithelial apoptosis and lung fibrosis by captopril or by a caspase inhibitor." Am J Physiol Lung Cell Mol Physiol **279**(1): L143-51.

Warburton, D. and S. Bellusci (2004). "The molecular genetics of lung morphogenesis and injury repair." Paediatr Respir Rev **5 Suppl A**: S283-7.

Warburton, D., M. Schwarz, et al. (2000). "The molecular basis of lung

morphogenesis." Mech Dev **92**(1): 55-81.

Ware, L. B. and M. A. Matthay (2000). "The acute respiratory distress syndrome." N Engl J Med **342**(18): 1334-49.

Ware, L. B. and M. A. Matthay (2001). "Alveolar fluid clearance is impaired in the majority of patients with acute lung injury and the acute respiratory distress syndrome." Am J Respir Crit Care Med **163**(6): 1376-83.

Watt, F. M. and B. L. Hogan (2000). "Out of Eden: stem cells and their niches." Science **287**(5457): 1427-30.

Webster, N. R., A. T. Cohen, et al. (1988). "Adult respiratory distress syndrome--how many cases in the UK?" Anaesthesia **43**(11): 923-6.

Weibel, E. R. (1984). The pathway for oxygen. Cambridge, Massachusetts and London, Harvard University Press.

Weibel, E. R. and D. M. Gomez (1962). "Architecture of the human lung. Use of quantitative methods establishes fundamental relations between size and number of lung structures." Science **137**: 577-85.

Weinstein, M., X. Xu, et al. (1998). "FGFR-3 and FGFR-4 function cooperatively to direct alveogenesis in the murine lung." Development **125**(18): 3615-23.

White, S. R., D. R. Dorscheid, et al. (1999). "Role of very late adhesion integrins in mediating repair of human airway epithelial cell monolayers after mechanical injury." Am J Respir Cell Mol Biol **20**(4): 787-96.

White, S. R., K. R. Wojcik, et al. (2001). "Airway epithelial cell wound repair mediated by alpha-dystroglycan." Am J Respir Cell Mol Biol **24**(2): 179-86.

Wiener-Kronish, J. P., K. H. Albertine, et al. (1991). "Differential responses of the endothelial and epithelial barriers of the lung in sheep to Escherichia coli endotoxin." J Clin Invest **88**(3): 864-75.

Williams, M. C. (2003). "Alveolar type I cells: molecular phenotype and development." Annu Rev Physiol **65**: 669-95.

Williams, M. C., Y. Cao, et al. (1996). "T1 alpha protein is developmentally regulated and expressed by alveolar type I cells, choroid plexus, and ciliary epithelia of adult rats." Am J Respir Cell Mol Biol **14**(6): 577-85.

Williams, M. C. and L. G. Dobbs (1990). "Expression of cell-specific markers for alveolar epithelium in fetal rat lung." Am J Respir Cell Mol Biol **2**(6): 533-42.

Wong, C. J., J. Akiyama, et al. (1996). "Localization and developmental expression of surfactant proteins D and A in the respiratory tract of the mouse." Pediatr Res **39**(6): 930-7.

Yano, T., R. J. Mason, et al. (2000). "KGF regulates pulmonary epithelial proliferation and surfactant protein gene expression in adult rat lung." Am J Physiol Lung Cell Mol Physiol **279**(6): L1146-58.

Zilberberg, M. D. and S. K. Epstein (1998). "Acute lung injury in the medical ICU: comorbid conditions, age, etiology, and hospital outcome." Am J Respir Crit Care Med **157**(4 Pt 1): 1159-64.